TÉCNICO LISBOA

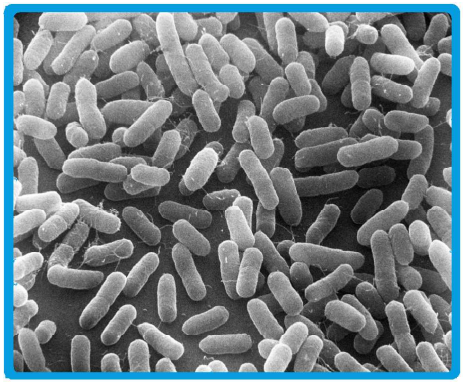

Development of Carbon Nanotube Field-Effect-Transistor (CNT-FET) biosensor with a point-of-care device for water quality analysis in terms of water-borne bacteria.

Miguel Nuno Mesquita Costa Rodrigues

Thesis to obtain the Master of Science Degree in

Bioengineering and Nanosystems

Supervisor: Prof. Susana Isabel Pinheiro Cardoso de Freitas

Examination Committee

Chairperson: Prof. Gabriel António Amaro Monteiro
Supervisor: Prof. Susana Isabel Pinheiro Cardoso de Freitas
Member of the Committee: Prof. Luís Joaquim Pina da Fonseca

November 2017

Dedicado aos meus pais, que sempre a mim me dedicaram todo o seu tempo paciência e amor.
Dedicado aos meus avôs, que sempre a mim me dedicaram todo o seu conhecimento.
Dedicado ao meu irmão, que sempre a mim me dedicou tudo aquilo que de melhor tem para partilhar.
Dedicado a todos os meus amigos e amigas (OS).

Mas acima de tudo...

Dedicado à minha queridíssima Avó Carochinha.
E dedicado à minha queridíssima Avó Lurdes.

Os meus anjos da guarda.

Acknowledgments

I would like to give my acknowledgements, firstly, to Professor Susana Cardoso Freitas without whom this study would not have been possible. Thank you, Professor, for providing me with the necessary sensors for this study, for arranging my visits to the University of Aveiro and above all, thank you Professor for your patience.

Secondly I would like to give my acknowlegments to Professor Teresa Rocha Santos at the CESAM department of the University of Aveiro, never forgetting assistant Professor João Costa and Post Doctoral student Celine Justino, who were always willing to help and whose knowledge was of great importance in order to accomplish this study.

Thirdly I would like to give my acknowledgements to Professor Umesh Vinaica Mardolcar and to assistant Professor Daniel Mendes from the Physics department at IST, for providing me with the materials and facilities to fabricate the necessary circuit boards for this study.

Of course, I would like to give my acknowledgements to Professor Gabriel Monteiro from the Bioengineering department of IST for providing me the necessary testing samples to calibrate the sensors.

Finally, I would like to give my acknowledgements to all the INESC-MN team Engineer Fernando Silva, Vania Silverio, Denis Santos, Rui Pinto, Natércia Correia and, above all to my fellow colleagues from INESC-MN, Rui Garcia, Pedro Alves, Jorge Perreira, Débora Albuquerque, João Serra, Tomás Ribeiro, Tiago Costa, Tomás Martins, Nuno Milhomens and all the others without whom this study would not have been possible.

Thank you.

Resumo

Este estudo aspira ao desenvolvimento de um dispositivo alternativo e não convencional capaz de analisar água numa perspectiva point-of-care. O objectivo primário é o de conseguir utilizar um computador pessoal para determinar a concentração de bactérias presentes em determinada amostra de água. O dispositivo base é um transístor de efeito de campo no qual o canal é uma malha de nanotubos de carbono de parede simples, esta malha possui um comportamento semiconductor do tipo-p.

Cada dispositivo foi fabricado em cinco passos. Em primeiro lugar, um passo de micro-fabricação no qual a base do dispositivo foi feita. Em segundo lugar, um passo de deposição por dielectroforese no qual a malha de nanotubos de carbono de parede simples foi depositada. Em terceiro lugar, um passo de funcionalização no qual um anticorpo específico foi adsorvido aos nanotubos de carbono. Em quarto lugar, bactérias *E. coli* da estirpe DH5α foram aplicadas em concentrações diferentes e conhecidas a dispositivos diferentes. Por último, a caracterização destes dispositivos foi feita usando o analisador de parâmetros de semicondutores, de modo a obter a curvas Id-Vd e Id-Vg dos transístores de efeito de campo.

Após todos os dados serem recolhidos e analisados foi obtida uma curva de calibração capaz de correlacionar a corrente de base do transístor com a concentração de *E. coli*, esta curva é essencial para o funcionar correcto do dispositivo point-of-care.

Este estudo explica não só os princípios de funcionamento por detrás dos transístores de efeito de campo baseados em nanotubos de carbono de parede simples, mas também, formas de melhorar a sua reprodutibilidade de resultados. O dispositivo point-of-care consiste num pico amperímetro rudimentar, capaz de ler as correntes de base dos sensores (pA), este pico amperímetro está conectado ao computador através de a uma placa de Arduino e do software MATLAB.

Palavras-chave: SWCNT, FET, CNT-FET, *E. coli*, Barreiras de Schottky, Transferência directa de cargas, Dispersões de CNT, Deposição dieletroforética de CNT.

Abstract

This study aspires to create an unconventional and alternative device capable of analysing water in a point-of-care perspective. The main objective is to assess, using a personal computer, the amount of water-borne bacteria present in a given water sample. The base device is a field-effect-transistor in which the channel is a single walled carbon-nanotube network, this network shows a p-type like semiconductor behaviour.

Each device was manufactured in five steps. Firstly, a microfabrication step in which the basis of the device was assembled. Secondly, a dielectrophoretic deposition step in which the carbon-nanotube network was deposited. Thirdly, a functionalization step in which a specific antibody is adsorbed on to the carbon-nanotubes. Fourthly, *E. coli* bacteria from the string DH5α were applied in different but known concentrations to different devices. Lastly, the characterization of these devices was done by obtaining the Id-Vd and Id-Vg curves of the field-effect-transistors using a semiconductor parameter analyser.

After the data was collected and analysed a calibration curve was obtained, capable of correlating the drain-current of the transistor with the *E. coli* concentration, this curve is essential to the proper working of the point-of-care device.

This study overviews the principles of working of the single walled carbon-nanotube field-effect-transistors as well as methods to improve their reproducibility of results. The point-of-care device is a rudimentary picoameter, capable of reading the devices drain-currents (pA), this picoameter is connected to a computer via an Arduino board and a MATLAB software.

Keywords: SWCNT, FET, CNT-FET, *E. coli*, Schottky Barriers, Direct charge transfer, CNT dispersions, dielectrophoretic deposition of CNTs.

Glossary

CNT-FET……..Carbon Nanotube Field-Effect-Transistor

FET……..Field-Effect-Transistor

Id-Vd……Drain-current vs Source-Drain Voltage curve

Id-Vg……..Drain-current vs Gate Voltage curve

MWCNT……Multi-Wall Carbon Nanotube

SB……..Schottky Barriers

SWCNT……..Single Wall Carbon Nanotube

UFC……..Colony Forming Units

|ΔI|……..Absolute Value for Drain current variation

Contents

Chapter 1

Introduction

The microbiological quality of water is a concern to consumers, water suppliers, regulators and public health authorities. The potential of water to transport microbial pathogens to great numbers of people, causing subsequent illness, is well documented in countries at all levels of economic development (1,2). Of course, water-associated diseases in developing countries are prevalent and, according to the World Health Organization (WHO), are amongst the world's major causes of preventable morbidity and mortality. Nevertheless waterborne diseases also present a great challenge in developed countries, for instance, the outbreak of cryptosporidiosis in 1993 in Milwaukee, Wisconsin (3), in the United States provides a good example. It is suspected that a major water purification plant was contaminated with Cryptosporidium, due to oocysts passing through the filtration system without being properly filtered. It was estimated that about 400 000 individuals suffered from gastrointestinal symptoms due, in a large proportion of cases, to this protozoan parasite. More recent outbreaks have involved E. coli O157:H7, the most serious of which occurred in Walkerton, Ontario Canada in the spring of 2000 (4), which resulted in six deaths and over 2 300 cases. In this study I will present a way to fabricate and calibrate a point of care bio sensor capable of detecting E. coli bacteria in water. The bio sensor is a carbon nanotube field effect transistor, none-the-less, in order interpret the values given by the sensor a device capable of correlating current values to bacterial concentration will be engineered. This study will serve has a proof of concept in order to prove that it is possible to quickly assess water quality. Over the past decade, electrical detection of biological species using novel nanostructure-based devices has attracted significant attention for chemical, genomics, biomedical diagnostics, and environmental applications (5). The use of nanostructured devices in biological sensors in place of conventional sensing technologies has advantages of high sensitivity, low energy consumption and potentially highly miniaturized integration.

A biological sensor can be defined as a device that responds to changes in its environment and converts this response into a signal that can be read. As for the basic characteristics of an useful sensor, its response should be predictable so that it scales with the magnitude of changes in the biological environment (6).

Along with the evolution of nanotechnology over the past years, came great progress in our fundamen-

tal understanding of the physical and chemical properties of nanomaterials as well as their synthesis process. This has stimulated interest in the incorporation of these novel materials into new sensor architectures. There are nanomaterials which are composed of one-dimensional nanostructures, meaning that at least one of their three dimensions is in the nanometers range, materials such as nanotubes and graphene sheets are one-dimensional nanostructures and seem to be ideal candidates for the development of new miniaturized chemical and biological sensors. Carbon nanostructures including CNTs and graphene are central materials in nanoscience (5). Their unique electrical, physical, mechanical and chemical properties are widely studied so as to develop high performance devices, in fact, ever since the discovery of the CNTs in 1991, they have quickly become a global research activity. It is well known that these materials present electrical properties that are very keen to be affected by exposure to biomolecules, this has led to the investigation of these materials as sensing elements for bio sensors, by a number of groups. The high surface-to-volume ratio of the CNT makes it possible to obtain very fast response times enabling the detection of biological species at low concentrations, this being said, CNT-based bio sensors are recognized to be a next generation building block for ultra-sensitive bio-sensing systems (7,8). Figure 1 gives the number of papers referring to CNT based bio sensors between 2000 and 2014. It is clear that the study of this type of bio sensors had a great acceptance from the scientific community, and one can see that after 2007 there was a very significant increment in the number of papers published regarding this issue, meaning that CNT based bio sensors is still a very young field of research.

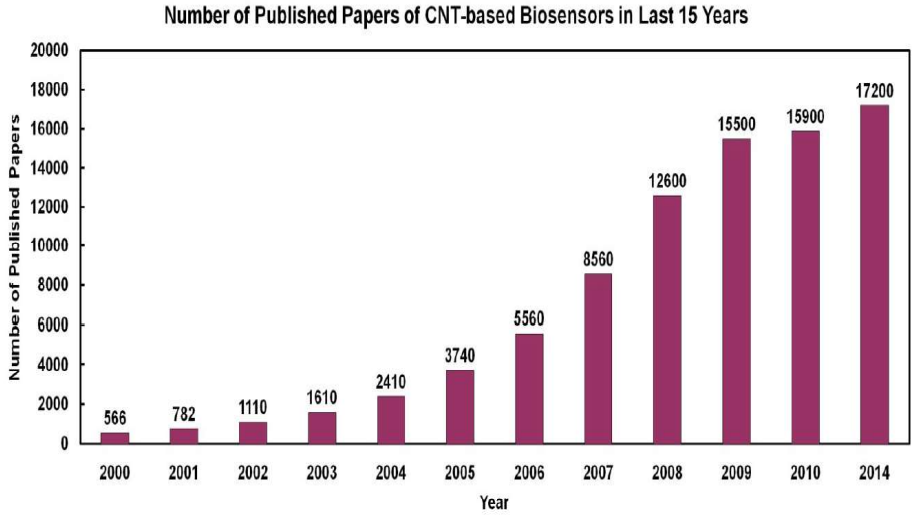

Figure 1 – Number of published scientific papers referring to CNT-based Bio sensors from 2000-20014.(6)

Current applications of CNT based bio sensor are immense, none-the-less, CNT field-effect-transistors are the ones that hold the greater promise in future years. Presently CNT-FET's are being used for gas-sensing, biological detection and miniaturized transistors for electronic device implementation. There is however a great difference between the three main applications of this type of transistor. For an electronic approach the objective is to use a single semiconducting carbon nanotube to create the transistor, this makes the fabrication process extremely difficult and expensive. In the other applications of these FET's, such as gas sensing and biological detection, a CNT network composed mainly of semiconduct-

ing CNT's is deposited in between the electrodes, this allows for an inexpensive device construction while sustaining a very solid and highly responsive platform. In fact, there are many reports of biological and gas detection using these types of sensors, Zhang et al. (9) in 2012 used a CNT-FET to assess water quality by detecting a very dangerous bacteria strain, E. coli O157 : H7. NASA is currently using these sensors for the detection of flammable gases for the petrochemical industry, quality control by the chemical industry, methane detection for the mine safety industry, environmental monitoring of toxic industrial gases and biomedical monitoring of gases in a patient breath (10). A common CNT-FET bio sensor includes the structure of a three-electrode transistor. The drain and source electrodes are interdigitated and are connected by a semiconductor channel, which in this case is a carbon nanotube random network, furthermore the gate electrode modulates conductance of this channel (11–13). The structure of a typical CNT-FET device is illustrated in Figure 2.

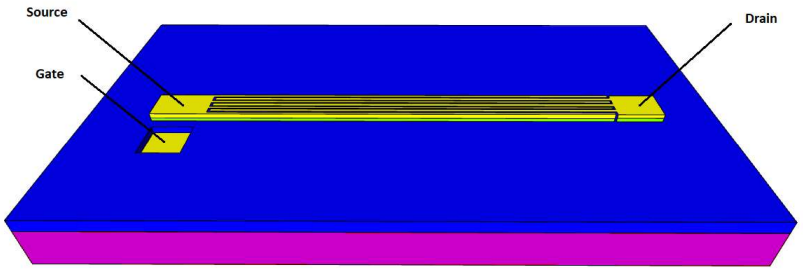

Figure 2 – Picture illustrating a back-gated CNT-FET for bio sensing application. In between the two interdigitated electrodes (Source and Drain) lies a network CNT's. The square pad is the gate electrode which connects to the Si layer below in order to apply the gate voltage through-out the channel. The FETs used in this study were provided by INESC-MN and have the same appearance as the one shown.

Since semiconducting SWCNTs are p-type under ambient conditions electron-donating, electron-accepting molecules or even whole cells interact with SWNTs resulting in charge-carrier recombination within the nanotube (7,12,14). This will cause a change in conductance and a shift in the transfers curves (Id - Vg) and (Id-Vd).

Knowing that currently the detection of biological and chemical compounds relies strongly in optical detection, mainly fluorescently-labeled biomolecules with dyes or quantum dots, and, that these artificial labelling methodologies are time-consuming, cost-intensive, and the introduction of labels weakens the interaction between receptor and target. The development of a fully electronic label free sensing device should be the future of biosensing.

CNT-FET bio sensors with different abilities and characteristics have been developed for biological applications. In the early stages of these sensors they were made directly from pristine CNTs, however, as the research developed some shortcomings of the pristine SWCNTs started to appear. The main problem was that the sensors usually showed a low sensitivity to the analytes this was due to, either, low adsorption from the analytes or low selectivity from the CNTs. To overcome the above shortcomings, many efforts have been made to modify CNTs, one of the strategies used to improve the sensing performance of the FETs was by functionalizing them with antibodies (11,15). In here I will focus mainly

in immunologically functionalized CNT-FETs. Immunologically functionalized CNT-FETs are bio sensors that possess, adsorbed to their carbon nanotube network, an antibody that binds to a specific biomolecule or particle. The premise behind the workings of these functionalized CNT-FETs is the same of the pristine CNT-FETs. When the transistor is in its operating point, a certain voltage is applied in the gate electrode and a bias voltage is applied between source and drain, due to this bias potential a current is induced to flow between the source and drain electrodes, usually this current is in the order of pico-amperes, when a given molecule sustains a physical contact with the CNT network or near the CNT/metal contact there is a variation of charge carrier density within the CNT network, this results in a shift of the current flowing between source and drain, this shift can be detected only if the variation is big enough to be detected by the apparatus used to interpret the signal. The only difference is that in this case, with antibody immobilization, there are no problems with adsorption of the analyte onto the CNT network because the antibody works has a receptor, this, as stated before, increases both the selectivity and sensitivity of the sensor.

Two different sensing mechanisms have been proposed in literature. The first one suggests that the charge transfer between the SWCNT/antibody complex and the analyte molecules that connect to this complex results in a change of the charge carrier density in the CNT network, due to direct charge transfer, and thus channel conductance change (12,16). The second mechanism resorts to the modification of the Schottky Barriers (SB) at the CNT/metal contacts due to the adsorption of molecules on the premises of these metal/semiconductor contacts (12,17,18). Depending on the specific analyte and the contact material, reports vary on which effect dominates.

1.1 Work Outline and Objectives

This thesis has the overall objective of optimizing a bio sensor capable of analysing water samples in terms of *E. coli* concentration. Accompanied with this bio sensor a point-of-care device capable of measuring the bio sensor results will also be fabricated. This study was done in collaboration with INESC-MN, Universidade de Aveiro and Instituto Superior Técnico. The FET chips and the antibody were provided by INESC-MN, the CNTs and surfactant were provided by the CESAM department at Universidade de Aveiro and the *E. coli* cells were provided by the IBB department at Instituto Superior Técnico.

1.1.1 Work Outline

This study can be divided into three steps. Studying the workings of a CNT-FET, this is, the principles behind the *E. coli* detection of these bio sensors. Sensor characterization, in here one will test the fabricated devices with multiple concentrations of *E.coli* with the intent of obtaining a calibration curve that correlates *E. coli* concentration with the current flowing on the bio sensors. Finally fabricating a point-of-care device capable of reading the bio sensors current-flow, import the analog values to a

personal computer and use the previously obtained calibration curve to assess the *E. coli* concentration present in the water sample.

1.1.2 Objectives

The major objectives to be achieved in this study are the following. In order for the sensors to work at their best potential one needs to improve their reproducibility of results, since the major factor for poor reproducibility from one CNT-FET to another is the CNT network in between the source and drain electrodes, one of the main objectives is to devise a strategy that allows for all CNT-FETs to work in the same range of values, this, in order to obtain a good calibration curve, for further implementation in the point-of-care device, ideally this calibration curve should show an almost linear behavior. Another objective is to understand the minimum threshold of detection for these devices. The final objective of this study is to fabricate a device capable of amplifying and reading the currents at which the CNT-FETs operate.

Chapter 2

Principles of Working

2.1 Semiconducting CNTs

CNTs can be thought of as the seamless hollow tubes obtained by rolling graphene sheets. According to the number of layers of graphene, the CNTs can be divided into two groups, multi-walled carbon nanotubes (MWCNTs) and single-walled carbon nanotubes (SWCNTs) (19) as shown in Figure 3a and Figure 3b respectively.

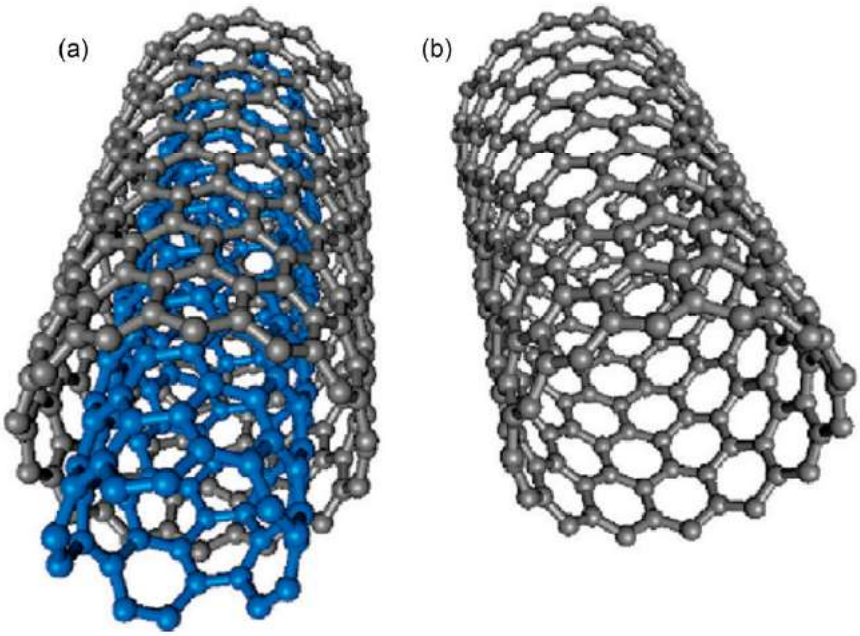

Figure 3 – Structure representations of (a) a MWCNT and (b) a SWCNT (6).

In general, SWCNTs are one-dimensional nanomaterials with a diameter in the range of 0.75nm to 3nm and a length of around 50 μm. Because MWCNTs are composed of more than two layers of graphene sheets, their diameter is bigger than the SWCNTs and it usually ranges from 2nm to 30nm with some MWCNT reaching even more than l00 nm, the distance between each layer is approximately 0.42 nm (overlapping of the electronic clouds) (6). Since in this study only SWCNT were used we will focus only on this group of carbon nanotubes.

As stated before carbon nanotubes can be seen as hollow tubes obtained by rolling up graphene sheets, although the synthesis of CNTs is not done like this, this allows us to have a better understanding of the CNTs properties and what structural differences give rise to such properties. For instance, the deformation of the hexagonal graphene lattice as shown in Figure 4 is useful to describe what differences give rise to which properties. The vector from A to A', which is called the chiral vector Ĉh and can be described by Equation 1, is a fundamental part of understanding the different types of SWCNTs.

$$Ch = na_1 + ma_2$$

Where Ĉh is a linear combination of the lattice basis vectors, ā1 and ā2 which correspond to the C-C bond length (0.12nm to 0.15nm), n and m are positive integers which are known as the chiral indices. In the process of rolling up the graphene sheet, once the integers n and m are affirmed the carbon atom A overlaps the carbon atom A', thus forming the carbon nanotube Figure 4. According to the different directions of winding, meaning different chiral vectors, SWCNTs are divided into three different types of structure: armchair type, zigzag type and chiral type, Figure 5. The structure types of CNTs are related to their chiral indices (n, m) and the spiral angle θ, which is the angle between the chiral vector and the a_1 unity vector. When n = m, the spiral angle θ is equal to $30°$, the type of CNT is called armchair. When m = 0, $\theta = 0°$ the type of CNT is called zigzag. When θ is different than $0°$ or $30°$ the type of CNT is called chiral. The electrical properties of SWCNTs strongly depend on their diameter and on their chiral indices. For instance, the nanotube diameter is inversely proportional to its energy gap, if this nanotube is a semiconductor (6,19–21).

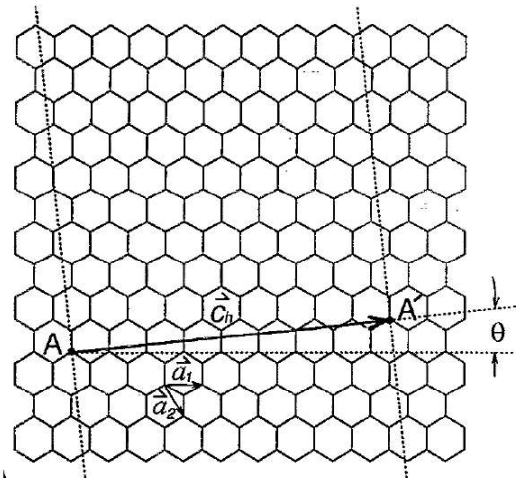

Figure 4 - The chiral vector AA' or Ch = na1 + ma2 is defined on the honeycomb lattice of carbon atoms by unit vectors a1 and a2 and the chiral angle θ with respect to the zigzag axis (21).

The chiral indices "n" and "m" dictate if the nanotube is metallic or semiconductor. For a SWCNT to be semiconductor the chiral indices of their chiral vector need to respect a simple relation given by Equation 2, (6,19–21).

$$n - m = 3r$$

Where r is an integer, therefore, whenever (n – m) is multiple of 3 the carbon nanotube is metallic. This is exemplified in Figure 5.

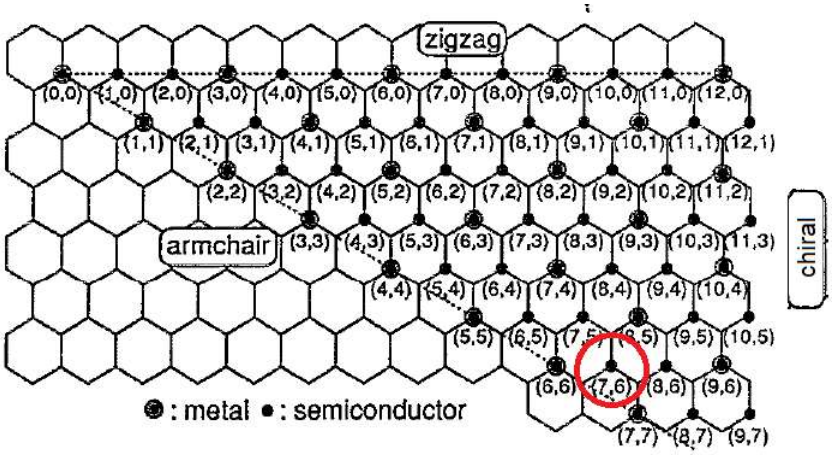

Figure 5 - Possible vectors specified by the pairs of integers (n, m) for general carbon tubules, including zigzag, armchair, and chiral tubules. The encircled dots denote metallic tubules while the small dots are for semiconducting tubules (21). The red circle corresponds to the SWCNT used in this study.

In this study the Carbon nanotubes used were provided by Prof. Teresa Santos group at the University of Aveiro, they were obtained from Sigma-Aldrich and were composed of 77% semiconducting carbon nanotubes with (7, 6) as chiral indices, Figure 5 (red circle) and Figure 6, having therefore a diameter of 0.7nm to 1.1nm, using Pitagoras $\sqrt{(0.12 * 6)^2 + (0.12 * 7)^2} = 1.1nm$. This is crucial as the sensor can only work if the CNT network deposited between Source and Drain is composed mainly of semiconducting CNTs.

Product Specification

Product Name:
carbon nanotube, single-walled - (7,6) chirality, carbon > 90%, 77%(carbon as SWNT), 0.7-1.1 nm diameter

Product Number: **704121**
CAS Number: 308068-56-6

Figure 6 – SWCNTs from Sigma Aldrich product specification datasheet (22)

2.2 CNT-FETs

As stated before carbon nanotube field effect transistors have the typical structure display of a three-electrode transistor. The drain and source electrodes are connected by the semiconductor channel, which in this case is a carbon nanotube random network, furthermore the gate electrode modulates

conductance of this channel (11,12,19). There is not yet a consensus about the primary method of conductance change within the channel, two different mechanisms to modulate the current within the channel have been proposed in literature (12,23,24) their main difference is related with the region of the device where the analyte adsorbs. The first one suggests that there is a charge transfer between the SWCNTs and the analyte molecules that adsorb on the SWCNTs surface, which then gives rise to a change in charge carrier density, thus leading to, channel conductance change. The second mechanism resorts to the modification of the Schottky Barriers (SB) at the CNT/metal contacts due to the adsorption of molecules on both the metal or the SWCNT. Depending on the quantity of analyte adsorbed onto the channel or near the metal-SWCNT contacts, conductance change, can be due mainly to charge transfer or Schottky barrier modification Figure 7.

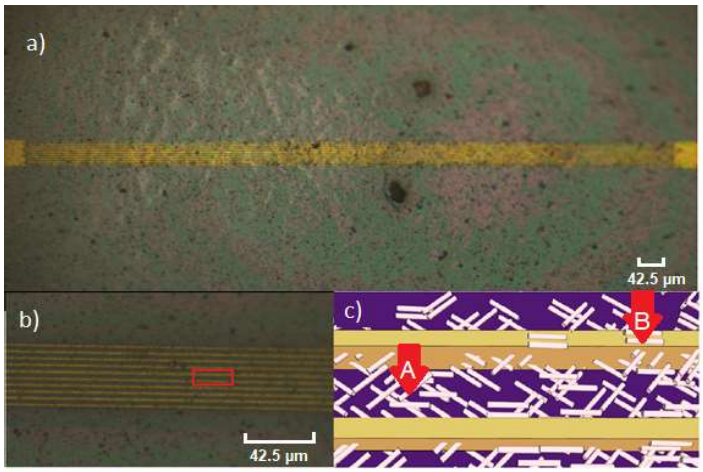

Figure 7 – a) Optical microscopy view (50x amplification) of the CNTFET interdigitated electrodes with the CNTs deposited on top. b) Optical microscopy view (1000x amplification) of the middle section of the electrodes. c) illustration depicting the possible analyte adsorption areas, in adsorption area "A" the effect that gives rise to the conductance change in the CNT channel is Charge transfer, in adsorption area "B" the effect that gives rise to the conductance change in the CNT channel is Schottky barrier modification. The CNT-FETs showed here were provided by INESC-MN.

When exposed to oxygen semiconducting SWCNTs begin to behave as p-type semiconductors with holes as main charge carriers (5,12,14,25). Given this fact, most CNT-FETs exposed to air show p-type behaviour but become more ambipolar in vacuum. Such doping effect can take place during the synthesis and handling of nanotubes or by oxygen adsorption on the CNT surface when exposed to air. This mechanism has been demonstrated when removing oxygen from a CNT-FET by annealing in vacuum. The transfer characteristics of the device gradually change from p-type to ambipolar as the oxygen was removed (12). This is crucial to explain how the sensors work in terms of conductance channel in the presence of the analyte.

2.2.1 Schottky barrier modification

A simplistic way of describing the current flow change in the nanotube due to Schottky barrier modification, starts by matching the valence band of the nanotube with the Fermi energy (Ef) of the contact

metal electrodes, since the SWCNT are p-type a depletion zone is created, this depletion zone otherwise known as Schottky Barrier can be modulated by a gate voltage, Figure 8, allowing or prohibiting the current flow. However, the electric field generated by the gate voltage which is needed to control the current flow through the CNT-network can easily be perturbed locally, this perturbation can occur by adsorption of molecules near the contacts ,Figure 7c adsorption area "B", which changes the applied electric field to the Schottky Barrier Figure 8.

Schottky Barriers are generally formed when a semiconductor is brought into direct contact with a metal due to the mismatch of the work functions of the metal and the CNT (12,18,26). A charge transfer occurs at the interface which results in the bending of the conduction and valence bands. Such bending generates a charge depletion (potential barrier) that opposes further charge transfer. There are two of such Barriers, one at the source electrode and another at the drain electrode and they can dominate the transport characteristics of the CNT network.

The thickness (SB_w) and height (SB_h), Figure 8, of such barrier can be increased or decreased with the electric field provided by the gate electrode, thus, modulating the current flow either of holes or electrons. Mechanisms based on tunneling processes and hence on the thickness of the barrier are more important at the CNT/metal contact interface than the ones depending on temperature which are more dependent on the height of the barrier. Therefore, when the Schottky barrier becomes thinner, tunneling effect of the charge carriers can favor the current flow in the CNT-FET (12,17,27,28). This is described by the Id-Vg curves for different Source-Drain voltages of the device where one can clearly see a change in drain current as a function of a change in the gate electrode voltage thus the electric field created near the contacts Figure 9.

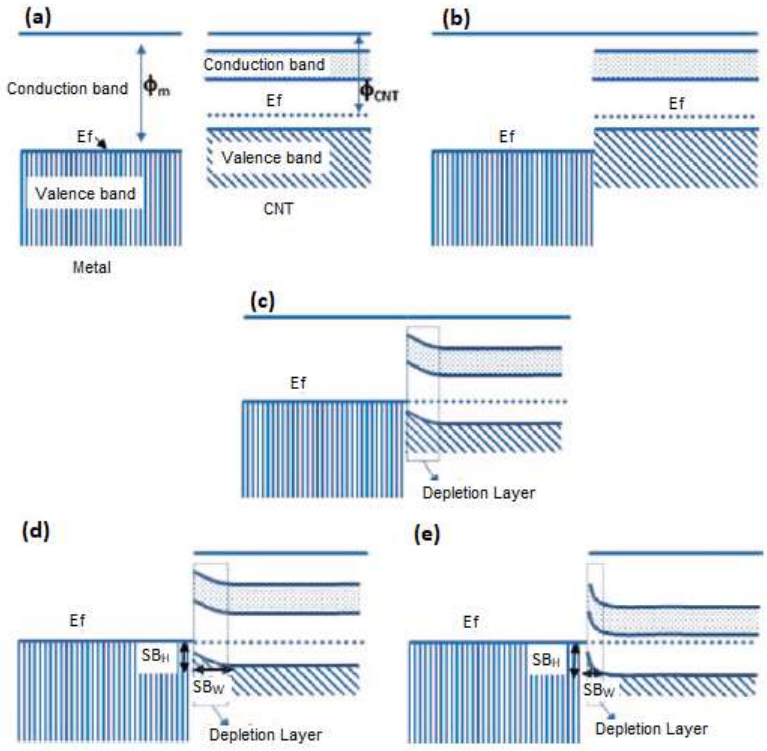

Figure 8 - Scheme illustrating the formation of Schottky barriers (SB). In (a) the band diagrams for the metal contact and for a semiconducting p-type nanotube are shown. The metal has a higher work function or barrier height (φ) than the CNT. The CNT has been schematized as a p-type since oxygen from the environment can dope the CNT with holes. In this case, the Fermi level of the CNT is close to the valence band. When the CNT and the metal contact are brought together (b), the Fermi level of both materials will try to equilibrate by flowing charge carriers between them (c). That results in a bending of the bands forming a depletion layer which gives place to the generation of Schottky barriers that inhibit the charge carrier transport. However, the height (SB_h) and thickness (SB_w) of the barrier can be changed with the gate voltage. In (d, e) the height and the thickness of the barrier height are indicated. It also shows how the thickness of the tunnelling barrier can be decreased with the gate voltage (12).

In Figure 9 one can see the Id-Vg curves of four pristine CNT-FETs. These curves are shown in order to understand how the gate voltage affects drain-current. Since in Figure 9 the CNT-FETs used were pristine which means that the channel had no molecule adsorbed. The change in drain current is only due to Schottky Barrier modulation as a function of the applied gate voltage. One can see that with a change with gate voltage from -5V to 5V the drain-current of the CNT-FETs decreases thus a thickening of the Schottky Barrier occurs.

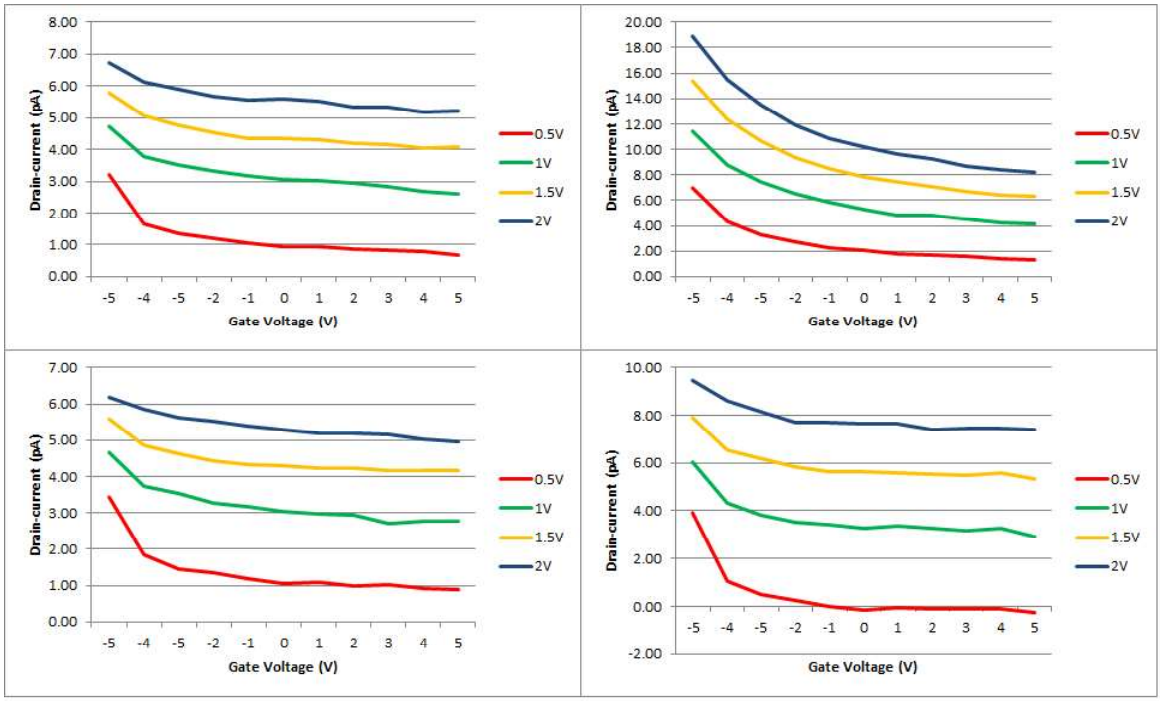

Figure 9 – Id-Vg Curves of four pristine CNT-FETs measured using Agilent 4155C (semiconductor parameter analyzer)at the University of Aveiro. Each of the coloured lines corresponds to a different Source-Drain bias voltage.

When a certain molecule adsorbs near the metal-semiconductor contact, Figure 7c adsorption area "B", where the Schottky barriers form, a change in channel conductance occurs, this can be due to two different phenomena. Firstly, the work function of metals is known to change when molecules are adsorbed on the surface (24,28,29). A change in the metals work function means a different alignment of the Fermi levels between the semiconducting SWCNT and the electrodes, this different alignment means that the Schottky barriers width and height are different, thus creating an influence in the tunnelling of charges, therefore allowing or prohibiting their passage through the barriers (30). Evidence suggests that there is a linear relation between the metals work function and surface coverage for certain molecules (19,28). The other process suggest that a surface dipole layer forms on the metal and CNT-network surfaces due to the applied electric field of the gate voltage. Any adsorption of molecules to these surfaces causes a disruption in this dipole layer (12,18,19), this dipole layer disruption locally influences the applied electric field created by the gate voltage which modulated the current flow. A change in this electric field near the CNT/metal contacts inherently carries a change in the Schottky barriers width resulting in a channel conductance change. In Figure 10 one can see how the molecule adsorption influences the dipole layer and the sensed electric field at the CNT/metal contacts.

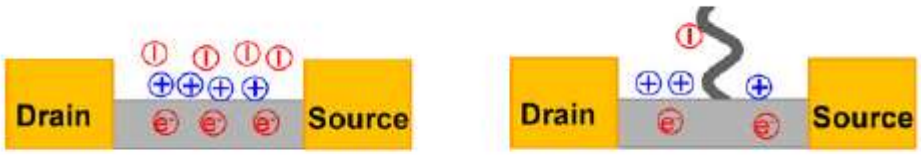

Figure 10 – How a dipole layer can be disrupted influencing the sensed field in the CNT-FET channel or near of the CNT/metal contacts, depending on the place of adsorption (31).

In Figure 11 one can see how the molecule adsorption changes the Schottky barriers which are modulated by the gate electrode. The adsorption of molecules influences the range of drain-current values which the gate voltage is able to modulate.

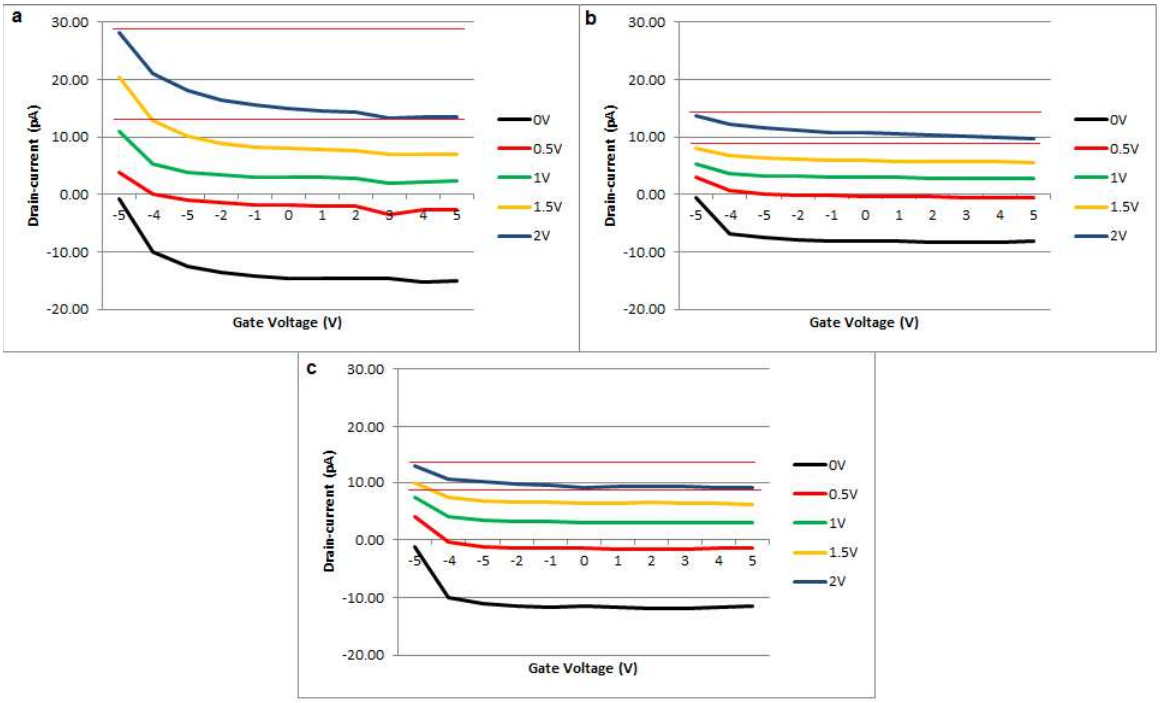

Figure 11 – Id- Vg Curves of the same CNT-FET obtained using Agilent 4155C (semiconductor parameter analyzer)at the University of Aveiro. a) Pristine CNT network. b) CNT network with antibody adsorbed. c) CNT network with antibody and analyte adsorbed. One can clearly see how molecule adsorption near the contacts influences the Schottky barriers, in a) the gate voltage modulates a drain current range of around 20pA, in b) after antibody adsorption the gate voltage modulates a drain current range around 5pA, in c) gate voltage modulates and drain current range lower than 5pA. The adsorption of molecules on the surface near the Metal/semiconducting CNT influences the formation of Schottky barriers and restricts the range of Drain current values that the gate voltage can modulate. Schottky Barrier modulation range is shown in between the parallel red lines.

2.2.2 Direct charge transfer to CNT network

Doping of electrons and holes into SWCNTs through molecular charge-transfer is of special interest. Non-covalent bonding offers non-invasive approaches to modify SWCNTs properties (16,25,29). The charge transfer between the SWCNT and adsorbed molecules vary to a large extent depending on the

nature of their interactions (32,33). Certain molecules have been proven to interact weakly with minimal charge transfer to CNTs while others have demonstrated noticeable charge transfer (19). All atoms of single-walled carbon nanotubes (SWNTs) reside at the surface this means that adsorption of electron-withdrawing/donating molecules that change the charge carrier density, can be used to modulate drain currents (16,32,34).

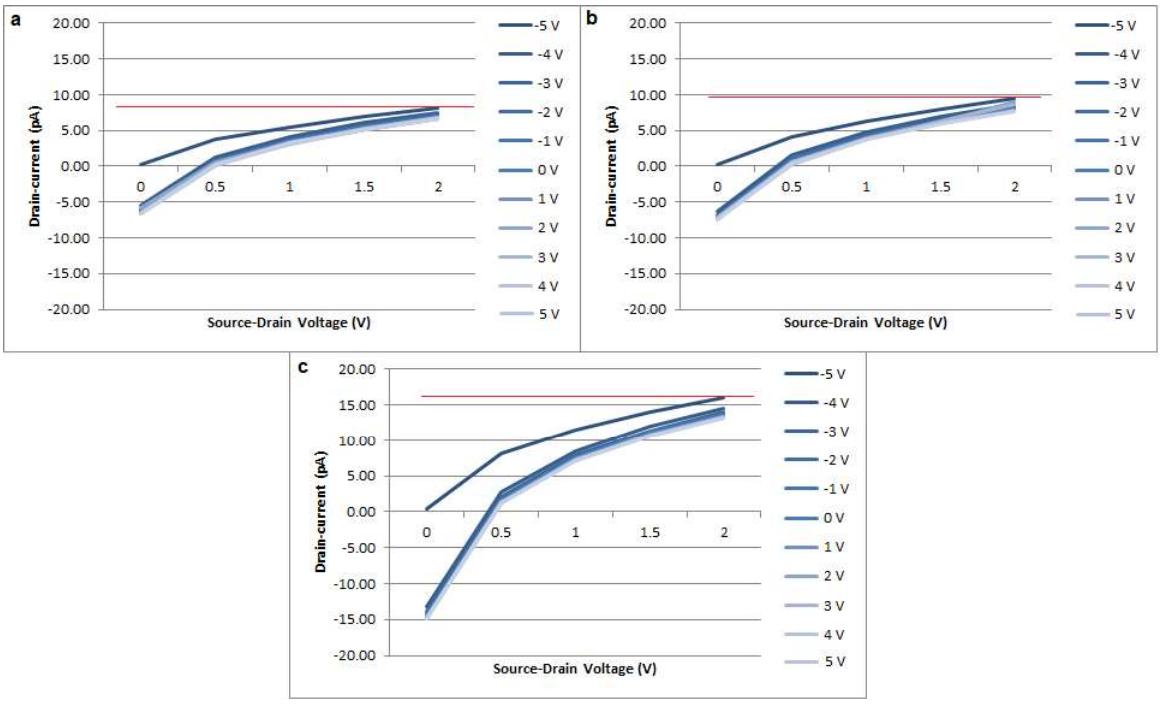

Figure 12 – Id-Vd curves of the same CNT-FET for different gate voltages [-5V, 5V] obtained using Agilent 4155C (semiconductor parameter analyzer)at the University of Aveiro. a) Is the Id-Vd curve for a device fabricated with pristine CNTs. b) Is the Id-Vd curve for a device in which the CNT network as a certain anti-body adsorbed c) Is the Id-Vd curve for a device in which the CNT network as both an anti-body and its analyte adsorbed. The curve shift upon molecule adsorption is shown as the horizontal red line in all three graphs.

In Figure 12 one can see that upon molecule adsorption the Id-Vd curves are shifted, in this case upwards. In p-type semiconducting SWCNTs when an electron-donating molecule adsorbs on the surface a recombination phenomenon occurs (21,29,34), this recombination leads to a decrease in the channel current (Source-Drain current). Also, in p-type semiconducting SWCNTs when an electron-withdrawing molecule adsorbs on the surface, charge carrier density increases, leading to a channel conductance increase. One should bare in mind that, the *E. coli* strain used in this study (DH5α) has a cell wall that might possess both electron-donating and electron withdrawing molecules. The direct charge transfer event can be described by plotting the CNT-FET Id-Vd curves using a pristine SWCNT network versus a SWCNT network with am antibody adsorbed and a SWCNT network with both antibody and analyte adsorbed (16,35), Figure 12. It is clearly seen in Figure 12 that when a certain molecule adsorbs to the CNT network there is a shift in the drain current this shift is proportional to the coverage done by the adsorbed molecule on the CNT network. In the case of Figure 12 the Drain-current increased with adsorption.

2.3 Reminiscent current

Another parameter to take in consideration with this type of sensor is the minimum Drain current, this happens due to the fact that the CNT network that composes the FET channel is a mixture of semiconducting CNT and metallic CNT. While with the use of electrostatic doping effects and Schottky barrier modulation one can control the current flow in the semiconducting CNT, one cannot control the current flow in the metallic CNT, this means that there will always be a reminiscent current inside the CNT-FET channel due to the metallic CNTs, therefore the CNT-FET will never reach an off-state (12), Figure 13.

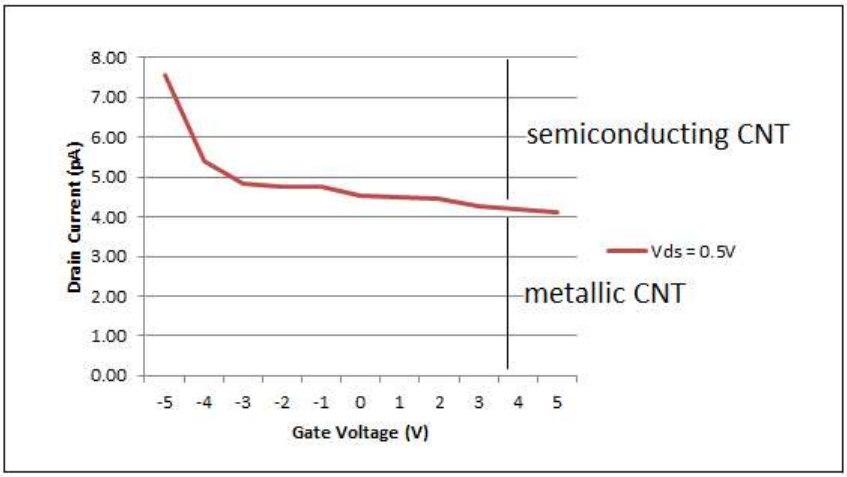

Figure 13 – An Id-Vg curve of a CNT-FET with a bias voltage between source and drain of 0.5V, this plot clearly evidences the effect of the presence of Metallic CNT on the device transfer curve. This was measured using Agilent 4155C (semiconductor parameter analyzer)at the University of Aveiro.

Chapter 3

Device Fabrication

3.1 FETs provided by INESC-MN

The CNT-FETs provided by INESC-MN consisted, as stated before, on a typical three electrode transistor display. There are however several parameters which are important to the workings of this device such as the device dimensions, device display and thickness of the layers used. INESC-MN fabricated a total of 360 FETs, 69 of which were used in this study the remaning FETs were to be used in University of Aveiro by Prof. Teresa Santos group (35). INESC-MN decided the FET design, affirming their dimensions and structure display according to the working principles of the sensors. The overall FET display can be seen in Figure 14 where the elongated pads (blue) are the source and drain electrodes and the square pad (red) is the gate electrode which is connected to the silicon wafer beneath.

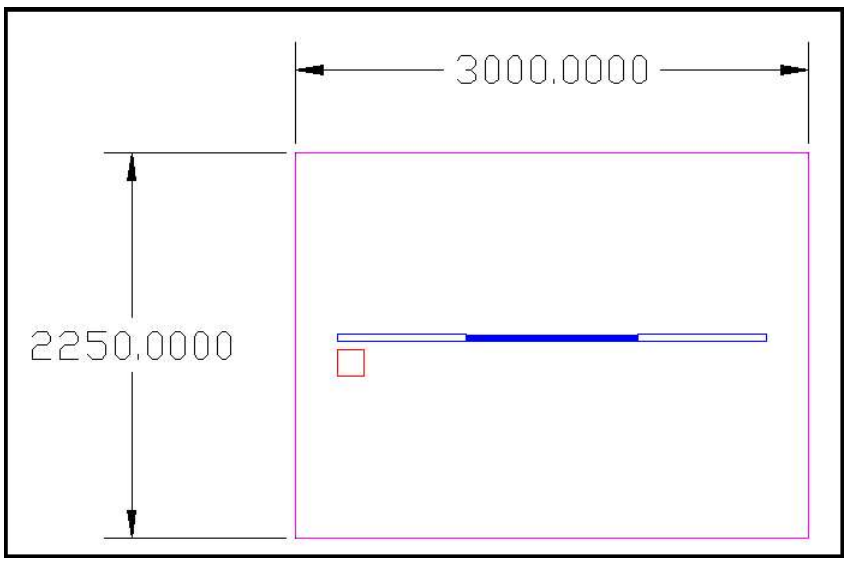

Figure 14 – Building block of the CNT-FET, overall display (μm), mask designed by INESC-MN, (35).

The site of CNT deposition was defined as an area in between 10 interdigitated electrodes as seen in Figure 15. Each branch of the interdigitated electrodes is 1,5 μm in width, 998,5 μm in length and separated by 2,5 μm from the adjacent branches Figure 15. The combination of the branches of each

electrode and the space between them is the effective area of SWCNT deposition. Within this area there will occur chemical doping through electrostatic charge transfer as well as Schottky barrier modulation.

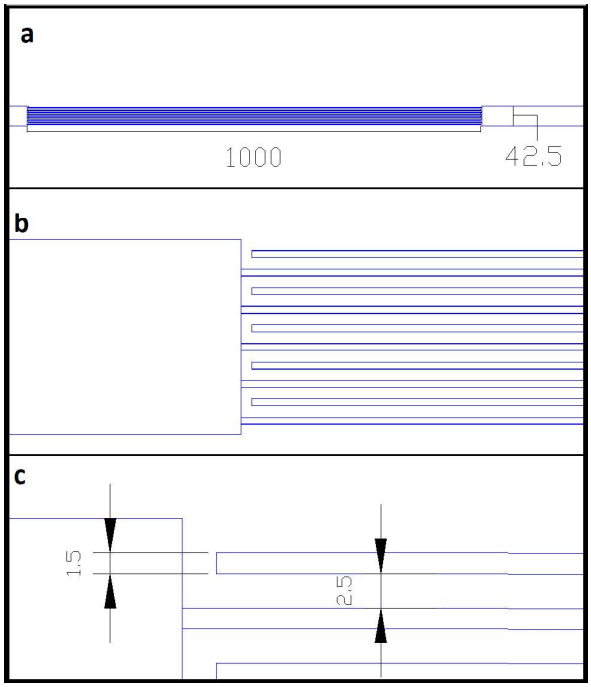

Figure 15 – Dimensions of the building block of the CNT-FET device (μm), a) sensor dimensions, b) interdigitated electrodes, c) electrode dimensions. Mask designed by INESC-MN,(35).

INESC-MN fabricated, on a 3-inch Silicon wafer wafer, a total of 360 FET devices. The layer composition of the FET devices provided by INESC-MN is shown in Figure 16. The first layer (red) is the Silicon wafer. The second layer (blue) is a 4000$\mathring{A}$ Silica layer to serve as an insultor, separating the gate electrode from the source and drain electrodes. The third layer (green) is a 100$\mathring{A}$ Titanium layer to secure the adhesion of the source and drain electrode to the Silica layer. The final layer are the source and drain electrode, which are comprised of 1000$\mathring{A}$ Gold layer. The square structure is a 4000$\mathring{A}$ hole through the Silica layer allowing the Silicon layer (Gate electrode) to be reachable from the top of the device, this perfuration was also filled with an 100$\mathring{A}$ Titanium layer and an 1000$\mathring{A}$ layer of Gold.

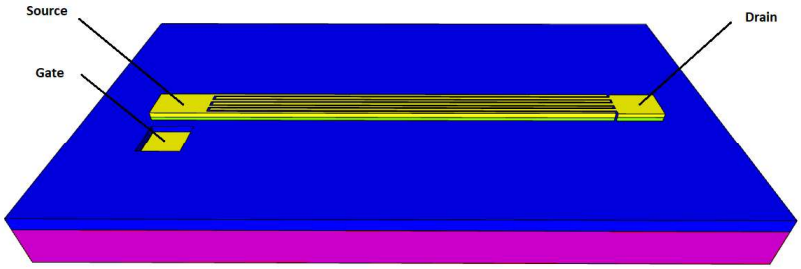

Figure 16 – Final FET device structure and composition. FET devices provided by INESC-MN

3.2 PCB fabrication

The printed circuit boards were manufactured at the Physics Laboratories of Instituto Superior Técnico and served the purpose of allowing an easier connection of the Gate, Source and Drain electrodes, to the sensor characterizing apparatus. Each PCB contains a total of 3 CNT-FETs as illustrated in Figure 17.

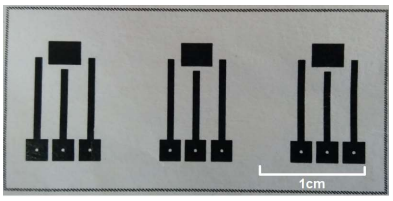

Figure 17 - Schematic of the PCB design with 3 CNT-FET incorporation. The outer pads are both the Source and Drain electrodes whereas the middle pad is the Gate electrode, (25).

The PCB fabrication started with two 200mm x 300mm PCB boards, these boards were cut into four 200mm x 150mm pieces, afterwards, the cut PCB boards were thoroughly cleaned and polished using acetone and Duraglit polisher cloths. The polishing process was done in order to promote the adhesion of the Photoresist spray.
Afterwards a positive Photoresist, (Positive-20 from Kontakt Chemie) was a applied via spraying, immediately after the Photoresist coating the boards were put away in a dark room in the Physics Laboratories of Instituto Superior Técnico to prevent the resist from deteriorating, Figure 18.

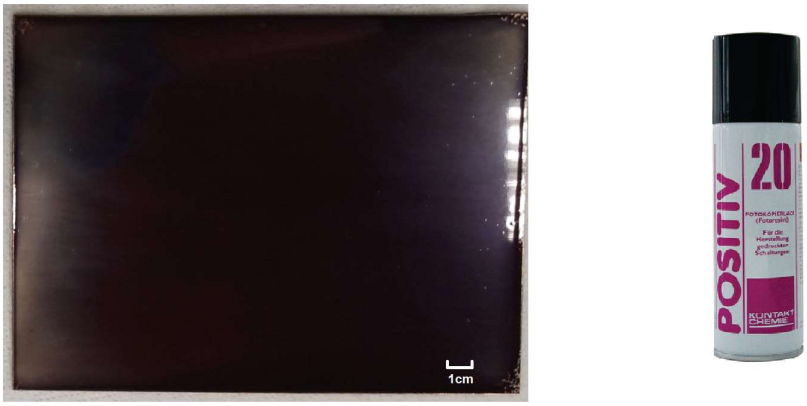

Figure 18 – PCB board after Photoresist coating and dark-room drying.

In order to pattern the PCB display onto the PCB boards a mask was designed. The overall yield of the process was 140 PCBs which was sufficient to mount 360 FETs with an excendent of 20 PCBs accounting for process errors. Due to the method used for Photoresist coating there is an uneven thickness of the resist throughout the board which means some of the PCBs were discarded for irregularities. In Figure 19 one can see the mask design baring 35 PCBs, four PCB boards were patterned using this mask design. Each mask was printed on high quality A4 tracing paper using a laser printer at INESC-MN.

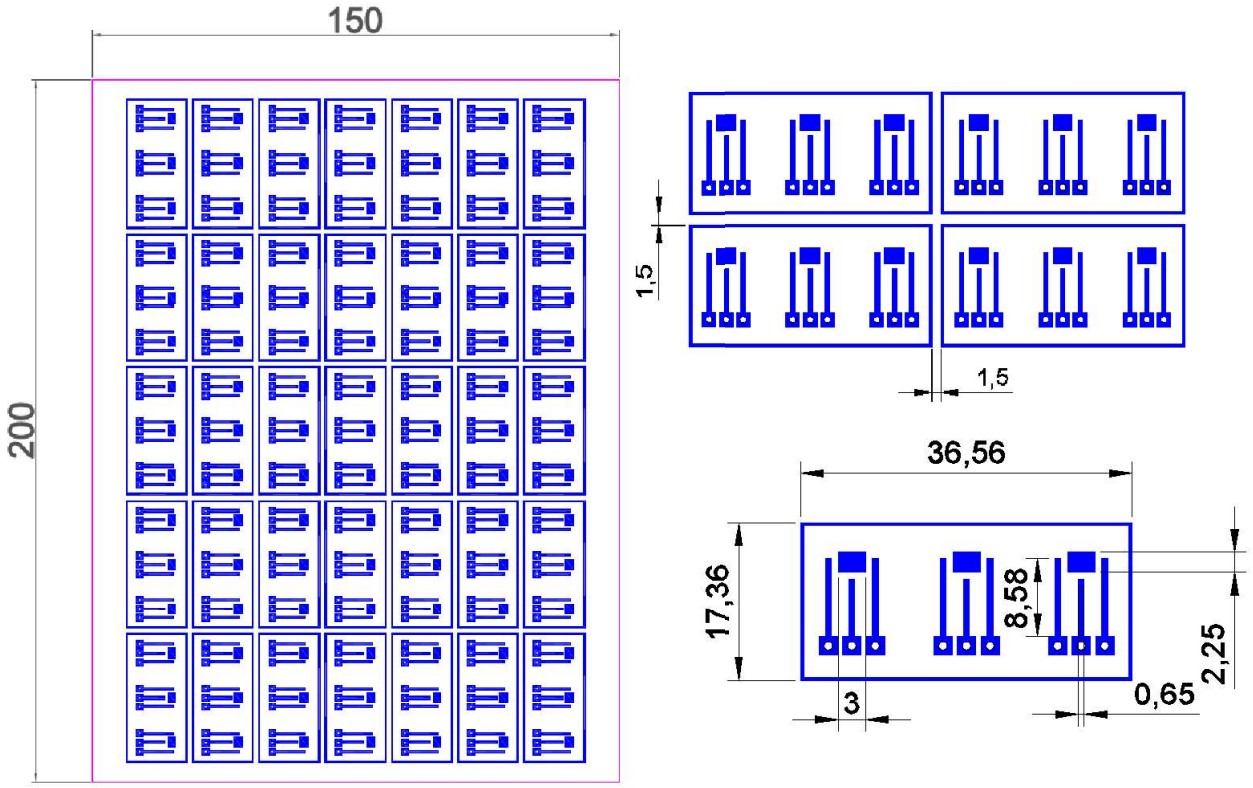

Figure 19 – Hard mask Mask design using AutoCad 2015 (mm). One can see that there is a separation between the PCBs and the edge of the copper board this is because at the edge of the printed circuit boards the Photoresist tends to be much thinner that in the middle and, therefore, more error prone. The separation of the PCBs in between themselves was 1,5 millimeters so that upon cutting there was a sufficient degree of freedom.

Once the masks were printed they were placed on top of the Photoresist coated copper boards and exposed to UV light for a total of 10min at the Physics Laboratories of Instituto Superior Técnico, using a Primelec CI 2645 machine, Figure 20.

Figure 20 – Photoresist coated copper board with hard mask (Left). Primelec CI 2645 machine (Right).

Once the UV light exposure was done the boards were submitted to a development treatment using a, stock undisclosed developing solution, which removed the Photoresist that was exposed to the UV light. Immediately after the resist development the boards were submerged on an Iron Perchlorate solution

and submitted to ultrasounds for 15min Using a MEGAelectronics ultrasound bath machine. After the circuits were printed on the PCB boards one needed to drill the holes in order to weld the pins. This step was done using a Dremel drill with a 1mm drill, at INESC-MN. The small circumference at the end of the pads, Figure 19, was done to facilitate the drilling procedure. Once drilling was done the PCBs were cut into individual pieces using a guillotine, thus finalizing the process of PCB fabrication, Figure 21.

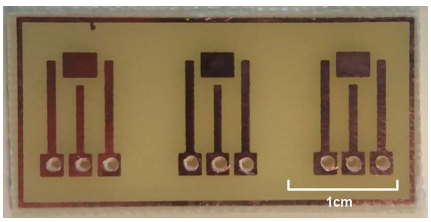

Figure 21 - Finalized PCB, (35).

Once all the PCBs were ready, the ones with the highest level of corrosion were compared with the normal PCBs. This was done to understand if the currents flowing through the copper layers could be different from PCB to PCB, this procedure led to the increasing the overall yield of PCB fabrication, thus allowing to mount all the FETs provided by INESC-MN while ensuring the correct functioning of all the devices. In order to assess this issue a profilometry test was done at INESC-MN in the majority of the PCBs, the average thickness of the cooper layer was around the 40 μm with a typical profile shown in Figure 22 (Left).

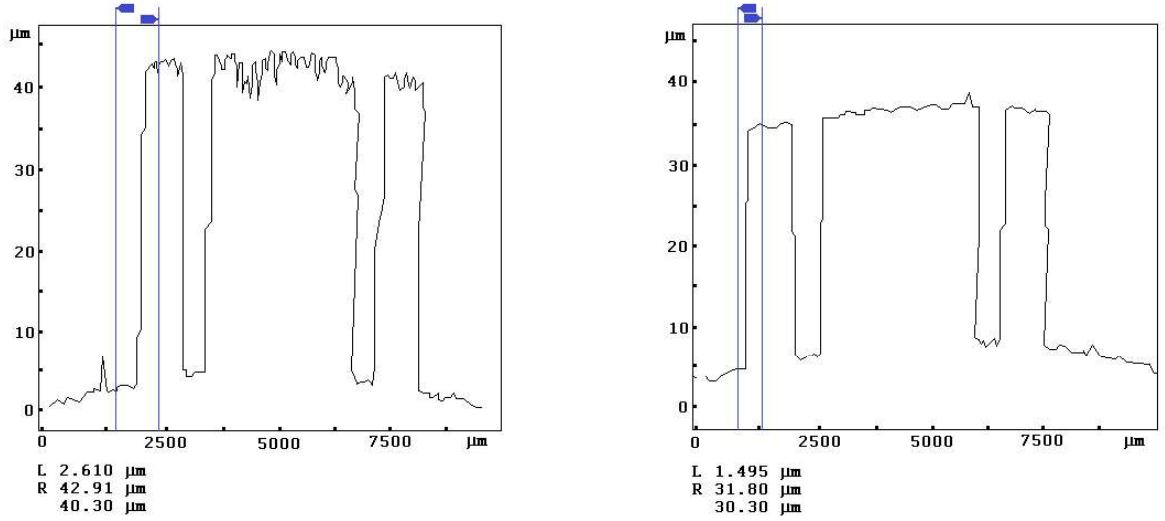

Figure 22 – Profilometry done at INESC-MN. (Left) Average profilometer of the copper layer in the PCBs ($40\mu m$); (Right) lowest measured profilometer of the copper layer in the PCBs.($30\mu m$).

The CNT-FETs completely assembled on the PCBs can be described as the circuit illustrated in Figure 23. Knowing that the copper resistivity for the bulk is around $1.68 * 10^{-8}\Omega/m$, a change of $10\mu m$ in film thickness for the same PCB copper line dimensions (width and length), would account in a 25% resistance change Equation 3, and using the actual dimension values of the PCB one can calculate the resistance in the PCB copper line. Has shown in Figure 19 the copper lines have a width of 0.65mm and the longest line has a length of 8,58mm. Using the resistivity equation, Equation 3.

$$\rho = \frac{\omega * t}{l} * R$$

$$\frac{\rho * l}{\omega} * t_1 R_1 = \frac{\rho * l}{\omega} * t_2 R_2$$

$$R_1 = \frac{30}{40} * R_2$$

$$R_1 = 5.5444 m\Omega \wedge R_2 = 7.392 m\Omega$$

None-the-less this type of circuit due to the poor conductance of the semiconducting CNTs have an average current flow of $10pA$, this means that the average resistance, for the range of bias source-drain voltages applied [0V; 2V], of the semiconducting CNT network is in the order of $200G\Omega$. Considering that the main resistor in in the Figure 23 circuit is a $200G\Omega$ and the other resistor is a variable one that ranges between $5.5m\Omega$ and $7.4m\Omega$. In the overall circuit this change due to the thickness of the copper layer correlates with a shift in current in the order of the $1 * 10^{-20}A$, which is a discriminable value.

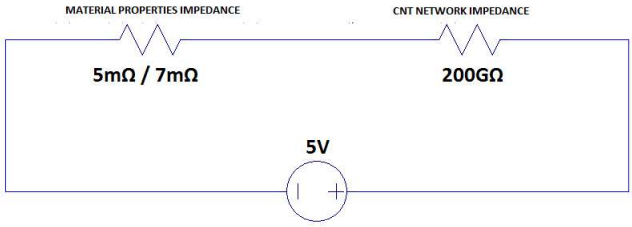

Figure 23 – Circuit illustrating the dominating voltage drop in the CNT-FETs.

3.3 PCBs and CNT-FET assembly

The assembly procedure of the CNT-FET onto the PCBs has the main objective of scaling up the CNT-FETs in order to, afterwards characterize these sensors using the appropriate apparatus.
The assembly itself is an overall simple procedure it can be divided into five steps: Breadboard pin welding, connection verification, gluing each FET device onto a PCB, wirebonding and silicone passivation.

The breadboard pin welding and connection verification was done using standard pins with a distance between pins compatible with that of a breadboard pin holes, the welding was done using a welding iron, solder and soldering paste at INESC-MN. After welding the pins on all the PCBs, each welding point was tested. Using a multimeter in short-circuit mode with one probe on the either the designated Source Drain or Gate pads and the other probe on the respective pin.

The gluing step uses a acrylic glue in order to fix the FET in place in this procedure one used a Loctite Superglue provided by INESC-MN, a small droplet of glue was placed on the big pad of the PCB

seen in Figure 21, afterwards the FET was placed on top of this droplet and aligned with margins of the pad this ensured a simpler wirebonding procedure, as the gate electrode is closer to the middle pad and the source and drain electrode are both closer to the outer pads of the PCB.

The wirebonding was done at INESC-MN using a, KULICKE and SOFFA industries wirebonding machine with a $25\mu m$ tungsten wire, each bond was done in a small loop in order to allow the full coverage of the tungsten wire in the silicone passivation step.

The passivation step was done using Elastoacil Silicone at INESC-MN using a $0.3mm$ blunt needle on a $10mL$ syringe. There are three main objectives with this step: preventing physical damage to the wirebonding, passivation to prevent any leakages currents of the device that could result in a abnormal result and creation of a 2μL well in order to place the water sample droplet to be tested, Figure 24.

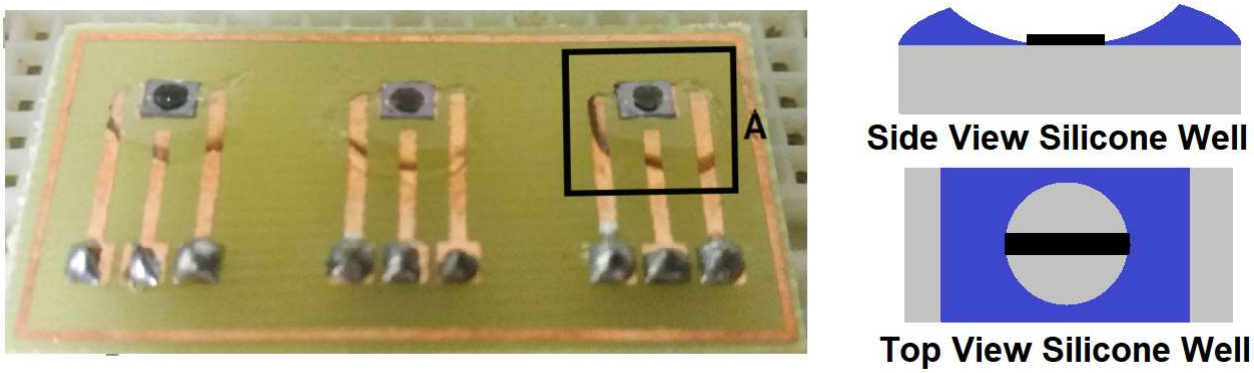

Figure 24 - In the left picture one can see a completely assembled PCB, the (A) square represents the silicone well. In the right picture one can see a schematic of such well.

Once every CNT-FET was completed, the majority of sensors were packaged and sent to University of Aveiro to the CESAM department to serve as a sensing platform for Prof. Teresa Rocha Santos research team (35). For this study 69 fully mounted FET in 23 PCBs were used as sensing platform for *E. coli*, In Figure 25 one can see the fully assembled sensors in their packaging.

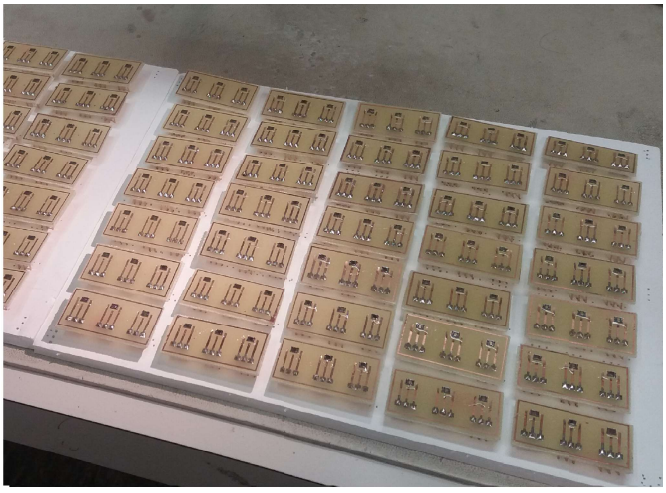

Figure 25 - Fully assembled sensors in their respective packaging.

3.4 CNT dispersions

The main part of every CNT-FET is its channel, in this case the transistor channel is a network of semiconducting carbon nanotubes. Since the chosen deposition method for the CNT network was by dielectrophoresis it is imperative that the CNT are suspended in a solution, therefore a CNT dispersion. The dispersions explained in this section were done at the University of Aveiro, the dispersions are comprised of three components milliQ water, CNTs and sodium cholate (surfactant)(35–38). Both the sodium cholate and the semiconducting CNT were provided by Prof. Teresa Santos team and were aquired from Sigma Aldrich, Figure 26. The CNTs were (7,6) as to their chiral vectors, therefore, semiconducting according to Figure 5, they were 90 % carbon with 77 % of the overall carbon being single wall carbon nanotubes. The sodium cholate($C_{24}H_{40}O_5$) was a standard sodium cholate solution from Sigma Aldrich.

Product Specification

Product Name:
carbon nanotube, single-walled - (7,6) chirality, carbon > 90%, 77%(carbon as SWNT), 0.7-1.1 nm diameter

Product Number:	**704121**
CAS Number:	308068-56-6

Product Specification

Product Name:
Sodium cholate hydrate - BioXtra >99%

Product Number:	**C6445**
CAS Number:	206986-87-0
MDL:	MFCD00150749
Formula:	C24H39NaO5 · xH2O
Formula Weight:	430.55 g/mol

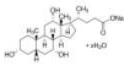

Figure 26 - Sigma Aldrich reagents to produce the SWCNT dispersion for dielectrophoresis deposition (22)(39).

The protocol used to produce the dispersions in question was obtained directly from Sigma Aldrich (37). The process behind debundling the SWCNT occurs due adsorption of the surfactants onto the surface of the CNT, Figure 27, when there is enough surfactant coverage on the CNT surface to permit the separation of an individual nanotube from the bundle the dispersion begins.

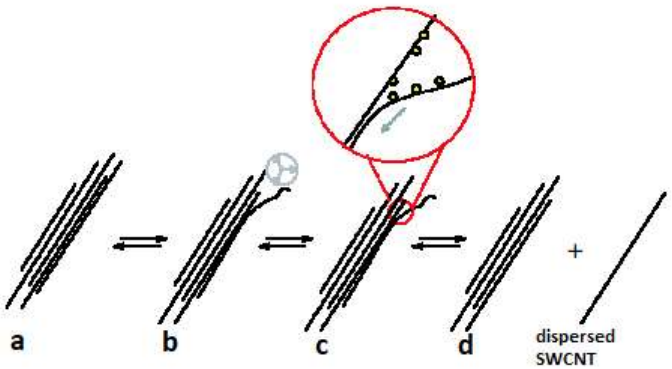

Figure 27 - Illustration of SWCNT debundling mechanism. SWCNT bundle (a), Ultrasonic processing "frays" the bundle end (b), which then becomes a site for additional surfactant adsorption. This latter process continues in an "unzippering" fashion (c) that terminates with the release of an isolated, surfactant-coated nanotube in solution (d).(37)

3.4.1 CNT dispersions methodology

The surfactant solution was done dissolving 100mg of sodium cholate ($C_{24}H_{40}O_5$) in 50mL of Milli-Q water, thus achieving a 0.2 % w/w concentration. Afterwards one weighed $\simeq$ 1-2mg of SWCNT in two different dilution balloons using a high precision scale. The next step was adding to each dilution balloon 14mL of surfactant solution (0,2 % w/w) suspending the previously weighed SWCNT. With the suspensions prepared they were submitted to ultrasounds bath for $\simeq$ 50min at 40 C$^\circ$ until the mixture sustained a black opaque like resemblance (40,37). Once the dispersions were done they were retrieved from their respective dilution balloons and placed into two 7mL Falcons per dilution balloon, therefore 4 Falcons in total, each Falcon contained 4mL of solution. The falcons were then centrifuged in a laboratory centrifuge machine at 2000Gs for 7min in order to precipitate the persistent SWCNT bundles. From each 4mL Falcon four 1mL flasks were filled, yielding a total of 8 flasks. The dispersions were characterized by UV-vis also at University of Aveiro and dilutions were made accordingly.

Chapter 4

Characterization and Results

4.1 UV-vis Characterization

UV-vis characterization was done at University of Aveiro. UV-vis can be used to determine the quality of the CNT dispersion (22,37,38,41), according to the degree of dispersed SWCNT the absorption curves will show higher peaks or lower peaks. In Figure 28 one can clearly see how the peak intensity decreases with the dilution degree of the dispersions. Since we are using these SWCNT dispersions to deposit a semiconducting channel for a CNT-FET device, it is important that the dispersions contain only trace amounts of metallic-SWCNT this ensures a small reminiscent current and an overall small current flow through the channel thus allowing for the detection of smaller concentrations of analytes because the change created by their adsorption on the channel is in the same order of magnitude as the current flow.

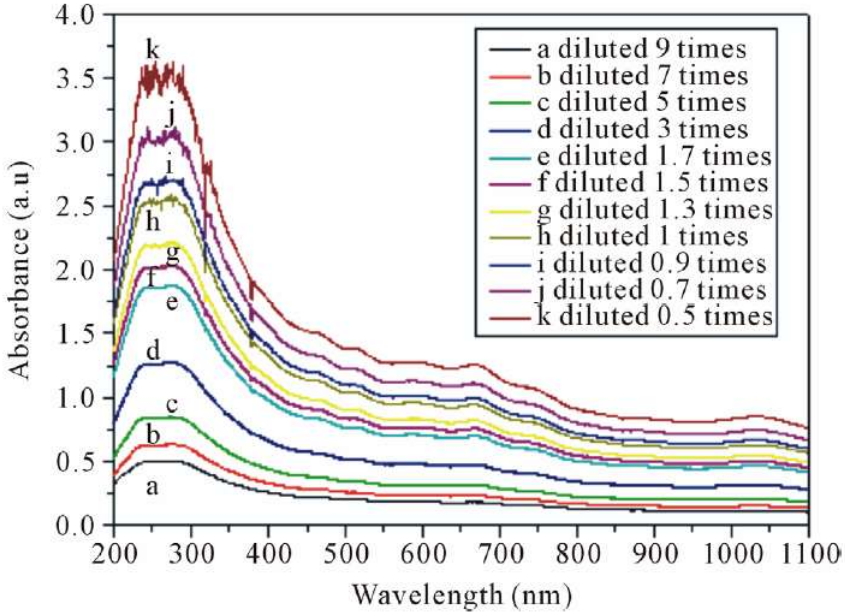

Figure 28 - Absorption curves of Different SWCNT dispersions obtained by dilution of an initial SWCNT dispersion (38).

After analysing the dispersions via UV-vis a typical curve was obtained, Figure 30, the λ range used in this test was between 200 and 600 nm which is the range where the metallic-SWCNT absorb, Figure 29.

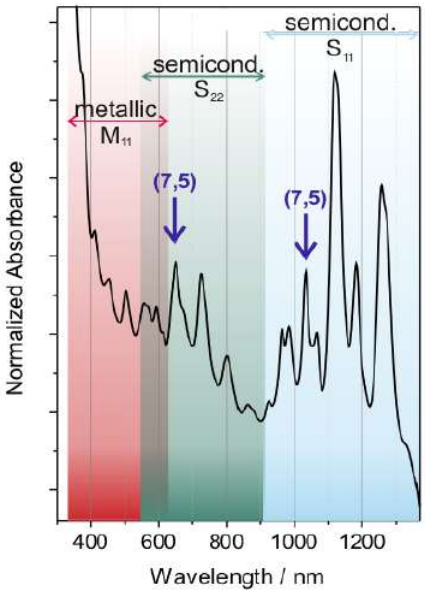

Figure 29 - Typical UV-vis absorption curve for the different types of SWCNTs (41).

Although the metallic-SWCNT type can compromise the functioning of the CNT-FET by increasing the overall reminiscent current in the CNT network, they serve has a good indicative about the quality of the dispersion because they are the ones that absorb light the most in the range of λ used in the UV visible light spectroscopy. The area under the peaks in both Figure 28 and Figure 30 is proportional to the metallic-SWCNT present in the media, according to Figure 29. If a good dispersion is achieved the peaks are well defined meaning there is a low presence of SWCNT's bundles, but to guarantee a functional device the area under the metallic SWCNT should not be very high as it is directly related to the amount of metallic-SWCNT present in the mixture. Since the bought SWCNTs were mainly semiconducting-SWCNT if the dispersions show a good degree of dispersion for metallic-SWCNTs one can assume that there is also a good dispersion of semiconducting-SWCNTs in the mixture.

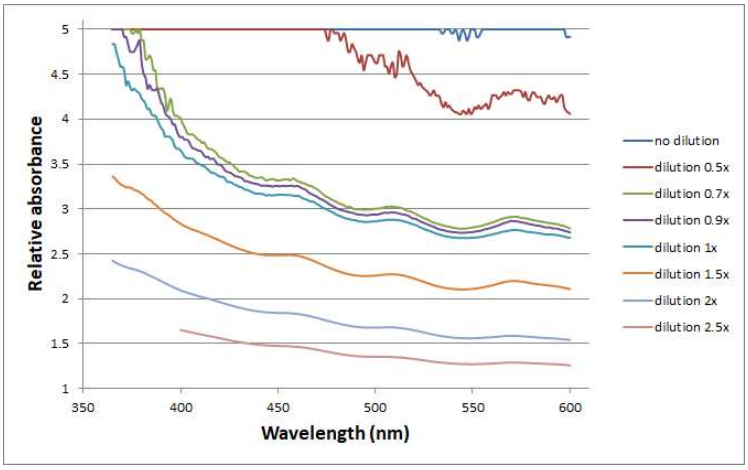

Figure 30 - UV-vis absorption curves for the dispersions obtained and the respective dilutions. These curves were measured at University of Aveiro using a SHIMADZU UV-2101PC UV-vis scanning machine.

Since the best dispersions show well defined peaks at 470 nm, 520 nm and 570nm. The dispersions that could be used in this study should be the mixtures with dilutions of either 0.7 times, 0.9 times or 1 time, Figure 30. To ensure the highest result reproducibility in the study only one dispersion was used. The mixture used had a dilution of 0.9 times, this mixture showed very well defined peaks and one can compare this peaks with the peaks described in the literature for a good SWCNT dispersion, Figure 31.

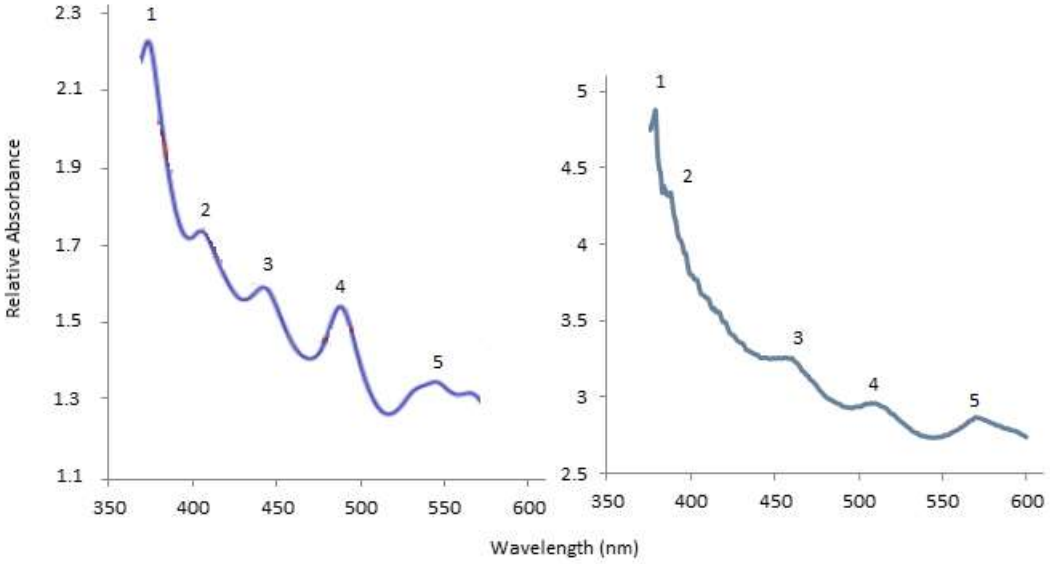

Figure 31 - Comparison between UV-vis curve of dispersion used in this study (right graph) and the UV-vis curve provided by the manufacturer (left graph)(37).

4.2 FET SWCNT deposition by dielectrophoresis

Once the dispersion was chosen the deposition proceeded, in order to achieve a high reproducibility with the CNT-FETs the deposition was done by dielectrophoresis by applying a electric field between the source and drain electrodes (42–45). This procedure was done at INESC-MN. The CNT-FETs were placed in a breadboard and afterwards the source and drain electrodes were connected to the Agilent arbitrary waveform generator machine, Figure 32 (top). Before deposition, the Agilent arbitrary waveform generator was turned on with a certain AC field applied in between the electrodes, Figure 32 (bottom). Next, a 2 μL drop of the chosen SWCNT dispersion was applied directly to the gap between electrodes using a high-precision pipette, the droplet was given enough time to completely dry before the applied field was turned off. The results were observed using an optical microscope to understand how the density of SWCNT within the channel changed with the different parameters of the electric field, and afterwards one used a set-up to obtain simple Id-Vg curves at INESC-MN.

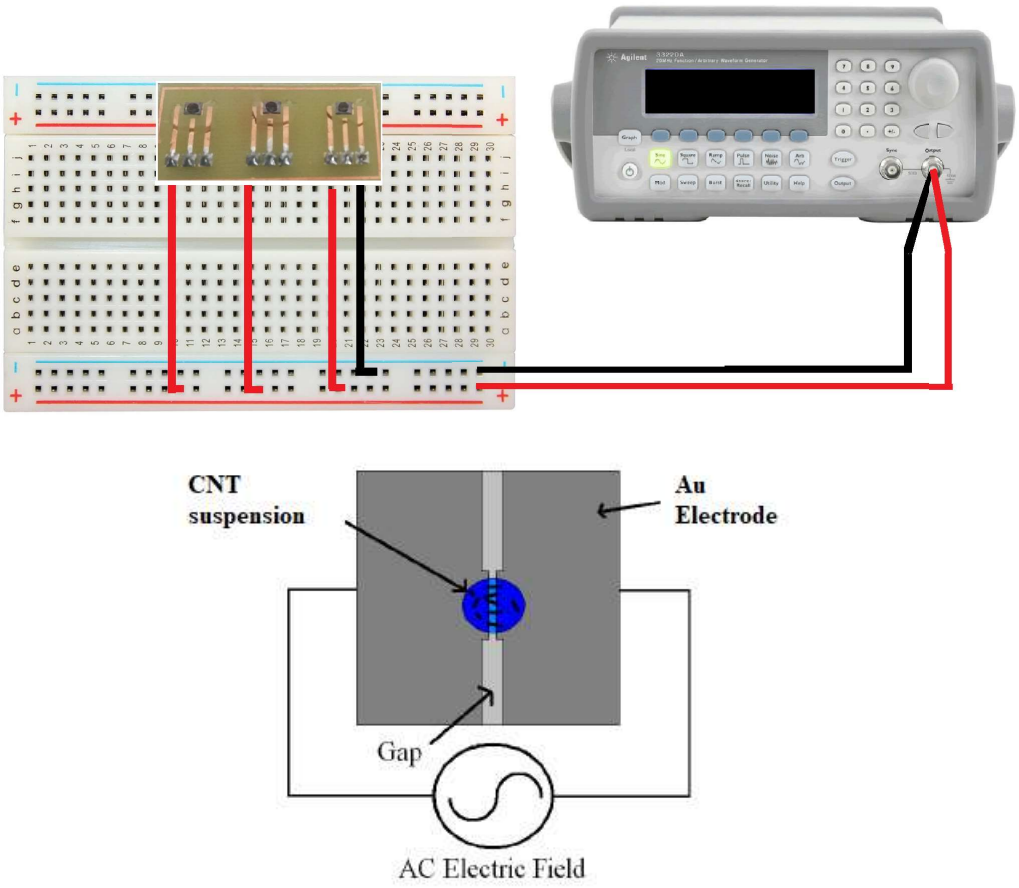

Figure 32 - Dielectrophoresis set-up(top) and schematic of the overall process(bottom)(42).

After deposition by dielectrophoresis using two different applied electric fields, the CNT-FET were visualized under an optical microscope. The fields used were: 3 MHz with 10 Vpp and 1.5 MHz with 10 Vpp. According to literature once the field frequency increases the SWCNT density in between the electrodes decreases (42,43), Figure 33. The FETs with the SWCNT deposited were then caracterized to obtain their Id-Vg Curves to understand if there were noticeably different.

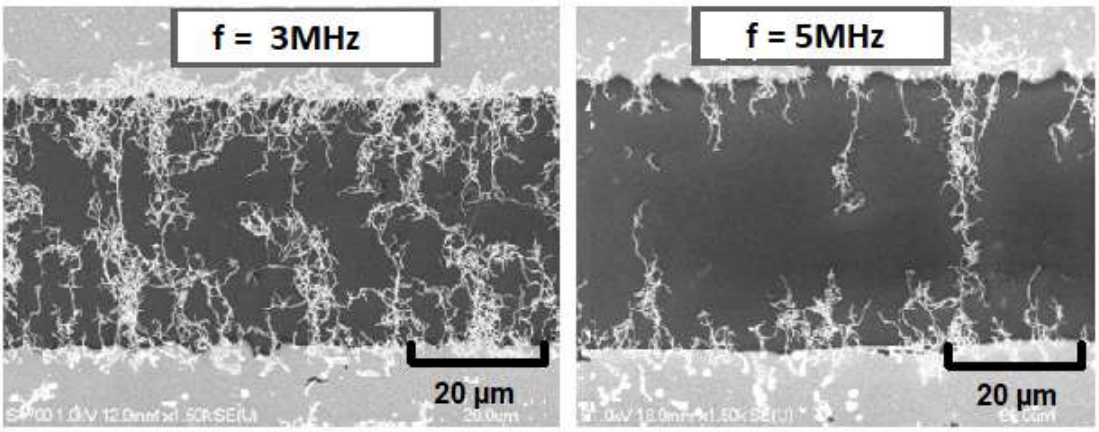

Figure 33 - SEM image from a research proving that by increasing the frequency of the applied field the SWCNT density decreases(42).

After completing the dielectrophoretic deposition the FETs were visualized under an optical micro-

scope to understand how the field would change the CNT network in between the electrodes. Figure 34 shows the best results gathered from the experiment, it was expected that the field with the highest frequency showed a lower density of SWCNT in between the electrodes(42,43).

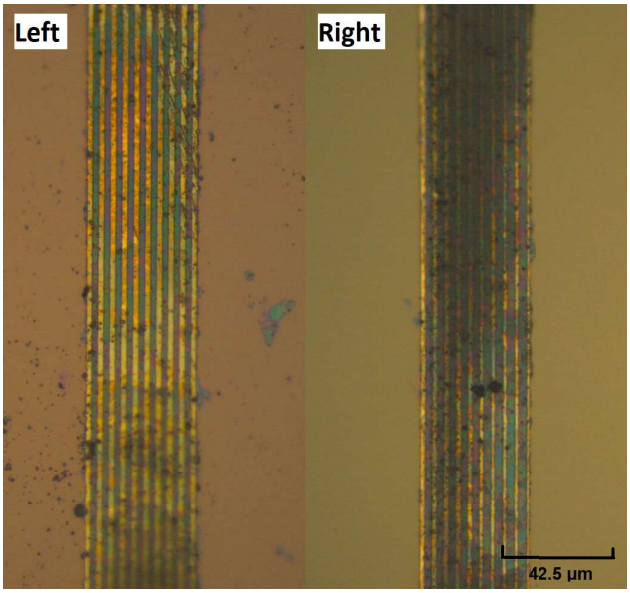

Figure 34 - Optical observation of the FETs after dielectrophoresis deposition. In the left image we see deposition with a field of 3 MHz and 10 Vpp whereas on the right image we see deposition using a field with 1.5 MHz and 10 Vpp. It is clearly seen that the 3 MHz field showed a lower density of CNTs in between the electrodes.

Afterwards the FETs were characterized using a picoameter (Keythley High Voltage Source Measure Unit) and a power supply (Hewlett Packhard E3612A). The picoameter does a DC voltage sweep from 0V to 2V with a step of 0.5V, while measuring the drain-currents of the CNT-FET. The power supply was used to apply the desired floating gate voltage which ranged between -5V to 5V with a step of 2.5V. The results are shown in Figure 35. It was expected that the CNT network which were deposited with a higher field frequency (3MHz) showed higher resistance due to the fact that CNT density in between the electrode was lower, and, for the lower field frequency (1.5MHz), the CNT network resistance should also be lower due to a higher density of SWCNT serving has conducting channel.

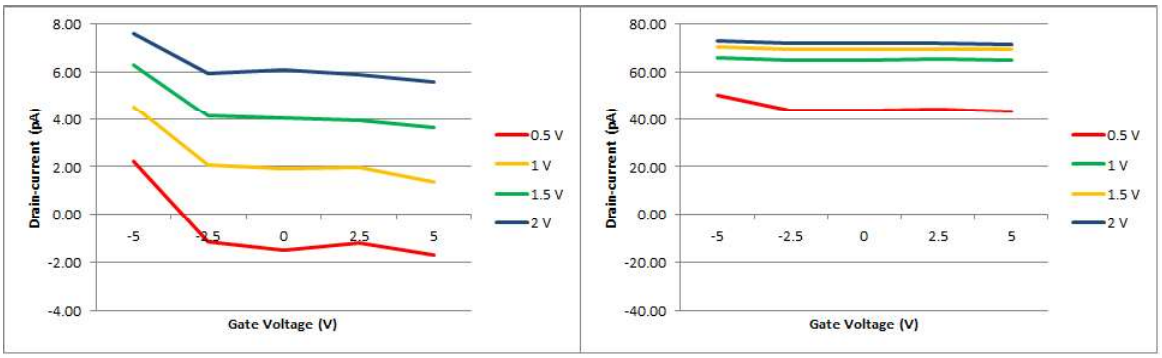

Figure 35 - Id-Vg curves of two different FET in which the SWCNT network was deposited using in the right curve (3MHZ with 10Vpp) and in the left curve (1.5MHz with 10Vpp). Each of the coloured lines corresponds to a different Source-Drain bias voltage.

In the graphic of Figure 35 one can see that once the field frequency for the deposition decreases the conductance of the channel increases. In the right graphic (1.5MHz) the drain current is almost constant around 60 to 70 pA with respect to the different applied bias voltages between source and drain electrodes, this is because the gate voltage needed to change the charge carrier density inside the channel is higher because there is a larger number of SWCNT deposited in between the electrodes, whereas in the left graphic (3MHz) where the amount SWCNT is lower the conductance is also lower and is easier to modulate the charge carrier density inside the channel with relatively small gate voltages. It is crucial in this study that the FETs are easily modulated, because one of the principles of operation of these sensors is by changing the Schotkky Barriers in the CNT/metal contacts. Also, it is important that these devices work with small drain currents, this because, in order, for small concentrations of analyte to be detected, the change in current upon adsorption should be in the same range of values has the drain current, or higher. Given this all the CNT-FETs in this study were deposited using an electric field of 3 MHz with 10 Vpp to ensure lower drain current and high modulability of the FET devices.

4.3 Sensor Characterization

This part of the study was done entirely at University of Aveiro. In this section a descripton of the results obtained will be done, mainly, by analyzing the curves obtained by the characterizing apparatus. In this study a total of 69 CNT-FETs were characterized using an Agilent 4155C Semiconductor Parameter Analyser machine, Figure 36. To obtain the curves the machine was connected to a personal computer using the Desktop EasyEXPERT software by Keysight. This procedure can be divided into three steps: pristine CNT-FET characterization, CNT-FET with immobilized antibody characterization and CNT-FET with immobilized antibody and *E. coli* characterization.

Figure 36 - Agilent 4155C machine.

4.3.1 Pristine CNT-FET characterization

The pristine CNT-FET characterization was done mainly to assess if all the CNT-FETs devices were working properly and in the desired range of values. Figure 37 shows the Id-Vg curves obtained for

two CNT-FETs, one had the most common drain currents registered and the other had the highest drain currents registered.

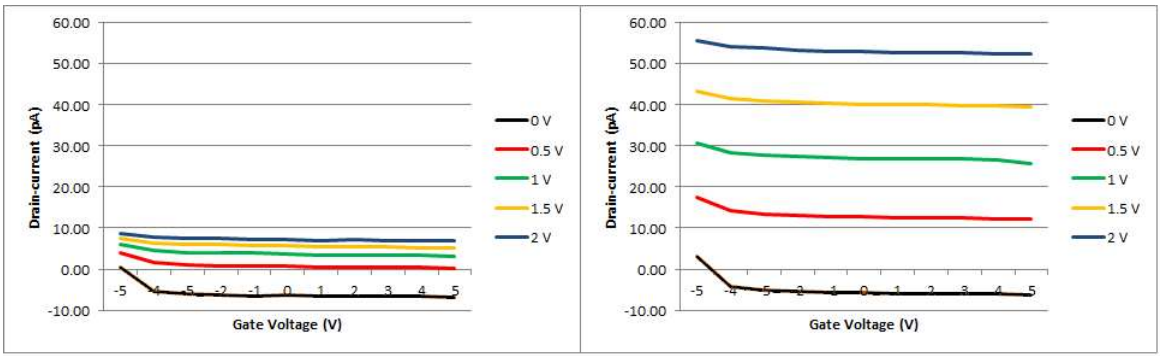

Figure 37 - Id-Vg curves of the average conductive FET (left curve) and the highest conductive FET (right curve). Each of the coloured lines corresponds to a different Source-Drain bias voltage.

Althought Figure 37 shows a large difference between the channel conductance of the two FET devices represented, both CNT-FETs were defined has working properly. The most common Id-Vg curves of the CNT-FETs characterized in this step were very similar to the left curve of Figure 37. In fact most of CNT-FETs had drain-currents which ranged between $-8 * 10^{-12}$A and $8 * 10^{-12}$A according to the Source-Drain bias voltages applied. As stated before, this study had a total of 69 FETs available after the first characterization meaning that even with some fluctuations of drain current from CNT-FET to CNT-FET all the characterized FETs showed good working parameters.

In Figure 38 graph a), one can see the average Id-Vd curve obtained for the pristine CNT-FETs, Figure 38 graphs b) to j) are the representations of the average drain-currents values for each of the gate voltages. The purpose of Figure 38 is to understand that from CNT-FET to CNT-FET the drain-current change was minimal. In order to understand to full extent of drain-current variation for the pristine CNT-FETs one calculated the average values and the standard deviation values of the characterized CNT-FETs, these results are shown in Figure 38 graphs b) to j), here one can see how far the measured drain-current values ranged apart from the average drain-current value. Each point in all the graphs b) to j) corresponds to the average drain-current of all the CNT-FETs for that specific combination of Gate Voltage and Source-Drain bias voltage. One can see that the standard deviations calculated are low which means that the FETs are all working in a well defined range of values, with the exception of the CNT-FET working with an applied gate voltage of 0V which showed very high standard deviation, thus having a graph with a different scale. From Figure 38 one can conclude that the dielectrophorstic deposition of the CNTs achieved the desired purpose of improving the reproducibility of results from CNT-FET to CNT-FET.

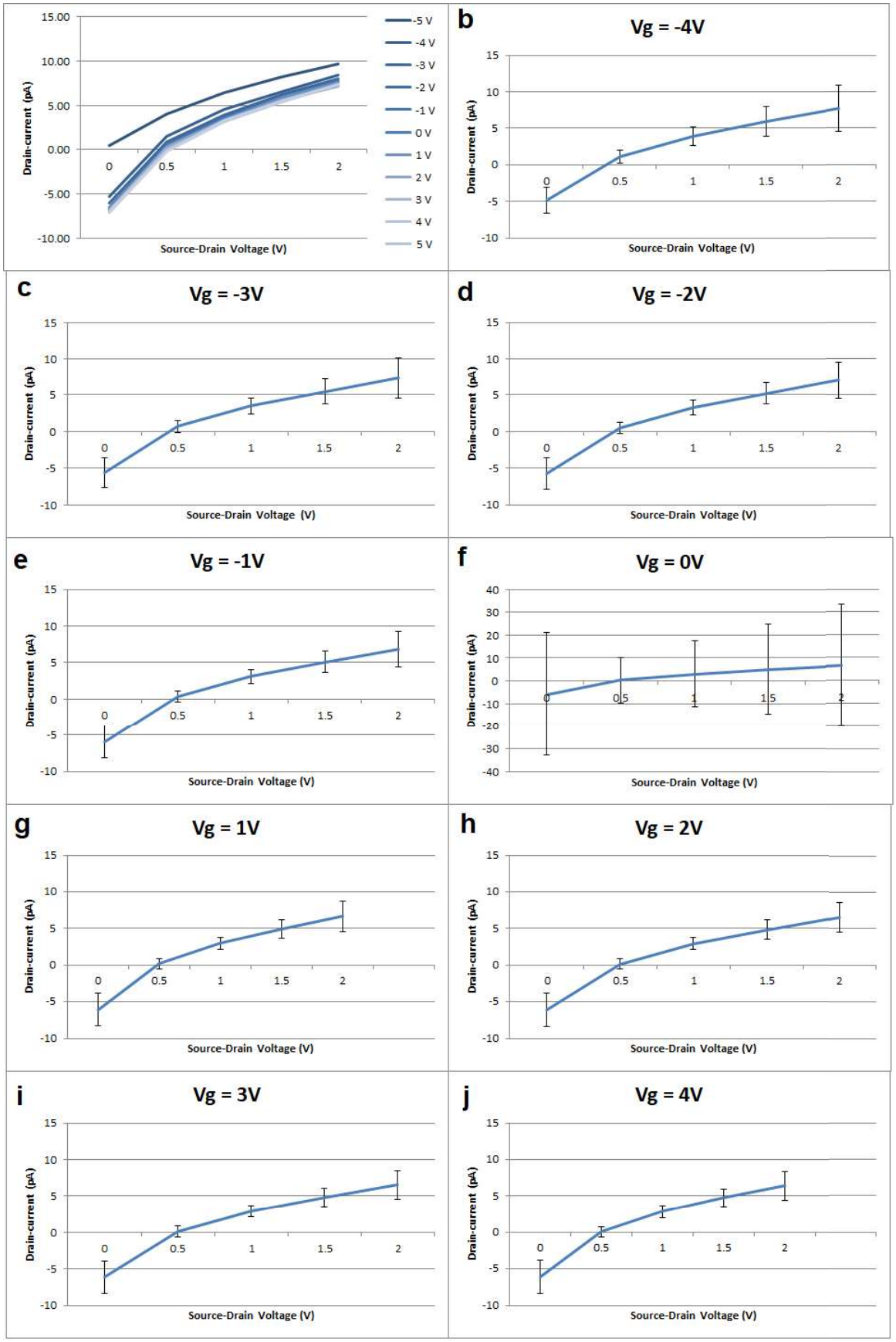

Figure 38 - a) The average Id-Vd curve obtained, each line corresponds to a different Gate Voltage. b) to j) The average drain-currents values with the respective error bars for the different applied gate voltages.

4.3.2 CNT-FET with immobilized antibody characterization

This characterization started with the preparation of an antibody solution. Since the objective of this study is to use a CNT-FET device to detect *E. coli* in water, the antibody of choice used in this study was an anti-*E. coli* antibody non-biotinated, which was provided by INESC-MN (46), this antibody allowed for a simpler and less expensive immobilization procedure. The method of immobilization was a simple adsorption. The procedure was done at University of Aveiro.

A 2 μL droplet of a diluted antibody solution was placed on top of the CNT-FET using a high-precision pipette and it was left to dry overnight on top of the SWCNT network. In Figure 39 one can see the antibody specifications.

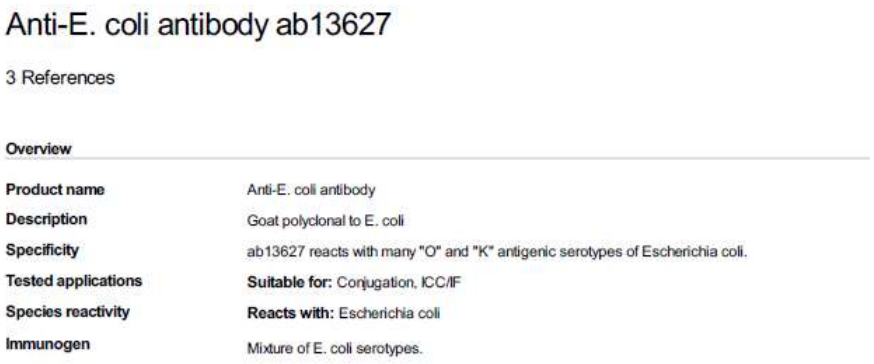

Anti-E. coli antibody ab13627

3 References

Overview

Product name	Anti-E. coli antibody
Description	Goat polyclonal to E. coli
Specificity	ab13627 reacts with many "O" and "K" antigenic serotypes of Escherichia coli.
Tested applications	**Suitable for:** Conjugation, ICC/IF
Species reactivity	**Reacts with:** Escherichia coli
Immunogen	Mixture of E. coli serotypes.

Figure 39 - Anti*E. coli* antibody datasheet (46).

The antibody solution prepared was done by diluting the stock solution of 4000 μg/mL in MilliQ water to achieve 10ng/μL. This ensured the SWCNT network had a good antibody coverage (35), thus ensuring the proper functioning of the device by allowing *E. coli* to connect with its complementary antibody anywhere on top of the device.

From this diluted antibody solution 2 μL were placed on top of the CNT-network of 66 of the FETs, 3 FETs were used as control with only MilliQ water. All the FETs were then placed in a refrigerator at 5 C$^\circ$ overnight to allow for the adsorption to take place.
Once the adsorption was concluded each CNT-FET was characterized. The characterization was done in the same Agilent 4155C machine. There were some discrepancies in the values measured, while some CNT-FETs showed an increase in their drain current with the adsorption of the antibodies, other CNT-FETs showed a decrease in their drain current, this was clearly assessed by their Id-Vg curves Figure 40. For instance in Figure 40, CNT-FET a) decreased its drain-current, the Id-Vg curves were all shifted downwards, the variation was $\approx 1pA$. The same happened for CNT-FET b) which shifted downwards ≈ 3 to $2pA$. On the other hand, in CNT-FET c) the drain-current increased, the id-Vg curve shifted upwards $\approx 1pA$, in CNT-FET d) the same happened, the Id-Vg curves were all shifted upwards $\approx 2pA$.

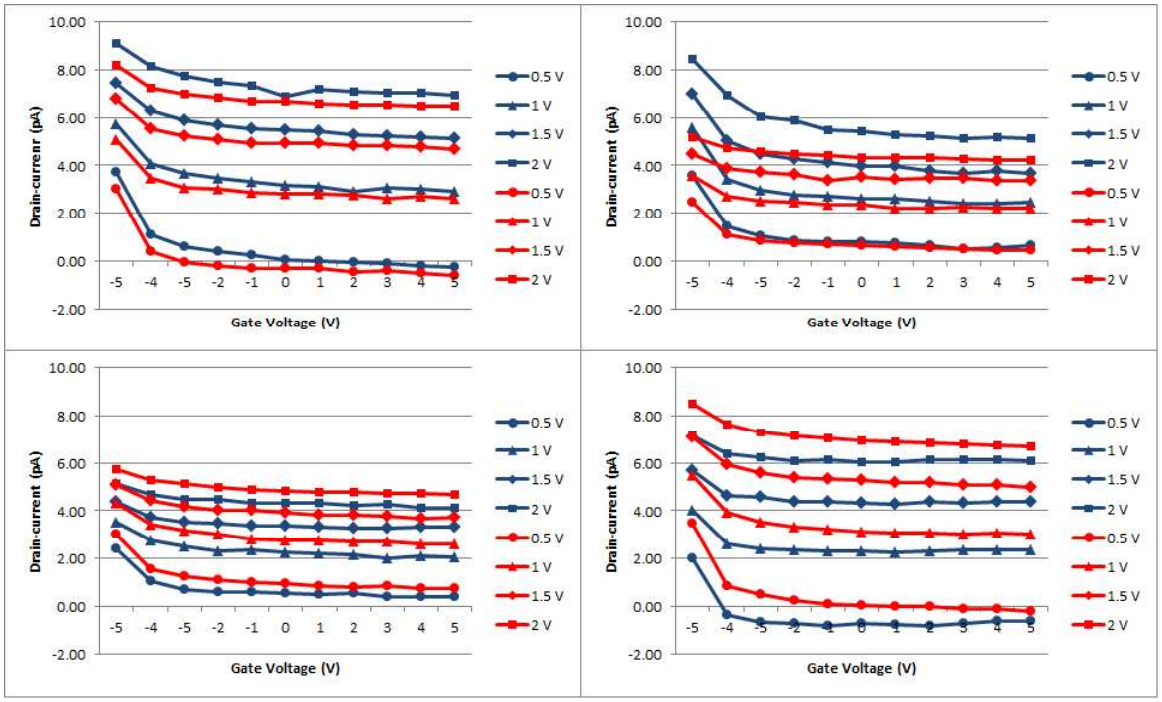

Figure 40 - Id-Vg curves of four different FETs before and after antibody adsorption, blue (before adsorption) and red (after adsorption). Each Line corresponds to a Source-Drain bias voltage.

This change, initially imposed a great challenge in the evolution of this study because the CNT-FETs did not show reproducibility of values upon molecule adsorption. But as one will see further, in the results chapter and also in data analysis chapter, one managed to achieve a good calibration curve in spite of these upwards and downwards discrepant shifts obtained for the drain current upon adsorption of molecules.

One possibility for this change is the fact that the antibody solution allows for a re-suspension of the CNT network which gets deposited in a slightly different way (35), this re-suspension, thus new deposition, thus new SWCNT network arrangement, translates in a different drain-current value than the previously assessed, however, the 3 control CNT-FETs tested with only MilliQ water showed very little difference in drain-current values when comparing with the changes registered for antibody adsorption Figure 41.

Since the drain-current change of the control CNT-FETs is different than the drain-current change for antibody adsorption, one deduces that it might not be due to a re-suspension of SWCNT network. Therfore, from the Id-Vg curves of the control CNT-FETs, Figure 41, one can formulate another hypothesis to explain these upwards and downwards discrepant shifts obtained for the drain current upon adsorption of antibody Figure 40. This hypothesis is based on the fact that the method of immobilization is random meaning that the antibodies do not adsorb on the SWCNT network in the same way Figure 42. This random adsorption accompanied by the fact that each zone of the antibody can possess different amounts electron donating molecules or electron withdrawing molecules, leads one to conclude that it is possible that the discrepant shifts measured are due to the random adsorption of antibodies which translate in a different charge transfer to the SWCNT network from CNT-FET to CNT-FET. Different charge transfer relate in different drain-current variations.

Afterwards these 3 control CNT-FETs were also functionalized with the antibody solution and characterized, this was done to increase the amount of tested samples, thus improving the calibration curve statistical significance.

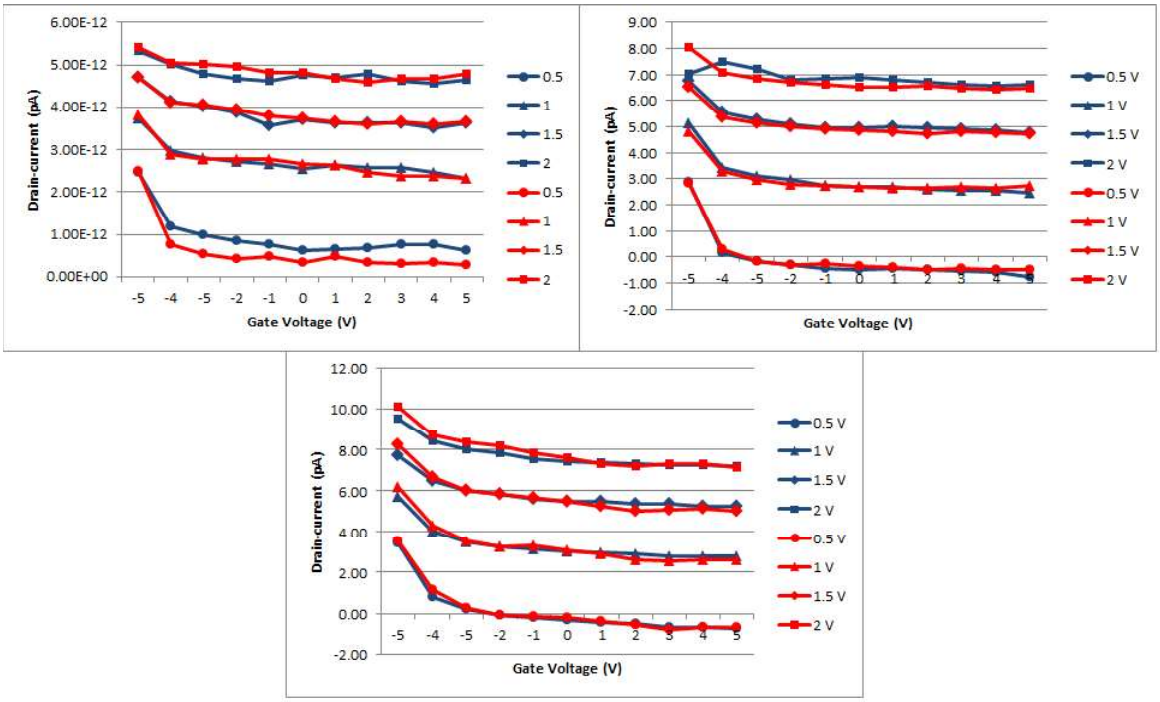

Figure 41 - Id-Vg curves of the control CNT-FETs (MilliQ water treatment) used for CNT-FET with antibody characterization, blue (before treatment) and red (after treatment). Each Line corresponds to a Source-Drain bias voltage.

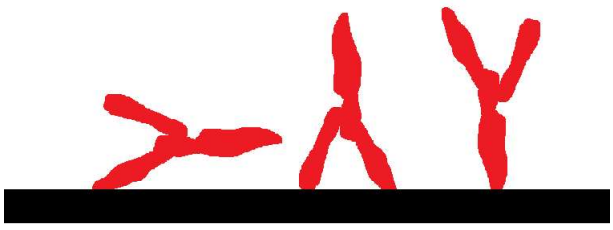

Figure 42 - Different possibilities of antibody adsorption leading to different charge transfer and different Schottky Barrier width.

4.3.3 CNT-FET with immobilized antibody and *E. coli* characterization

Now a group of 3 FETs with already adsorbed antibody were used as control. These 3 FETs used as control were treated with a 2 μL drop of MilliQ water instead of any *E. coli* concentration and, for all three FETs the drain current showed very small variations, in fact in Figure 43 one can see that the Id-Vg curves almost did not shift either upwards or downwards.

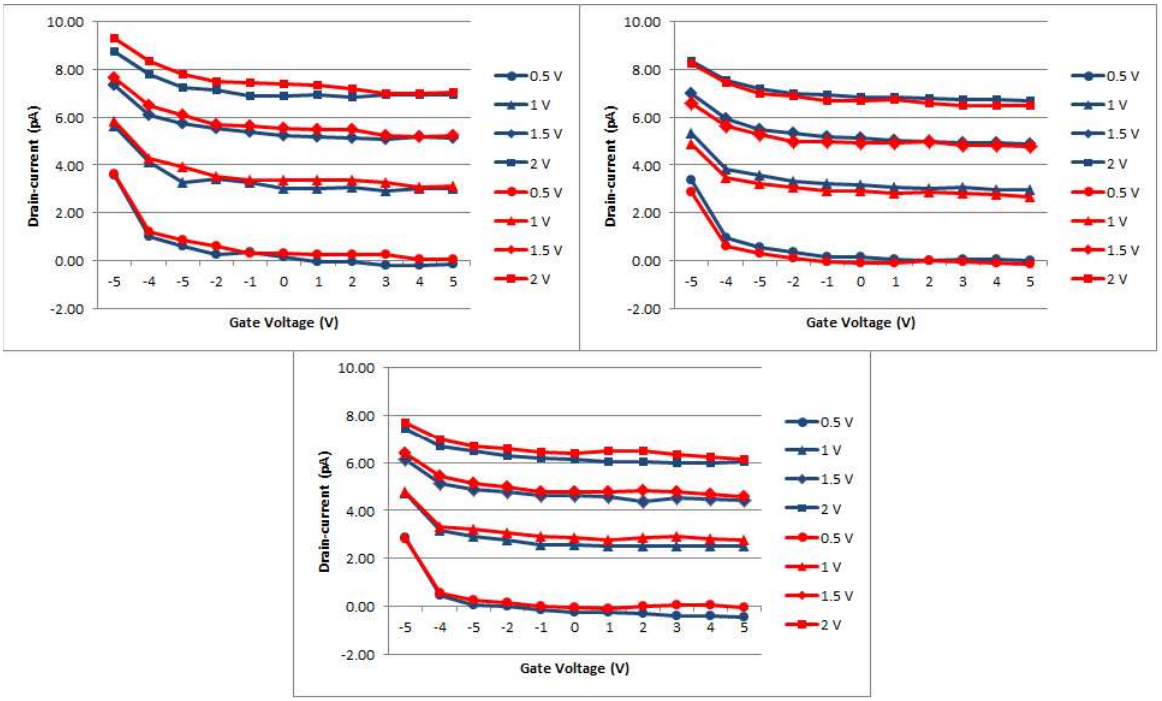

Figure 43 - Id-Vg of the control FETs as one can see the differences in drain-current are minimal, blue (before treatment) and red (after treatment). Each Line corresponds to a Source-Drain bias voltage.

Since the control CNT-FETs showed no change one decided to incorporate them in the next step, in order to increase the amount of tested samples, thus improving the calibration curve statistical significance.

This is the most crucial part of this study, the outcome of this procedure is a calibration curve that will allow the fabrication a point of care device. Since the study comprised a total of 69 CNT-FETs, one decided to test seven different *E. coli* concentrations. For each of the seven concentrations there were 10 CNT-FETs allocated, except for one concentration, which had only 9 CNT-FETs allocated, this concentration was the highest one as the intention was to also be able to understand the minimum threshold of detection of these sensors. Since the silicone well defined for the application of the droplets could only support a volume of 2 μL. In order to test the minimum threshold of detection for the CNT-FETs, one decided to test concentrations as low as 3 bacteria in order to understand if the sensors had the ability to detect close to a single bacteria.

To do so, one had to manage a way to have approximately one bacteria in 2 μL of water, therefore, 1 UFC (Colony Forming Unit) in 2μL. However, $\frac{1}{2}$ UFC/ μL is in fact a very large concentration (500 UFC/mL).

To prepare the different *E. coli* concentrations, one started with a fairly common *E. coli* string the DH5α, provived by the IBB department of Instituto Superior Tecnico, on a frozen pellet containing 10^7 UFCs, therefore, aproximately 10^7 bacteria. This pellet was dissolved in 1 mL of MilliQ water, from this 10^7 UFC/mL solution, successive dilutions were done to achieve the seven concentrations shown bellow, the dilutions were done at INESC-MN.

Table 1 - *E. coli* concentrations used.

Allocated CNT-FETs	100 µL Volume	2 µL Volume
9	10000 UFC/100 µL	200 UFC/2 µL
10	5000 UFC/100 µL	100 UFC/2 µL
10	2500 UFC/100 µL	50 UFC/2 µL
10	1250 UFC/100 µL	25 UFC/2 µL
10	500 UFC/100 µL	12,5 UFC/2 µL
10	250 UFC/100 µL	6 UFC/2 µL
10	125 UFC/100 µL	3 UFC/2 µL

Once all the concentrations were prepared one placed the samples in the CNT-FETs well and allowed the samples to dry, subsequently, one proceed with the characterization measurements using the same Agilent 4155C machine. Similarly to what happened upon antibody adsorption, when comparing the Id-Vg curves there were some FETs that showed an increase in drain current while other CNT-FETs showed a decrease in drain current, Figure 44.

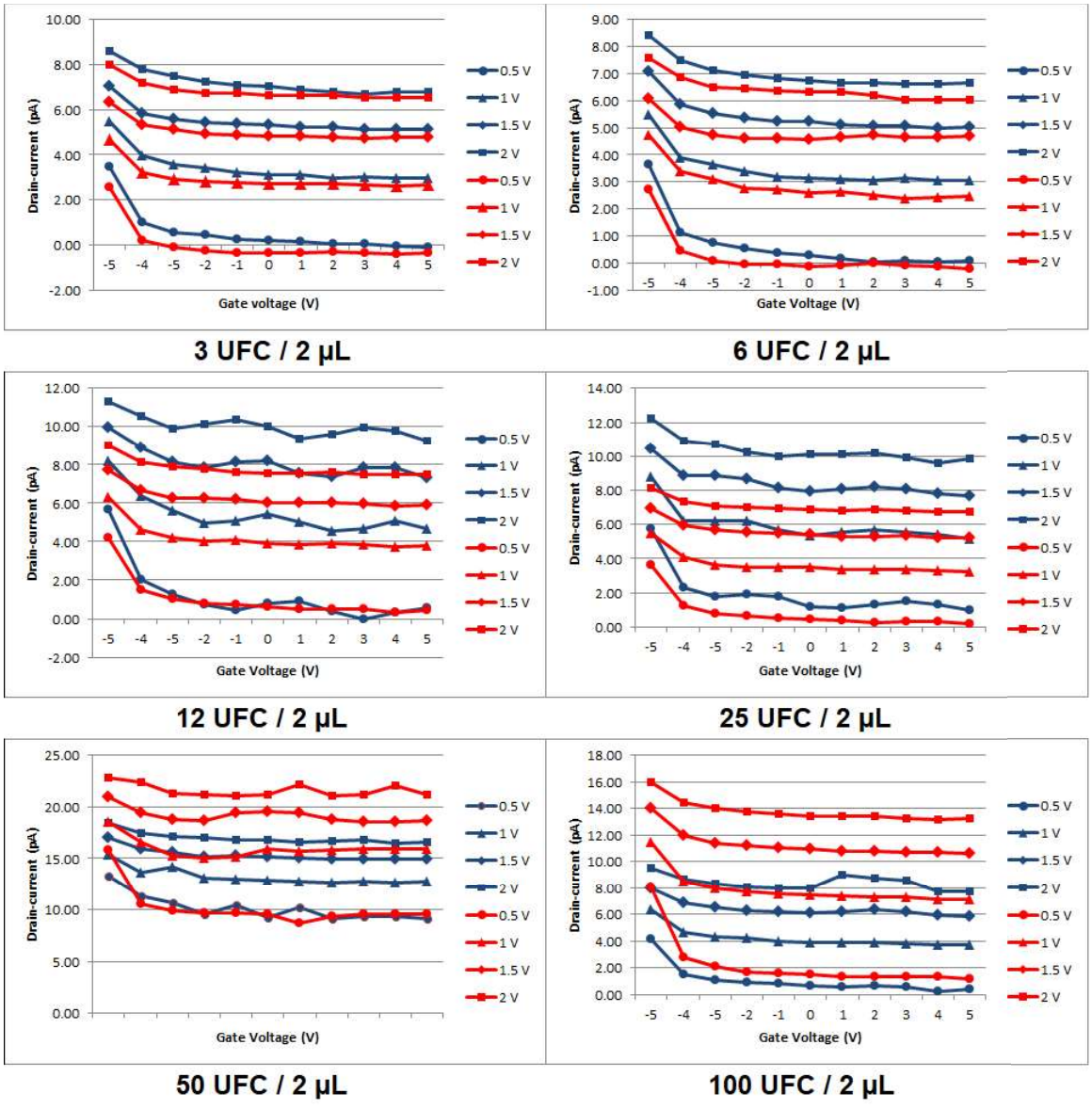

Figure 44 - Id-Vg curves of the most promising CNT-FETs for each of the used *E. coli* concentrations, blue (before *E. coli*) and red (after *E. coli*). Each Line corresponds to a Source-Drain bias voltage.

In Figure 44 one can see that some of the CNT-FET devices, upon connection with different concentrations of *E. coli* increased their drain-currents, for instance the CNT-FETs treated with 100 UFC/2 μL and 50 UFC/2 μL, while others decreased their drain-currents, for instance CNT-FETs treated with 25 UFC/2 μL, 12,5 UFC/2 μL, 6 UFC/2 μL and 3 UFC/2 μL.

However the differences between the drain-currents measured obey the expected rule, lower concentrations of *E. coli* created lower variations in the drain-current of the CNT-FETs while higher concentrations of *E. coli* created higher variations in the drain-current of the CNT-FETs, Figure 45.

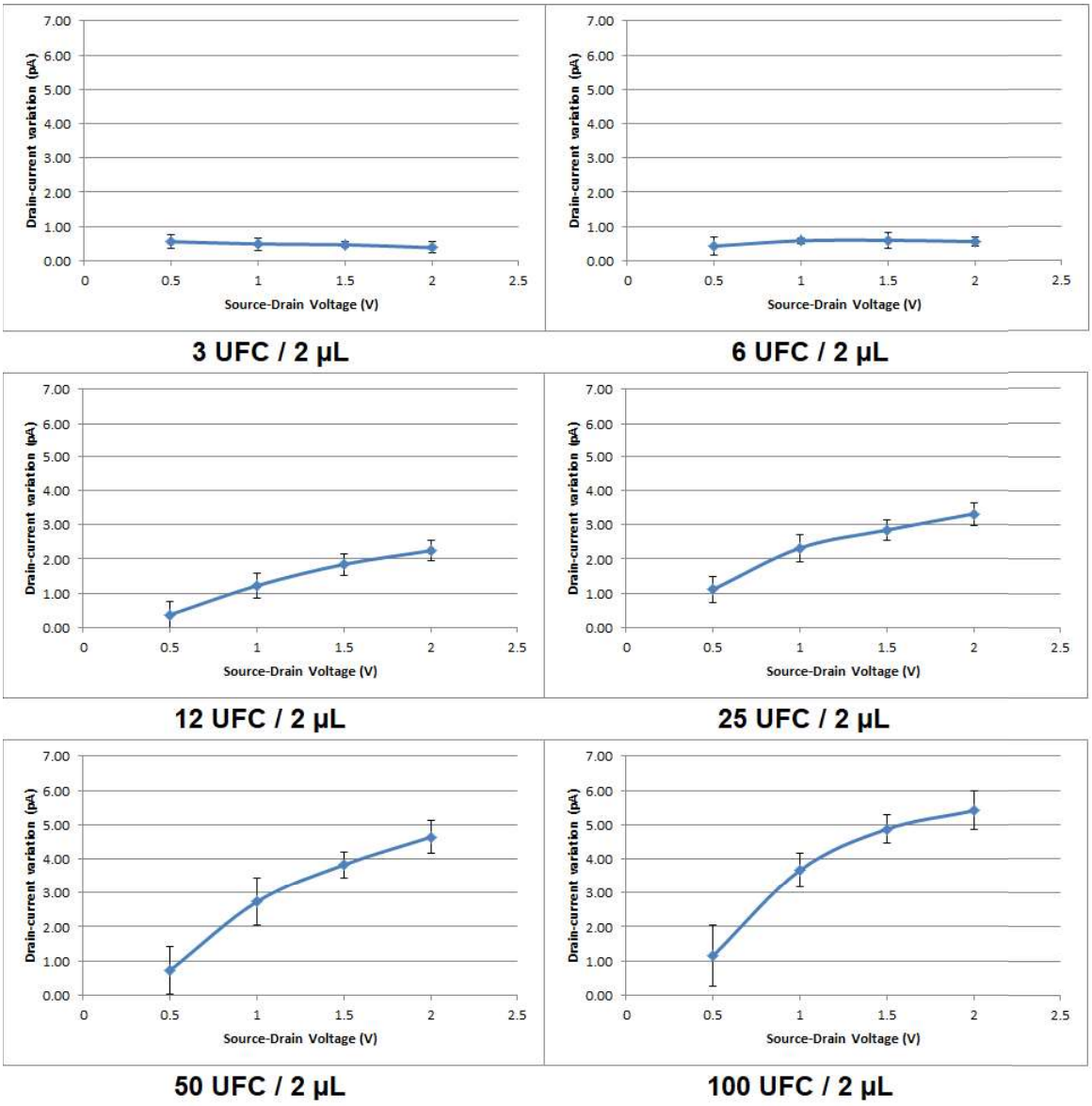

Figure 45 - Absolute average drain-current variation for each of Source-Drain voltages of the CNT-FETs tested in Figure 44.

Figure 45 shows the absolute average drain-current variation for each of source drain voltages of the CNT-FETs tested in Figure 44. Meaning, that each point is the the average between the differences registered for the before and after *E. coli* treatment Source-Drain Voltages along all the gate voltages, showed in Figure 44. The error bars represent the drain-current variation within the same source-drain voltage due to the different gate voltages. For example, in the 3 UFC/2 μL concentration, one substracted all the drain current values from the before and after curves of source drain voltages and averaged them

to obtain an average variation for each of the source drain voltages (0.5V, 1V, 1.5V and 2V). In Figure 45 the average drain-current variation of the 3 UFC/2 μL concentration for the source drain voltage of 0.5V was around $0.5pA$. Figure 45 serves the purpose of showing that, in fact, with increasing concentrations of *E. coli* the drain-current variation also increases, this is clearly evident in the curves showing the concentrations from 12,5 UFC/2 μL to 100 UFC/2 μL, where one can see that the average variation values become increasingly higher.

Chapter 5

Data Analysis

The main problem with the analysis of the data collected from the different FETs lied on the fact the the drain-current shifts upon molecule adsorption were discrepant , meaning that, sometimes drain-current would increase and other times the drain-current would decrease. Inspite of this fact the absolute value of the drain-current variation, obeyed, in fact a rule. For lower *E. coli* concentrations the absolute value of the drain-current variation was lower than for higher *E. coli* concentrations.

Since this study has the objective of developing a point-of-care device capable of measuring *E. coli* concentrations in water, and knowing that such device is a very rudimentary Picoameter not capable of doing DC voltages sweeps either on the Gate electrode or on the Source-Drain electrodes, one needs to define the overall best working parameters of the FET devices. Therefore, one needs to define a bias gate voltage and a bias source-drain voltage to apply on the FET's in order to read the Drain-current from a point-of-care perspective.

5.1 Absolute Drain current variation value $|\Delta I|$

From all the collected data the first step of the analysis was to obtain the absolute value for the drain-current variation $|\Delta I|$ between CNT-FETs with antibody and CNT-FETs with antibody and *E. coli*. This step was done for every CNT-FET along all the gate voltage/source-drain voltage combinations available. All the data was analysed using Microsoft Excel.

Table 2 - Drain Current values (pA) of a CNT-FET with antibody adsorbed. These values were obtained in University Of Aveiro using an Agilent 4155C Semiconductor Parameter Analyser machine.

	Vg=-5V	Vg=-4V	Vg=-3V	Vg=-2V	Vg=-1V	Vg=0V	Vg=1V	Vg=2V	Vg=3V	Vg=4V	Vg=5V
Vds=0V	0.76	-2.36	-2.72	-2.90	-2.98	-2.94	-3.10	-3.14	-3.20	-3.23	-3.24
Vds=0.5V	2.66	1.31	1.08	0.88	0.84	0.71	0.71	0.71	0.65	0.74	0.64
Vds=1V	3.85	2.97	2.82	2.73	2.64	2.59	2.50	2.51	2.47	2.44	2.39
Vds=1.5V	4.77	4.21	3.98	3.90	3.74	3.62	3.63	3.58	3.55	3.55	3.50
Vds=2V	5.43	4.94	4.76	4.77	4.62	4.59	4.57	4.55	4.50	4.47	4.46

Table 3 - Drain Current values (pA) of a CNT-FET with antibody adsorbed and a *E. coli* concentration of 50 UFC / 2μL. These values were obtained in University Of Aveiro using an Agilent 4155C Semiconductor Parameter Analyser machine.

	Vg=-5V	Vg=-4V	Vg=-3V	Vg=-2V	Vg=-1V	Vg=0V	Vg=1V	Vg=2V	Vg=3V	Vg=4V	Vg=5V
Vds=0V	3.01	0.41	0.19	0.09	0.06	-0.03	-0.22	-0.21	-0.24	-0.27	-0.30
Vds=0.5V	4.91	3.88	3.63	3.61	3.50	3.45	3.33	3.26	3.21	3.19	3.13
Vds=1V	6.13	5.47	5.29	5.14	5.04	4.98	4.93	4.81	4.81	4.80	4.55
Vds=1.5V	6.83	6.42	6.33	6.30	6.20	5.97	6.00	5.95	5.95	5.80	5.74
Vds=2V	7.61	7.36	7.26	7.19	7.06	6.89	6.90	6.93	6.84	6.69	6.63

If one plotted the values shown in Table 1 and 2 one would obtain a typical Id-Vg curve or Id-Vd curve similar to the curves shown in the Sensor Characterization section of Chapter 4. In fact by plotting the data represented in Table 1 and Table 2 one obtains the curves shown in Figure 46.

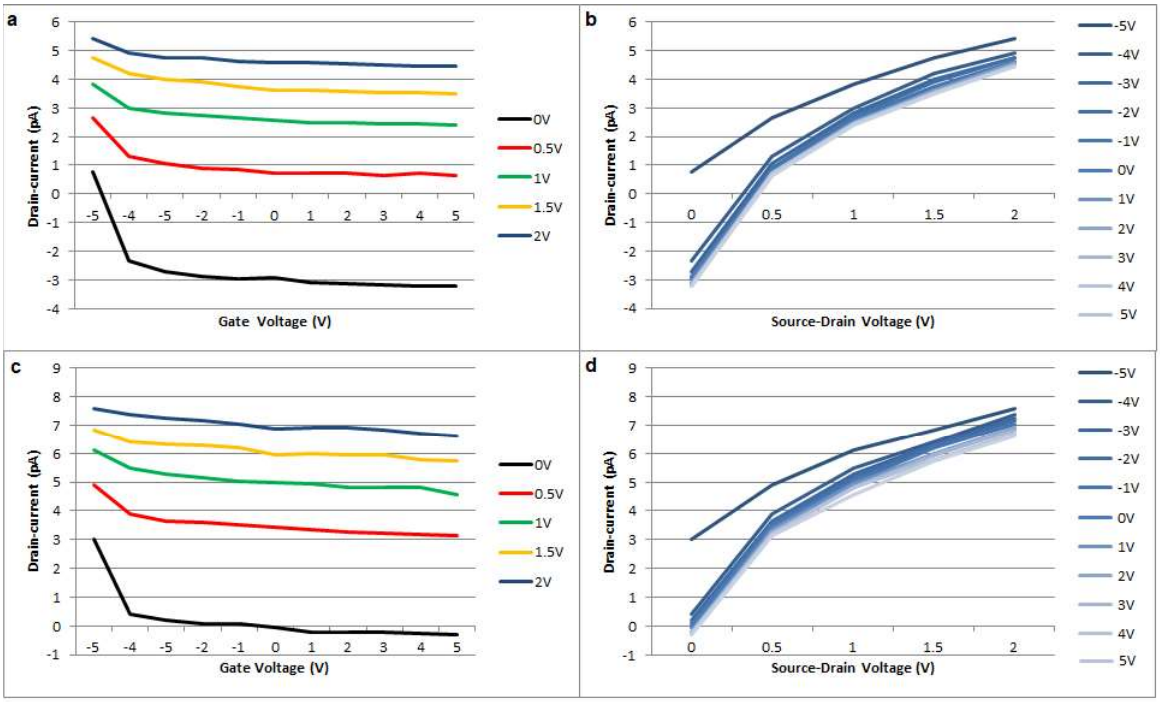

Figure 46 - Id-Vg and Id-Vd curves of a CNT-FET treated with 50 UFC / 2μL concentration of *E. coli*. graphs a) and b) correspond to the Id-Vg and Id-Vd curves, respectively, of the CNT-FET before treatment with *E. coli* (only antibody adsorbed). Graphs c) and d) correspond to the Id-Vg and Id-Vd curves, respectively, of the CNT-FET after treatment with *E. coli*. Graphs a) and c) each line plot correspond to a Source-Drain Voltage. Graphs b) and d) each line plot correspond to a Gate Voltage..

Afterwards one subtracted the values of Table 2 from the values of Table 1 and did the modulus of each value, thus obtaining the absolute drain-current variation $|\Delta I|$, Table 3

Table 4 - Absolute drain current variation values ($|\Delta I|$) (pA) for one CNT-FET using a 50 UFC / 2μL *E. coli* concentration.

	Vg=-5V	Vg=-4V	Vg=-3V	Vg=-2V	Vg=-1V	Vg=0V	Vg=1V	Vg=2V	Vg=3V	Vg=4V	Vg=5V
Vds=0V	2.255	2.764	2.915	2.99	3.039	2.905	2.879	2.928	2.956	2.957	2.935
Vds=0.5V	2.254	2.568	2.549	2.724	2.659	2.736	2.619	2.551	2.553	2.45	2.498
Vds=1V	2.279	2.495	2.473	2.414	2.403	2.389	2.432	2.309	2.342	2.359	2.164
Vds=1.5V	2.06	2.212	2.351	2.403	2.458	2.345	2.368	2.378	2.394	2.245	2.243
Vds=2V	2.174	2.424	2.503	2.417	2.438	2.295	2.327	2.374	2.348	2.22	2.17

5.2 Average $|\Delta I|$ values

The $|\Delta I|$ were obtained, as explained in the previous section, for every CNT-FET.

As stated before there were allocated for each *E.coli* concentration a total of 10 CNT-FETs, with the exception of one concentration which only had 9 CNT-FETs allocated. Therefore for every *E. coli* concentration, except for one, one obtained 10 Tables similar to Table 3 corresponding to the $|\Delta I|$ of the CNT-FET allocated to that specific *E. coli* concentration. For instance, the $|\Delta I|$ values for the 10 CNT-FETs treated with 50 UFC / 2μL are shown in Tables 5 to 14.

Table 5 - $|\Delta I|$ (pA) values for the first FET of 50 UFC / 2μL *E. coli* concentration. (same as Table 4).

	Vg=-5V	Vg=-4V	Vg=-3V	Vg=-2V	Vg=-1V	Vg=0V	Vg=1V	Vg=2V	Vg=3V	Vg=4V	Vg=5V
Vds=0V	2.255	2.764	2.915	2.99	3.039	2.905	2.879	2.928	2.956	2.957	2.935
Vds=0.5V	2.254	2.568	2.549	2.724	2.659	2.736	2.619	2.551	2.553	2.45	2.498
Vds=1V	2.279	2.495	2.473	2.414	2.403	2.389	2.432	2.309	2.342	2.359	2.164
Vds=1.5V	2.06	2.212	2.351	2.403	2.458	2.345	2.368	2.378	2.394	2.245	2.243
Vds=2V	2.174	2.424	2.503	2.417	2.438	2.295	2.327	2.374	2.348	2.22	2.17

Table 6 - $|\Delta I|$ (pA) values for the second FET of 50 UFC / 2μL *E. coli* concentration.

	Vg=-5V	Vg=-4V	Vg=-3V	Vg=-2V	Vg=-1V	Vg=0V	Vg=1V	Vg=2V	Vg=3V	Vg=4V	Vg=5V
Vds=0V	5.449	3.564	3.401	3.253	2.144	1.958	0.919	0.629	0.389	1.676	1.799
Vds=0.5V	6.985	6.367	5.785	5.058	5.003	5.018	4.919	4.582	4.248	4.304	4.444
Vds=1V	7.439	6.856	6.204	4.794	6.3	5.737	6.104	5.706	5.085	4.914	4.927
Vds=1.5V	7.498	7.148	6.6	6.579	6.661	5.698	6.029	5.932	5.411	5.434	5.212
Vds=2V	7.7	9.622	6.697	5.814	7.2	5.941	6.245	5.981	5.325	6.069	5.645

Table 7 - $|\Delta I|$ (pA) values for the third FET of 50 UFC / 2μL *E. coli* concentration.

	Vg=-5V	Vg=-4V	Vg=-3V	Vg=-2V	Vg=-1V	Vg=0V	Vg=1V	Vg=2V	Vg=3V	Vg=4V	Vg=5V
Vds=0V	1.686	2.548	2.59	2.674	2.623	2.596	2.549	2.58	2.639	2.576	2.522
Vds=0.5V	1.708	2.076	2.138	2.154	2.11	2.085	2.033	2.082	2.052	2.054	1.955
Vds=1V	1.483	1.774	1.85	1.771	1.861	1.863	1.823	1.821	1.653	1.722	1.743
Vds=1.5V	1.692	1.852	1.878	1.832	1.747	1.784	1.842	1.829	1.797	1.807	1.623
Vds=2V	1.662	1.898	1.701	1.764	1.82	1.786	1.78	1.691	1.639	1.551	1.508

Table 8 - $|\Delta I|$ (pA) values for the forth FET of 50 UFC / 2μL *E. coli* concentration.

	Vg=-5V	Vg=-4V	Vg=-3V	Vg=-2V	Vg=-1V	Vg=0V	Vg=1V	Vg=2V	Vg=3V	Vg=4V	Vg=5V
Vds=0V	2.608	3.267	3.54	3.661	3.498	3.521	3.49	3.427	3.374	3.503	3.389
Vds=0.5V	2.296	2.682	2.97	2.839	2.912	2.755	2.696	2.728	2.728	2.875	2.786
Vds=1V	2.06	2.529	2.556	2.584	2.572	2.549	2.556	2.547	2.527	2.441	2.318
Vds=1.5V	2.029	2.405	2.406	2.447	2.372	2.247	2.464	2.327	2.311	2.488	2.263
Vds=2V	2.163	2.247	2.363	2.368	2.155	2.356	2.294	2.369	2.223	2.083	2.027

Table 9 - $|\Delta I|$ (pA) values for the fifth FET of 50 UFC / 2μL *E. coli* concentration.

	Vg=-5V	Vg=-4V	Vg=-3V	Vg=-2V	Vg=-1V	Vg=0V	Vg=1V	Vg=2V	Vg=3V	Vg=4V	Vg=5V
Vds=0V	1.865	2.289	2.454	2.462	2.498	2.504	2.493	2.493	2.405	2.29	2.588
Vds=0.5V	1.535	1.871	1.978	1.963	2.028	2.067	1.962	1.876	1.962	1.977	1.867
Vds=1V	1.463	1.489	1.652	1.768	1.751	1.649	1.529	1.565	1.574	1.656	1.646
Vds=1.5V	1.362	1.582	1.602	1.704	1.645	1.614	1.663	1.729	1.764	1.82	1.665
Vds=2V	1.535	1.642	1.753	1.759	1.81	1.597	1.617	1.605	1.625	1.629	1.552

Table 10 - $|\Delta I|$ (pA) values for the sixth FET of 50 UFC / 2μL *E. coli* concentration.

	Vg=-5V	Vg=-4V	Vg=-3V	Vg=-2V	Vg=-1V	Vg=0V	Vg=1V	Vg=2V	Vg=3V	Vg=4V	Vg=5V
Vds=0V	2.628	2.741	2.758	2.664	2.63	2.449	2.613	2.667	2.515	2.568	2.397
Vds=0.5V	2.615	2.69	2.351	2.249	2.208	2.195	2.222	2.208	2.146	2.087	1.957
Vds=1V	2.451	2.521	2.204	2.316	2.24	2.303	2.332	2.251	2.187	2.194	2.134
Vds=1.5V	2.829	2.184	2.357	2.253	2.294	2.403	2.251	2.224	2.119	1.972	2.098
Vds=2V	2.825	2.074	2.186	2.193	2.23	2.284	2.159	2.183	1.977	2.095	2.303

Table 11 - $|\Delta I|$ (pA) values for the seventh FET of 50 UFC / 2μL *E. coli* concentration.

	Vg=-5V	Vg=-4V	Vg=-3V	Vg=-2V	Vg=-1V	Vg=0V	Vg=1V	Vg=2V	Vg=3V	Vg=4V	Vg=5V
Vds=0V	1.875	2.56	2.794	2.809	2.873	2.857	2.925	2.97	2.906	2.967	2.885
Vds=0.5V	1.416	0.987	0.71	0.727	0.616	0.533	0.531	0.529	0.533	0.566	0.575
Vds=1V	4.372	4.099	3.835	3.722	3.794	3.605	3.753	3.705	3.624	3.603	3.639
Vds=1.5V	7.437	7.11	7.002	6.939	6.898	6.873	6.893	6.869	6.859	6.757	6.918
Vds=2V	10.597	10.304	10.112	10.093	9.997	9.973	9.976	10.009	10.044	9.951	10.029

Table 12 - $|\Delta I|$ (pA) values for the eighth FET of 50 UFC / 2μL *E. coli* concentration.

	Vg=-5V	Vg=-4V	Vg=-3V	Vg=-2V	Vg=-1V	Vg=0V	Vg=1V	Vg=2V	Vg=3V	Vg=4V	Vg=5V
Vds=0V	9.275	9.258	8.908	8.74	8.089	7.873	7.559	7.408	7.213	6.882	6.777
Vds=0.5V	9.134	8.794	8.486	7.997	7.596	7.486	7.211	7.076	6.717	6.378	6.67
Vds=1V	8.951	8.691	8.297	7.719	7.453	7.247	7.008	6.756	6.324	6.086	6.09
Vds=1.5V	8.801	8.51	7.981	7.617	7.36	7.181	6.961	6.645	6.314	6.214	6.143
Vds=2V	8.903	8.5	7.997	7.679	7.409	7.24	6.866	6.559	6.362	6.269	6.119

Table 13 - $|\Delta I|$ (pA) values for the ninth FET of 50 UFC / 2μL *E. coli* concentration.

	Vg=-5V	Vg=-4V	Vg=-3V	Vg=-2V	Vg=-1V	Vg=0V	Vg=1V	Vg=2V	Vg=3V	Vg=4V	Vg=5V
Vds=0V	1.654	2.127	2.249	2.219	2.343	2.418	2.472	2.441	2.522	2.62	2.588
Vds=0.5V	1.446	1.929	1.969	2.252	2.488	2.252	2.274	2.316	2.328	2.348	2.327
Vds=1V	1.823	2.004	2.072	2.073	2.071	2.068	2.097	2.103	2.214	2.066	2.128
Vds=1.5V	1.533	1.749	2.073	2.104	2.024	2.091	2.074	2.255	2.261	2.185	2.335
Vds=2V	1.736	2.023	2.21	2.022	2.126	2.239	2.187	2.27	2.187	2.135	2.251

Table 14 - $|\Delta I|$ (pA) values for the tenth FET of 50 UFC / 2μL *E. coli* concentration.

	Vg=-5V	Vg=-4V	Vg=-3V	Vg=-2V	Vg=-1V	Vg=0V	Vg=1V	Vg=2V	Vg=3V	Vg=4V	Vg=5V
Vds=0V	0.069	0.202	0.38	0.455	0.562	0.691	0.763	0.795	0.727	0.773	0.901
Vds=0.5V	0.007	0.171	0.282	0.306	0.553	0.606	0.679	0.743	0.726	0.746	0.864
Vds=1V	0.262	0.211	0.25	0.386	0.492	0.648	0.552	0.568	0.505	0.719	0.715
Vds=1.5V	0.281	0.328	0.367	0.525	0.57	0.702	0.674	0.742	0.861	1.019	1.134
Vds=2V	0.397	0.46	0.469	0.715	0.778	0.811	0.797	0.853	0.959	1.014	0.898

Afterwards one averaged the values from all the Tables 5 to 14 to obtain the average drain-current variation value for the CNT-FETs treated with a certain *E. coli* concentration, in this case 50 UFC / 2μL. The end result is Table 15 which shows the average $|\Delta I|$ values for every gate voltage/source-drain voltage combination available. This process was done for all the seven *E. coli* concentrations with their respective CNT-FETs.

Table 15 - Average $|\Delta I|$ (pA) values for every gate voltage/source-drain voltage combination available within the 50 UFC / 2μL *E. coli* concentration CNT-FETs.

	Vg=-5V	Vg=-4V	Vg=-3V	Vg=-2V	Vg=-1V	Vg=0V	Vg=1V	Vg=2V	Vg=3V	Vg=4V	Vg=5V
Vds=0V	2.9364	3.132	3.1989	3.1927	3.0299	2.9772	2.8662	2.8338	2.7646	2.8812	2.8781
Vds=0.5V	2.9396	3.0135	2.9218	2.8269	2.8173	2.7733	2.7146	2.6691	2.5993	2.5785	2.5943
Vds=1V	3.2583	3.2669	3.1393	2.9547	3.0937	3.0058	3.0186	2.9331	2.8035	2.776	2.7504
Vds=1.5V	3.5522	3.508	3.4617	3.4403	3.4029	3.2938	3.3219	3.293	3.2091	3.1941	3.1634
Vds=2V	3.9692	4.1194	3.7991	3.6824	3.7963	3.6522	3.6248	3.5894	3.4689	3.5016	3.4502

By plotting the average $|\Delta I|$ values shown in Table 14, Figure 47, one can understand how the drain-current of CNT-FETs treated with a 50 UFC / 2μL *E. coli* concentration changed upon *E. coli* adsorption. For instance for a Source-Drain bias voltage of 1.5V the average $|\Delta I|$ was around 3.5 pA, whereas for a Source-Drain bias voltage of 0.5V the average $|\Delta I|$ was around 2.7 pA, Figure 56.

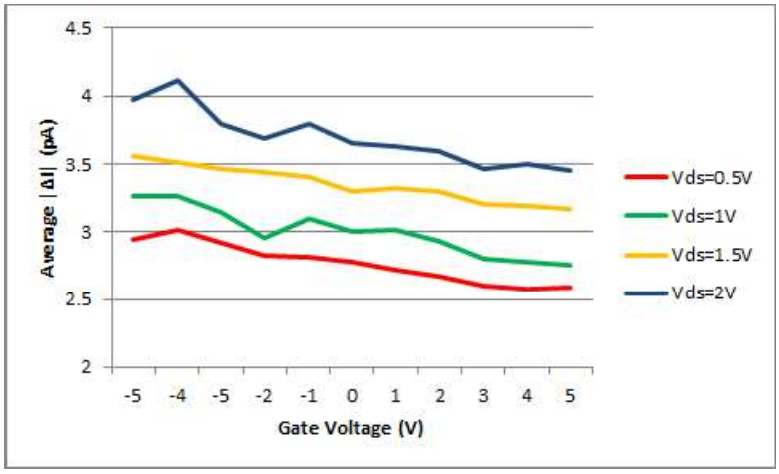

Figure 47 - Average | ΔI | values for the 10 CNT-FETs treated with 50 UFC / 2μL *E. coli*.

For example, on Figure 47 one can see that the CNT-FETs treated with a 50 UFC / 2μL *E. coli* concentration working with Vd= 1.5V and Vg = 3V, had an average variation of drain current between before and after *E. coli* of $\approx 3.3pA$. The steps described in this section were repeated for all the seven *E. coli* concentrations used, therefore one obtained seven Tables similar to Table 15.

5.3 Average drain current values screening

As stated before the objective of this study was to fabricate a point-of-care device capable of reading the CNT-FETs drain-currents, therefore a pico-ammeter. However, this pico-ammeter is quite rudimentary, and it will not be able to do DC sweeps, thus one needs to decide the best working parameters of the CNT-FET devices, a bias Gate voltage and a bias Source-Drain voltage. The gate voltages used in the CNT-FET characterization ranged from [-5V; 5V]. In order to fabricate a point-of-care device it is less expensive and space consuming to avoid negative voltages as they require in their simplest form two batteries. Therefore while choosing the operating parameters, in order to construct a calibration curve for CNT-FETs, one discarded the negative Gate voltages as well as gate voltage 0V as they would be harder to implement in a point-of-care device.

Another key factor of this screening to further help with the construction of a calibration curve was the discarding of the bias Source-Drain voltage of 0V, this measurement existed due the Agilent 4155C machine DC sweep method of operation.

After gathering the average | ΔI | for the seven *E. coli* concentrations used, explained in the "Average | ΔI | values" section. One obtained seven Tables similar to Table 15. Once the negative gate voltages and the 0V voltages were discarded, Table 15 became Table 16 without the negative Gate voltages and the null Source-Drain voltage average | ΔI | values. Therefore, Table 16 is comprised only of the average | ΔI | which correspond to Gate voltage/Source-Drain voltages that can be implemented in the point-of-care device. For instance, one can compare Table 15 with Table 16 to understand the screening.

Table 16 - The possible average | ΔI | values (pA) to implemented on the point-of-care device for the 50 UFC / 2μL *E. coli* concentration FETs.

	Vg=1V	Vg=2V	Vg=3V	Vg=4V	Vg=5V
Vds=0.5V	2.7146	2.6691	2.5993	2.5785	2.5943
Vds=1V	3.0186	2.9331	2.8035	2.776	2.7504
Vds=1.5V	3.3219	3.293	3.2091	3.1941	3.1634
Vds=2V	3.6248	3.5894	3.4689	3.5016	3.4502

This screening was done in all the data gathered for the CNT-FETs, and the end result were the Tables 17 to 23.

Table 17 - The possible average | ΔI | values (pA) to implemented on the point-of-care device for the 3 UFC / 2μL *E. coli* concentration FETs.

	Vg=1V	Vg=2V	Vg=3V	Vg=4V	Vg=5V
Vds=0.5V	1.381	0.830714286	0.896857143	0.595142857	0.894
Vds=1V	2.598571429	1.140142857	2.281857143	0.913	3.060142857
Vds=1.5V	2.769142857	1.219	1.289714286	1.388714286	2.975571429
Vds=2V	1.649714286	1.264	1.427142857	1.767285714	2.163428571

Table 18 - The possible average | ΔI | values (pA) to implemented on the point-of-care device for the 6 UFC / 2μL *E. coli* concentration FETs.

	Vg=1V	Vg=2V	Vg=3V	Vg=4V	Vg=5V
Vds=0.5V	0.94	1.1258	1.2066	1.2755	1.0106
Vds=1V	2.9173	2.8762	2.9117	2.8438	2.8037
Vds=1.5V	3.5961	3.4673	3.5111	3.3259	2.735
Vds=2V	3.4557	3.6009	3.3607	3.2651	3.078

Table 19 - The possible average | ΔI | values (pA) to implemented on the point-of-care device for the 12.5 UFC / 2μL *E. coli* concentration FETs.

	Vg=1V	Vg=2V	Vg=3V	Vg=4V	Vg=5V
Vds=0.5V	2.065222222	2.074222222	1.964222222	1.839555556	1.782222222
Vds=1V	2.712111111	2.690555556	2.632	2.583	2.781444444
Vds=1.5V	3.281777778	3.153333333	3.161888889	3.161888889	3.758555556
Vds=2V	3.548555556	3.559222222	3.443	3.486888889	3.822333333

Table 20 - The possible average | ΔI | values (pA) to implemented on the point-of-care device for the 25 UFC / 2μL *E. coli* concentration FETs.

	Vg=1V	Vg=2V	Vg=3V	Vg=4V	Vg=5V
Vds=0.5V	2.53	2.5019	2.3576	2.4727	2.3069
Vds=1V	2.9142	2.6756	2.6563	2.6045	2.5352
Vds=1.5V	3.4827	3.2851	3.002	2.9921	2.8405
Vds=2V	32.5241	31.9755	31.285	30.7446	30.5545

Table 21 - The possible average | ΔI | values (pA) to implemented on the point-of-care device for the 50 UFC / 2μL *E. coli* concentration FETs. (same as Table 15).

	Vg=1V	Vg=2V	Vg=3V	Vg=4V	Vg=5V
Vds=0.5V	2.7146	2.6691	2.5993	2.5785	2.5943
Vds=1V	3.0186	2.9331	2.8035	2.776	2.7504
Vds=1.5V	3.3219	3.293	3.2091	3.1941	3.1634
Vds=2V	3.6248	3.5894	3.4689	3.5016	3.4502

Table 22 - The possible average | ΔI | values (pA) to implemented on the point-of-care device for the 100 UFC / 2μL *E. coli* concentration FETs.

	Vg=1V	Vg=2V	Vg=3V	Vg=4V	Vg=5V
Vds=0.5V	3.4297	3.2227	3.0739	3.0018	2.9373
Vds=1V	5.9469	5.6769	5.5272	5.4165	5.2962
Vds=1.5V	8.4682	8.2063	8.0037	7.8358	7.7297
Vds=2V	11.0638	10.7098	10.468	10.2341	10.1424

Table 23 - The possible average $|\Delta I|$ values (pA) to implemented on the point-of-care device for the 200 UFC / 2μL *E. coli* concentration FETs.

	Vg=1V	Vg=2V	Vg=3V	Vg=4V	Vg=5V
Vds=0.5V	5.401	6.9436	7.3959	5.5748	5.2865
Vds=1V	9.5047	9.9751	9.7961	9.4504	9.6982
Vds=1.5V	12.4796	12.7684	11.9713	12.4534	12.5139
Vds=2V	13.6654	14.1673	13.7028	13.6535	13.8115

5.4 Calibration Scatter-plots

The scatter-plots obtained in this section were a critical step towards the correct design of the point-of-care device. To create the scatter-plots one organized the data from each of the Tables 17 to 23, according to the Gate Voltage/Source-Drain Voltages combinations, Tables 17 to 23 coloured cells are represented in Table 24. After organizing every value of the average $|\Delta I|$ per *E. coli* concentration one obtained Table 24.

Table 24 - Average $|\Delta I|$ values (pA) for all the *E. coli* concentration FETs, after organization. The coloured cells correspond to the coloured cells represented in Tables 17 to 23 and serve the purpose of simplifying the method of data organization according to the Gate voltage/Source-Drain voltage combinations for each *E. coli* concentrations.

Gate Voltage | Source-Drain Voltage	3.00	6.00	12.00	25.00	50.00	100.00	200.00
Vg=1V | Vds=0.5V	1.38	0.94	2.07	2.53	2.71	3.43	5.40
Vg=1V | Vds=1V	2.60	2.92	2.71	2.91	3.02	5.95	9.50
Vg=1V | Vds=1.5V	2.77	3.60	3.28	3.48	3.32	8.47	12.48
Vg=1V | Vds=2V	1.65	3.46	3.55	32.52	3.62	11.06	13.67
Vg=2V | Vds=0.5V	0.83	1.13	2.07	2.50	2.67	3.22	6.94
Vg=2V | Vds=1V	1.14	2.88	2.69	2.68	2.93	5.68	9.98
Vg=2V | Vds=1.5V	1.22	3.47	3.15	3.29	3.29	8.21	12.77
Vg=2V | Vds=2V	1.26	3.60	3.56	31.98	3.59	10.71	14.17
Vg=3V | Vds=0.5V	0.90	1.21	1.96	2.36	2.60	3.07	7.40
Vg=3V | Vds=1V	2.28	2.91	2.63	2.66	2.80	5.53	9.80
Vg=3V | Vds=1.5V	1.29	3.51	3.16	3.00	3.21	8.00	11.97
Vg=3V | Vds=2V	1.43	3.36	3.44	31.29	3.47	10.47	13.70
Vg=4V | Vds=0.5V	0.60	1.28	1.84	2.47	2.58	3.00	5.57
Vg=4V | Vds=1V	0.91	2.84	2.58	2.60	2.78	5.42	9.45
Vg=4V | Vds=1.5V	1.39	3.33	3.16	2.99	3.19	7.84	12.45
Vg=4V | Vds=2V	1.77	3.27	3.49	30.74	3.50	10.23	13.65
Vg=5V | Vds=0.5V	0.89	1.01	1.78	2.31	2.59	2.94	5.29
Vg=5V | Vds=1V	3.06	2.80	2.78	2.54	2.75	5.30	9.70
Vg=5V | Vds=1.5V	2.98	2.74	3.76	2.84	3.16	7.73	12.51
Vg=5V | Vds=2V	2.16	3.08	3.82	30.55	3.45	10.14	13.81

The curves in Figure 48 were obtained for each of the gate voltage/source-drain voltage combinations by doing a scatter-plot using Microsoft Excel.

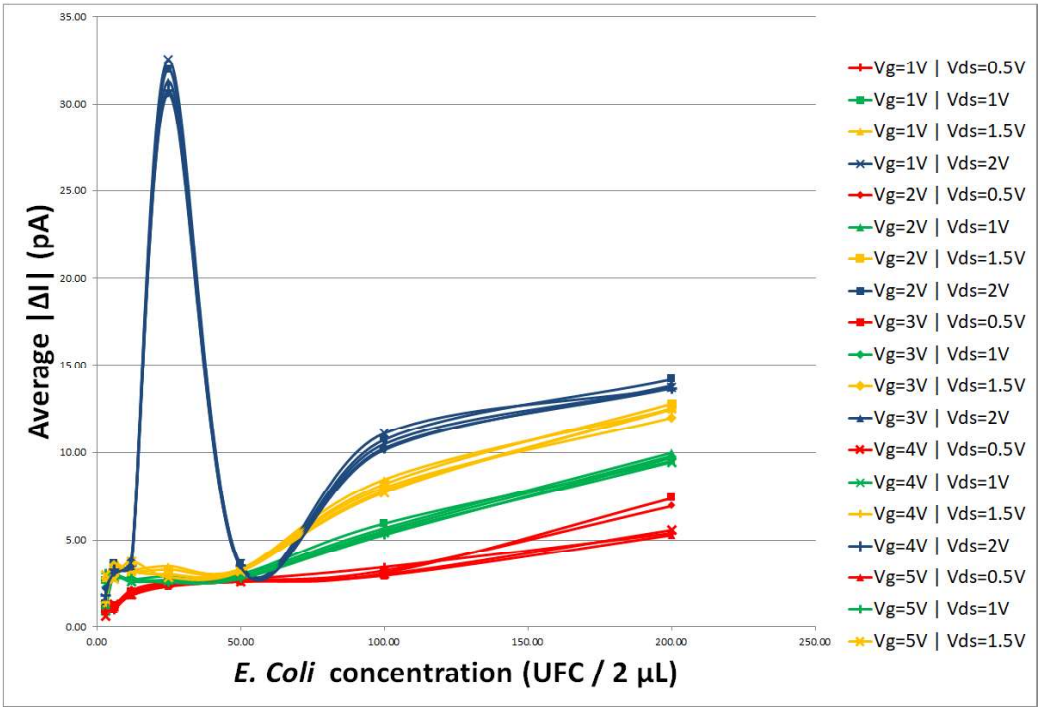

Figure 48 - Different scatter-plots obtained for each of the respective parameter combinations. Each scatter-plot corresponds to a Gate Voltage/Source-Drain Voltage combination.

As one can see, the scatter-plots obtained when the FETs are working with a Source-Drain bias voltage of 2V show a very peculiar peak of the average $|\Delta I|$ values at 25 UFC / 2 μL, therefore constructing a calibration curve with Vds = 2V was ruled out. Figure 49 shows the same line plots without Vds = 2V.

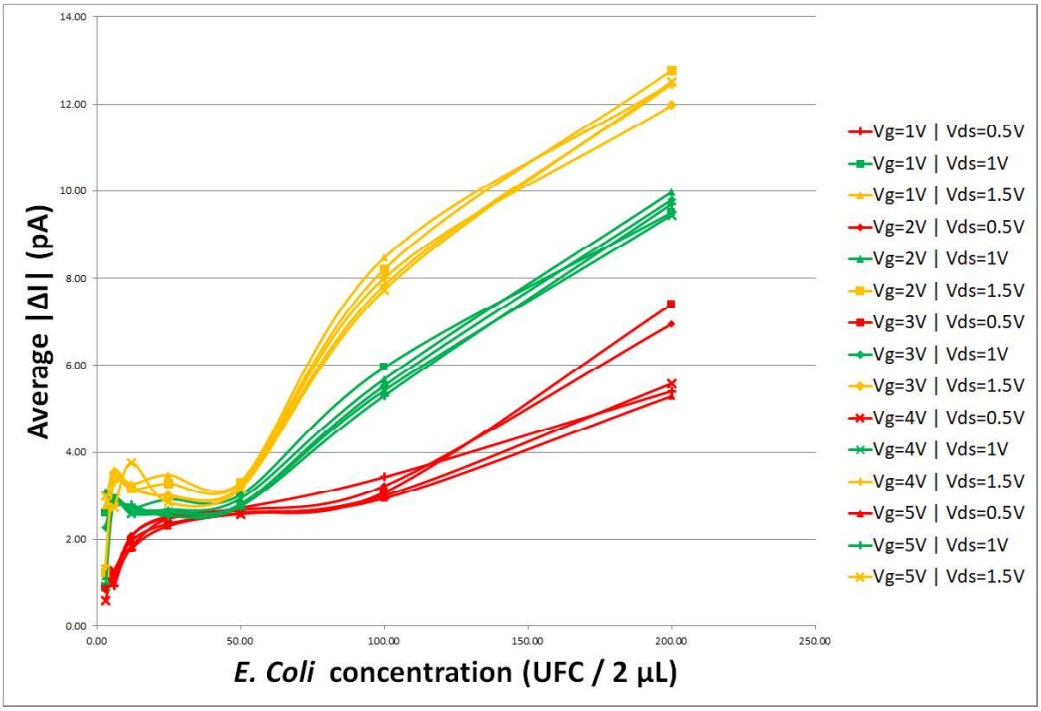

Figure 49 - Different scatter-plots obtained for each of the respective parameter combinations. Each scatter-plot corresponds to a Gate Voltage/Source-Drain Voltage combination.

By looking at all three scatter-plots present in Figure 49 one can distinguish three different zones in all three. From 0 to 25 UFC / 2μL there is a increase in the average $\mid \Delta I \mid$ this increase is rather abrupt. From 25 to 50 UFC / 2μL there is a period were apparently the average $\mid \Delta I \mid$ remains the same. Finally for the zone between 50 and 200 UFC / 2μL the device shows a splendid scatter-plot very close to a linear behaviour, which was the objective.

There is a possible explanation for these zones. The first zone (0 to 25 UFC / 2μL), which in fact is the detection of 3, 6, 12 and 25 bacterias, appears to be the range of concentration values in which Schotkky Barrier modulation dominates the sensing mechanism of the device. One deduces this zone as the Schottky Barrier zone of influence because Schottky Barriers are very sensitive to molecule adsorption and the adsorption of such a small number of *E. coli* cells does not carry a sufficient charge transfer to severely change the drain-current. As stated before, Schottky Barriers can change by adsorption of cells directly in the metal, changing its work function giving rise to a different alignment of the Fermi levels, which will lead to a thinning or thickening of the depletion zone culminating in a different drain-current. Or, Schottky Barriers can change when adsorption occurs in the surface of CNT-network near the metal/CNT contacts this changes the dipole layer and the applied electric field (gate voltage) around that space acting like an increased or a decreased gate voltage and inducing the depletion zone to change. In conclusion Schottky Barriers are very sensitive thus one supposes that they are responsible for the sensing at low concentrations.

Once enough bacteria adsorb in the premises of the contacts the Schottky Barriers reach a state where they can no longer can change, similar to the off-state or a saturation zone of a field-effect-transistor, it is not really an off state because the CNT-network, as seen before, contains metallic-SWCNTs that always conduct current thus a reminiscent current is present. This zone of either saturation of the CNT-FET or reminiscent ccurrent of CNT-FET would be zone 25 to 50 UFC / 2μL where the average $\mid \Delta I \mid$ remains the same.

The final zone 50 to 200 UFC / 2μL is the direct charge-transfer zone which apparently shows a linear behaviour, the more cells adsorbed the higher the average $\mid \Delta I \mid$ value.

While the Schottky barrier zone shows an overall increasing behaviour when the concentration increases, this zone has many irregularities. Therefore, according to these scatter-plots the minimum threshold of detection of these CNT-FET devices rests at 50 UFC / 2μL. And therefore the point-of-care device will aimed at testing concentrations no lower than 50 UFC / 2μL. Having reached this conclusion the average $\mid \Delta I \mid$ values for concentrations lower than 50 UFC / 2μL were discarded due to irregularities.

Althought the Scatter-plot that showed the best results between the 50 UFC / 2μL and 200 UFC / 2μL *E. coli* concentrations was the one shown in Figure 50 (Graph B), the Scatter-plot in (Graph A) also showed promising results, on top of these promising results was the fact that the source-drain bias voltage used in (Graph A) was 1.5V. Knowing that, in order to fabricate a point-of-care device one needs floating voltage supplies. One decided to chose the data represented in graph A to construct a calibration curve, this because 1.5V floating voltage supplies are quite common (Triple A batteries), whereas 1V batteries do not exist. Therefore one decided that the source-drain bias voltage to be used in order to operate the

CNT-FET devices was 1.5V for easiness of fabrication.

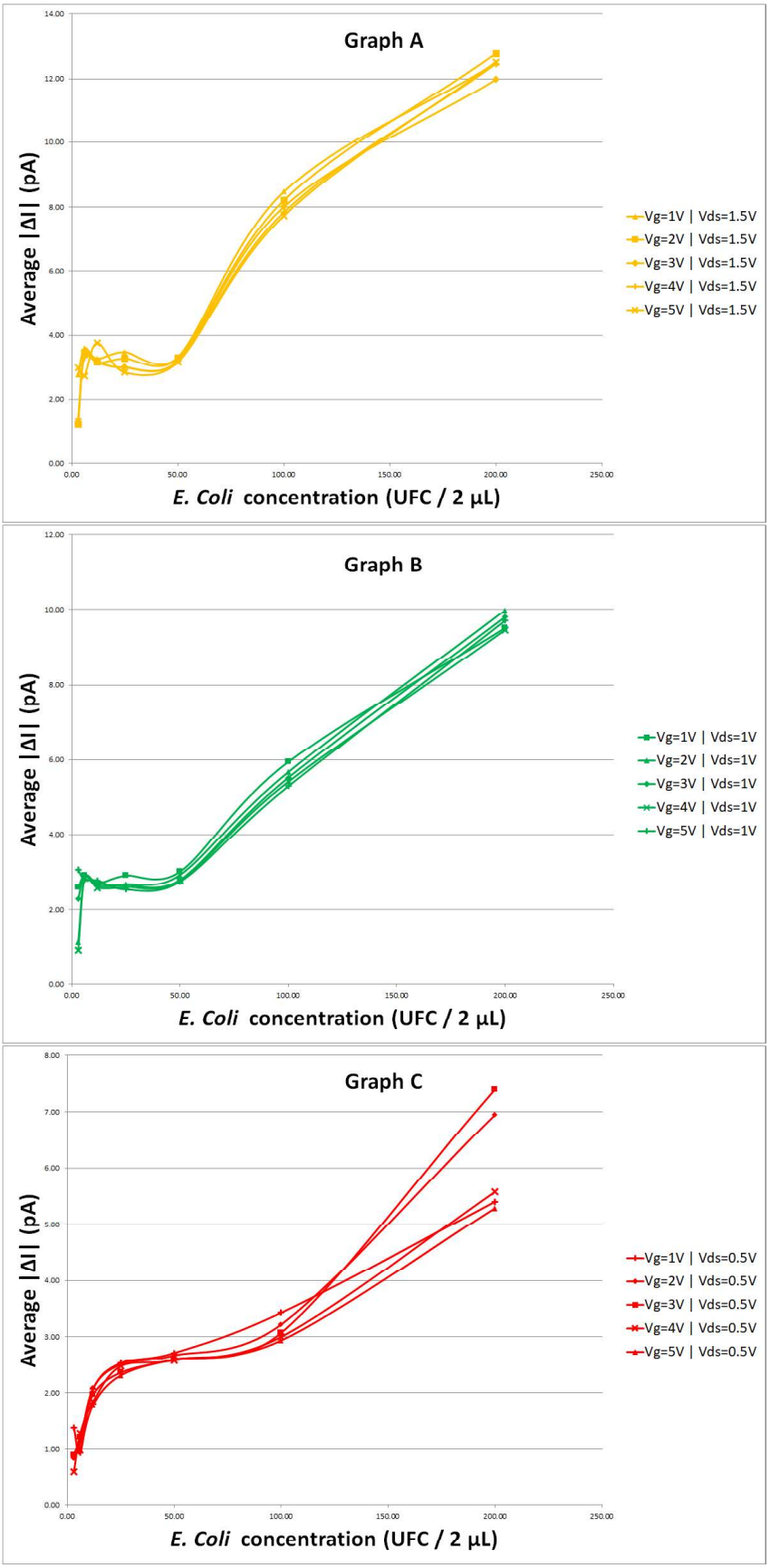

Figure 50 - Scatter-plots.In graph A Vds = 1,5 V. In graph B Vds = 1 V. Graph C Vds = 0,5 V. Each scatter-plot corresponds to a Gate Voltage/Source-Drain Voltage combination.

Now one needed to define the optimum gate voltage for the FETs to operate in. The main factor that came into play here was the fact that the gate voltage also needed to be a floating voltage supply, and, since the Arduino board has a 3.3 V floating voltage source and 3V batteries are rare. One decided to operate the CNT-FETs at around 3V (3.3V) for a mere easiness of fabrication. This was possible because all the gate voltages of Figure 50, Graph A, showed good scatter-plots, with very little difference between them. Figure 51 shows the scatter-plot after the screening of values and after determining the limits of detection of these CNT-FETs.

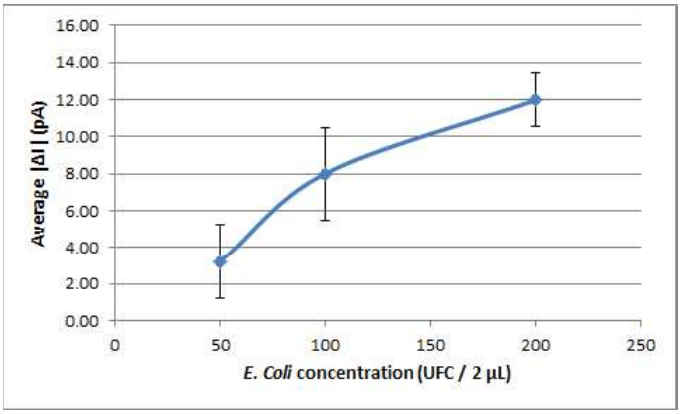

Figure 51 - Gate voltage of 3V and Source-Drain bias voltage of 1.5V scatter-plot, with respective error bars.

Since the error bars shown in Figure 50 show minimal overlapping of the average $\mid \Delta I \mid$ from one *E. coli* concentration to the other, one concluded this scatter-plot was a good candidate to construct our calibration curve. In order to obtain a more linear scatter-plot a Log_{10} normalization of the *E. coli* concentration values was done, Afterwards a linear regression was done in order to obtain the calibration curve. Figure 52 shows a scatter-plot of the normalized values, the calibration curve and the calibration curve equation.

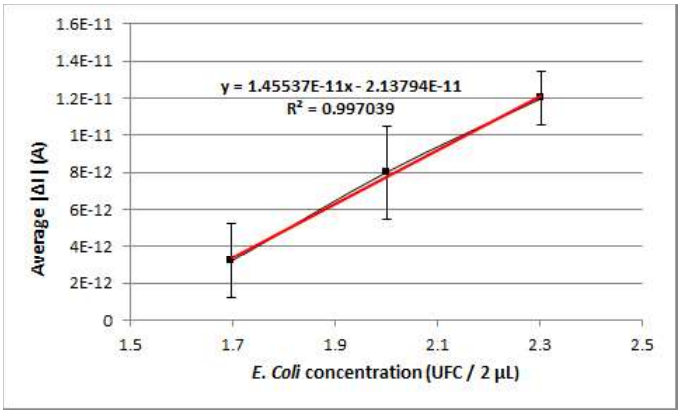

Figure 52 - Scatter-plot of the normalized values, the linear regression, calibration curve equation and R^2 test value.

As depicted in Figure 52 and according to the R^2 test value, which was above 0.99, the equation to be used in the point-of-care device is $y = 1.45537 * 10^{-11}x - 2.13794 * 10^{-11}$, however, accounting the Log_{10} normalization, the final equation to be implemented in the point-of-care device is Equation 4.

$$[E.Coli] = 10^{\frac{(\mid \Delta I \mid + 2.13794 * 10^{-11})}{1.45537 * 10^{-11}}}$$

Chapter 6

Implementation

6.1 Point-of-care device overview

As stated in the previous chapters of this study it was intended to build a point-of-care device capable of reading the drain currents of the FET devices using a personal computer. This device is a rudimentary DC picoameter, there is a lot of information mainly available in online forums that explain how to build such devices and the fundamental principles behind their workings (47–49). The premiss behind the workings of a picoameter is to amplify the currents while converting them into voltages. Since the CNT-FET operate with DC currents which are quite stable the most crucial step in the point-of-care device is the current amplification. It is imperative that the right operation amplifier (Op-Amp) is chosen, thankfully in this era of integrated circuits it is quite easy to acquire Op-Amps with extremely low input bias currents. This means that the Op-Amp is as close to an ideal Op-Amp as possible, although not ideal. The chosen Op-Amp for this study was a Texas Instruments LMC662 which has an ultra-low input bias current of 2 femto-ampere (50) this means that the Op-Amp draws in a 2 fA current which is lost and cannot be amplified, since the FETs operate at $\approx$ 10 pico-ampere the current drawn by the LMC662 Opamp is not relevant in the overall gain of the circuit. Figure 53 shows the LMC662 Opamp datasheet.

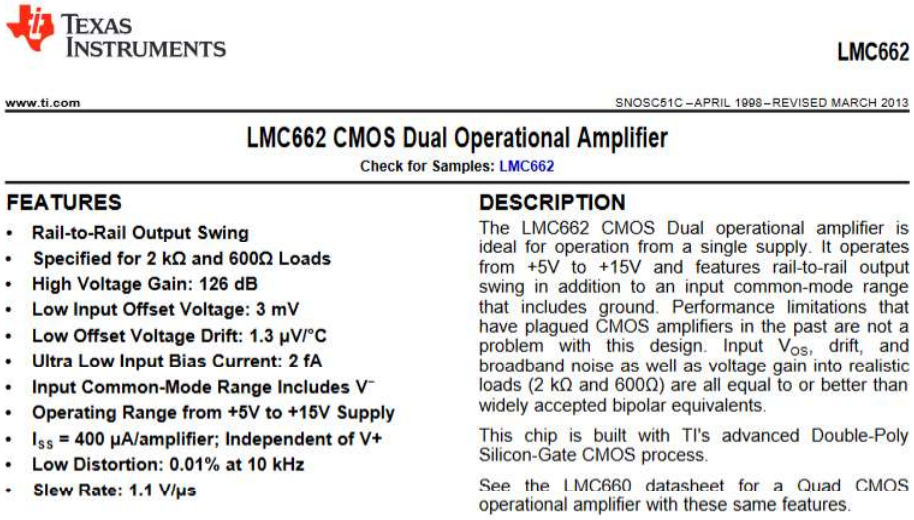

TEXAS INSTRUMENTS

LMC662

www.ti.com

SNOSC51C – APRIL 1998 – REVISED MARCH 2013

LMC662 CMOS Dual Operational Amplifier

Check for Samples: LMC662

FEATURES

- Rail-to-Rail Output Swing
- Specified for 2 kΩ and 600Ω Loads
- High Voltage Gain: 126 dB
- Low Input Offset Voltage: 3 mV
- Low Offset Voltage Drift: 1.3 µV/°C
- Ultra Low Input Bias Current: 2 fA
- Input Common-Mode Range Includes V^-
- Operating Range from +5V to +15V Supply
- I_{SS} = 400 µA/amplifier; Independent of V+
- Low Distortion: 0.01% at 10 kHz
- Slew Rate: 1.1 V/µs

DESCRIPTION

The LMC662 CMOS Dual operational amplifier is ideal for operation from a single supply. It operates from +5V to +15V and features rail-to-rail output swing in addition to an input common-mode range that includes ground. Performance limitations that have plagued CMOS amplifiers in the past are not a problem with this design. Input V_{OS}, drift, and broadband noise as well as voltage gain into realistic loads (2 kΩ and 600Ω) are all equal to or better than widely accepted bipolar equivalents.

This chip is built with TI's advanced Double-Poly Silicon-Gate CMOS process.

See the LMC660 datasheet for a Quad CMOS operational amplifier with these same features.

Figure 53 - Texas Instrumets LMC662 datasheet (50).

A typical current to voltage amplifying circuit is a simple inverting Opamp with a resistor as depicted in Figure 54.

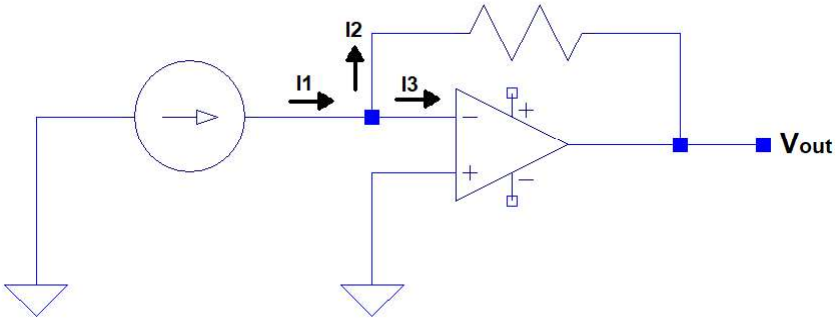

Figure 54 - current to voltage amplifying circuit.

The circuit shown above, Figure 54, works according to the following principles. Since the input bias current of the Opamp ($I3 = 2fA$) is around 4 orders of magnitude lower than the drain-current ($I1 \approx 10pA$) of the CNT-FET device, exemplified in Figure 54 as a current source, one can say that I1 = I2, thus by Ohm's law $V_{out} = I1 * R$. Knowing this, by changing the resistor one can change the gain of the circuit, a high resistance resistor sustains a higher gain for the circuit. Knowing that the CNT-FETs operate at ≈ 10 pA and that the Arduino board can measure current in the mV range, the resistor chosen to operate this circuit was a 10GΩ Resitor ($1 * 1^{10}\Omega$) acquired from eBay, this allowed for an overall gain of $1 * 1^{10}$ times, meaning 10pA current could be transformed into 10mV voltages. Similar circuits have been constructed by engineers, Figure 55 shows one of the circuits in which this device was based.

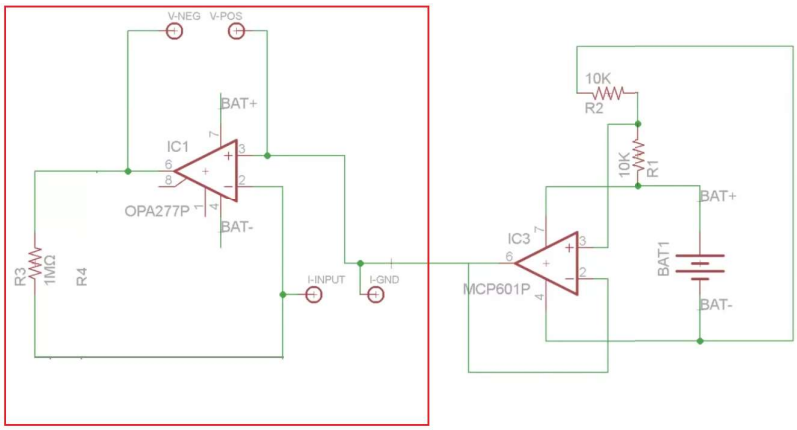

Figure 55 - Precision low current ammeter. The red square represents the current to voltage amplifying circuit (49).

Comparing the red square from Figure 55 with the circuit from Figure 54, one can understand better the circuit, the "I-INPUT" in Figure 55, is the current source (CNT-FET device) in Figure 54, "V-NEG" is V_{out}, the ground references in Figure 54 are "V-POS" and "I-GND" in Figure 55 and the R3 resistor in Figure 55 is the 10GΩ Resitor shown in Figure 54. In order to maintain this device portable, instead of bench-top power supplies to provide the gate voltage, the source-drain voltage and the Opamp supply voltages, one used the 3.3V output pin of the Arduino board, a triple A 1.5V battery and two 9V batteries

to provide +9V and -9V to the Opamp, respectively (51,52). The overall schematic of the circuit can be seen in Figure 56(a). This circuit was assembled in a bread board has shown in Figure 56(b).

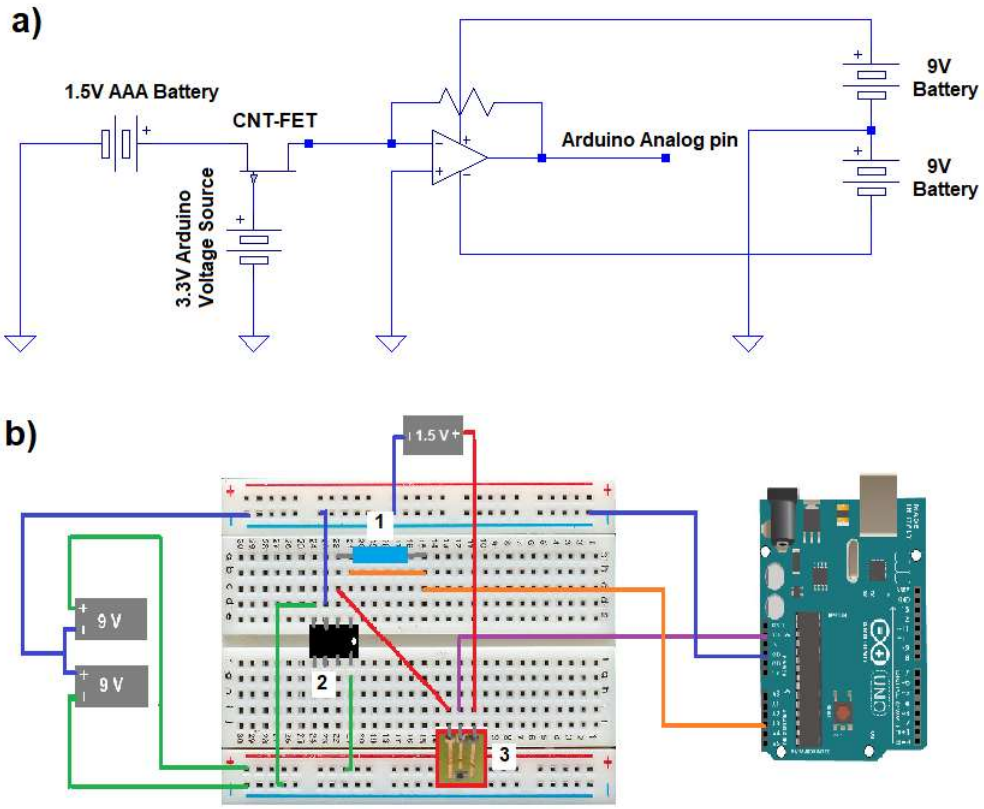

Figure 56 - (a) Schematic of the point-of-care device circuit, (b) circuit assembled in a Breadboard. (1) 10Gohm Resistor, (2) Texas Instruments LMC662 Op-Amp, (3) CNT-FET.

6.2 Arduino board and floating voltage supplies

In this section this device was to be connected to an Arduino UNO board in order to transform the DC analog voltage signal into a digital signal so that MATLAB could interpret this signal. To achieve that the Arduino board GND pin was connected to the ground reference of the circuit shown in Figure 56(a), the 3.3 V voltage source (floating voltage source) pin was connected to the gate electrode, and V_{out} was connected to one of the analog input pins of the Arduino board (A1 to A5), Figure 56(b) shows the wiring of the Arduino board connected to the breadboard circuit, the analog pin chosen was pin A3.

The floating voltage supplies as stated before, were done using batteries. A triple A 1.5V battery was used to provide the floating voltage of 1.5V needed to apply the source-drain bias voltage, Figure 56 shows the battery wiring. The last voltage sources of the circuit were the Opamp suppliers which needed to output a floating voltage anywhere between $\pm$ 5V to $\pm$ 15V as shown in Figure 53, to accomplish this two 9V batteries were connected in series and the ground reference of these two batteries was placed in between them, this allowed one to obtain -9V and +9V. Since the current to voltage amplifier intended to amplify pA into mV having an Op-amp working in a range between -9V and 9V ensured that the device

would not saturate, Figure 56 shows the wiring of the 9V batteries. The whole device was placed inside a shielding aluminium box to prevent any current leakages of the system, Figure 57.

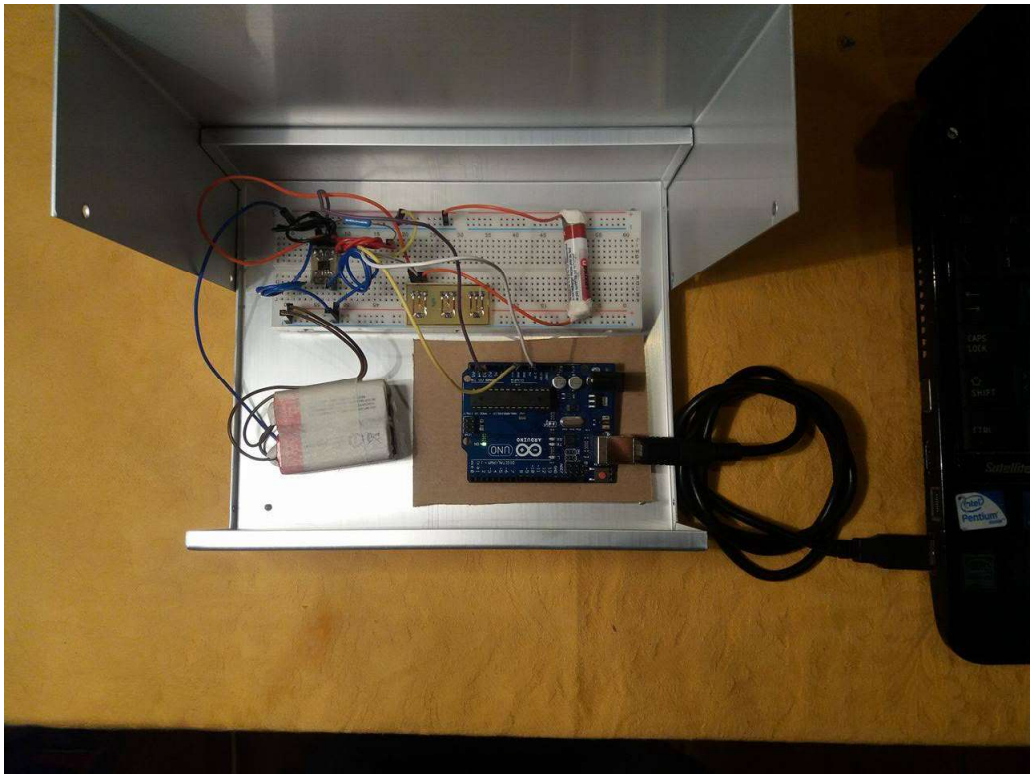

Figure 57 - Point-of-care device circuit inside shielding box connected to a personal computer. The Arduino board is on top of an insulating material to prevent short-circuiting.

6.3 MATLAB

One of the fundamental functions of the Arduino board for this device was the ”readVoltage” function which allows one to read the input voltage at any of the Arduino UNO analog pins (A1 to A5), this function can be called via MATLAB. To connect the Arduino board one needs to install the Arduino package in MATLAB this allows to create a bridge between the Arduino and MATLAB directly. To establish such connection one needs to call the ”arduino” function, and, afterwards the ”readVoltage” function, Figure 58.

Figure 58 - MATLAB Arduino connection and "readVoltage" function, this function was used until the voltage stabilized in this case at ≈ 0.17V taking into consideration the overall gain of this circuit $1 * 10^{10}$ times, the current flowing in the CNT-FET channel is around 17pA or $1.7 * 10^{-11}$A.

As seen in the data analysis chapter this device works by doing the difference in drain-current between the CNT-FET with antibody and the CNT-FET with antibody and *E. coli*.
This point-of-care device was tested, mainly to assess its quality, with the already used CNT-FETs, not only to quickly see if the drain-current values measured were in agreement with the ones obtained in University of Aveiro using the Agilent 4155C machine, but also to serve has a proof of concept that these FETs can be used in a point-of-care system to quickly assess water quality.

The CNT-FET used for this experiment, Figure 58, was treated with 100 UFC / 2μL of *E. coli* concentration. Further one will calculate the difference in current between the FET with antibody (previously gathered data in University of Aveiro) and the FET with antibody and *E. coli* (data gathered with the point-of-care device) and understand if this $\mid \Delta I \mid$ value corresponds, in fact, to the 100 UFC / 2μL concentration in the calibration curve obtained in the data analysis chapter.

To accomplish this one needed to created a simple table of values corresponding to the drain current of the all CNT-FETs when immobilized solely with antibody and working with Vg = 3V and Vd = 1,5V. The fact that the FETs were immobilized with the exact same quantity of antibody allowed, by averaging all the drain current values of the FETs in the working parameters of the point-of-care device, to obtain an average drain-current value for the CNT-FETs with only antibody immobilized. This value of drain-current would serve was the initial drain-current in order to obtain $\mid \Delta I \mid$. Table 25 shows all the collected drain-current values for the CNT-FETs operating with Vg = 3V and Vd = 1.5V, while immobilized solely with anti-*E. coli* antibody.

Table 25 - All drain current values (A) of the 69 FETs immobilized solely with antibody.

Id Value	FET Nº	Id Value	FET Nº	Id Value	FET Nº
2.63E-12	1	7.29E-12	24	2.59E-12	47
3.38E-12	2	2.99E-12	25	2.13E-11	48
4.65E-12	3	3.06E-12	26	2.18E-12	49
6.54E-11	4	3.27E-12	27	2.76E-12	50
1.36E-11	5	3.25E-11	28	2.34E-12	51
7.45E-12	6	2.93E-12	29	2.81E-12	52
9.67E-12	7	9.26E-12	30	2.50E-12	53
4.44E-12	8	1.87E-12	31	3.24E-12	54
3.04E-12	9	2.62E-12	32	2.43E-12	55
3.12E-12	10	4.27E-11	33	2.40E-12	56
2.72E-12	11	2.71E-12	34	5.17E-12	57
1.27E-11	12	4.51E-11	35	2.38E-12	58
3.04E-12	13	4.02E-12	36	2.39E-12	59
5.01E-11	14	2.46E-12	37	6.36E-12	60
6.42E-12	15	2.24E-12	38	2.35E-12	61
3.29E-12	16	2.72E-12	39	2.71E-12	62
3.48E-12	17	2.46E-12	40	2.60E-12	63
6.49E-11	18	2.62E-12	41	2.28E-12	64
9.92E-12	19	2.38E-12	42	2.37E-12	65
1.16E-11	20	2.47E-12	43	2.63E-12	66
4.11E-11	21	9.36E-12	44	9.36E-12	67
3.29E-12	22	2.57E-12	45	7.27E-12	68
3.44E-11	23	2.53E-12	46	6.33E-12	69

The average value of the drain-current measured was $9.49594202 * 10^{-12}A$ roughly $9.5 * 10^{-12}A$, this as stated before is a crucial value in the development of the point-of-care device as it is the base value to calculate the $\mid \Delta I \mid$ value that correlates with the *E. coli* concentration in the water as seen in Figure 59. Therefore, using the values obtained in Figure 58 one can calculate the current variation $\mid \Delta I \mid = 17 * 10^{-12} - 9.4959420 * 10^{-12}$. In this case $\mid \Delta I \mid = 7.5 * 10^{-12}A$. Using the calibration curve, Equation 4, Figure 59, one can quickly see that the CNT-FET tested in this experiment has a drain current variation that in fact correlates with a 100 UFC / 2μL *E. coli* concentration.

$$[E.Coli] = 10^{\frac{(7.5 * 10^{-12} + 2.13794 * 10^{-11})}{1.45537 * 10^{-11}}}$$

$$[E.Coli] = 96.45\frac{UFC}{2\mu L}$$

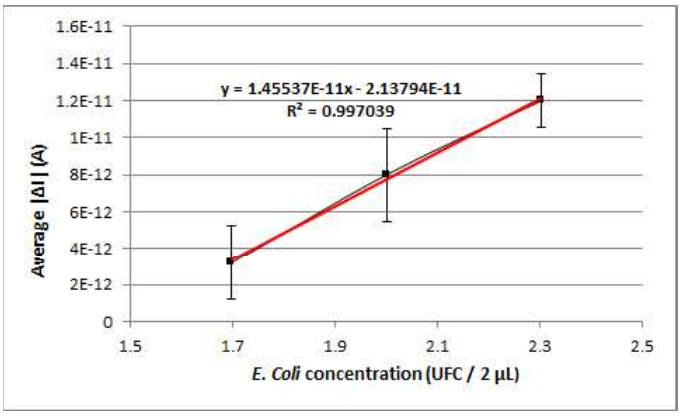

Figure 59 - Scatter-plot of the normalized values, the linear regression, calibration curve equation and R^2 test value.

6.4 Final MATLAB script

One key parameter to reduce error in the point-of-care device readouts was to implement an average making function, this function averages 100 values of the ”readVoltage” function into a value that will correspond to the drain-current in the FET channel in a more accurate way.

Another part of the MATLAB script was the implementation of a function that correlated the voltage sensed in the analog pin of the Arduino board with the drain-current flowing inside the CNT-FET channel (gain of the circuit). This function is a mere division of the average ”readVoltage” function values by the overall gain of the circuit ($1 * 10^{10}$).

Also one needed to calculate the $\mid \Delta I \mid$ value using the base value of $9,50 * 10^{-12} A$. Lastly, one needed to implement the calibration curve, Equation 4, onto the script so that the script could give out a *E. coli* concentration value. Figure 60 shows the final MATLAB script.

```
1     %a = arduino;
2 -   NumberOfReadings = 100;
3 -   analog = zeros(1,NumberOfReadings);
4 -   test = 0
5
6
7 -       test = 1;
8 -       AllValues = 0;
9
10 -  for index = 1:NumberOfReadings
11 -      analog(index) = readVoltage(a,'A3');
12 -      AllValues = analog(index) + AllValues;
13 -      pause (.1);
14 -      plot (analog);
15 -      ylim([-1 1]);
16 -      ylabel('Voltage');
17
18 -  end
19
20 -  AveValue = AllValues/NumberOfReadings;
21 -  DrainCurrent = AveValue/(1*10^11);
22 -  DeltaCurrent = ((DrainCurrent - (9.4959420*10^-12))^2)^(1/2);
23 -  E.Coli = 10^((DeltaCurrent+(2.13794*10^(-11)))/(1.45537*10^(-11)));
24 -  fprintf ('test %d = %.4f \n', test, AveValue)
25 -  fprintf ('Drain Current = %.14f \n', DrainCurrent)
26 -  fprintf ('Current Variation = %.14f \n', DeltaCurrent)
27 -  fprintf ('E.coli = %.3f \n', E.Coli)
28
29
```

Figure 60 - MATLAB script.

The script shown in Figure 60 starts by defining the number of readings which were set at 100 readings, next a zeros matrix with one column is defined with a number of rows equal to the number of readings. The ”for” cycle reads the analog pin voltage of pin A3 in the Arduino board and adds it to the AllValues string, each readout value has an interval of 0.1 seconds, while the ”for” cycle is running each value is plotted on the Graph window. The final steps are the conversion ones. Firstly, the average value of all the 100 readings is calculated (AveValue - Line 20) then the overall gain of the circuit is taken into consideration to calculate the drain-current of the CNT-FET (DrainCurrent - Line 21). Using the base value of $9,50 * 10^{-12} A$ the current variation is obtained (DeltaCurrent - Line 22) and using Equation 4

$$[E.Coli] = 10^{\frac{(\mid \Delta I \mid + 2.13794 * 10^{-11})}{1.45537 * 10^{-11}}}$$

the *E. coli* concentration is calculated (E. Coli - Line 23). Finally, each value is printed in the command window, (Lines 24-27).

For a CNT-FET with 100 UFC / 2μL the following results were obtained, Figure 61. Drain-Current 2,8pA. Current Variation 6,68pA. *E. coli* $\approx$85 UFC / 2μL.

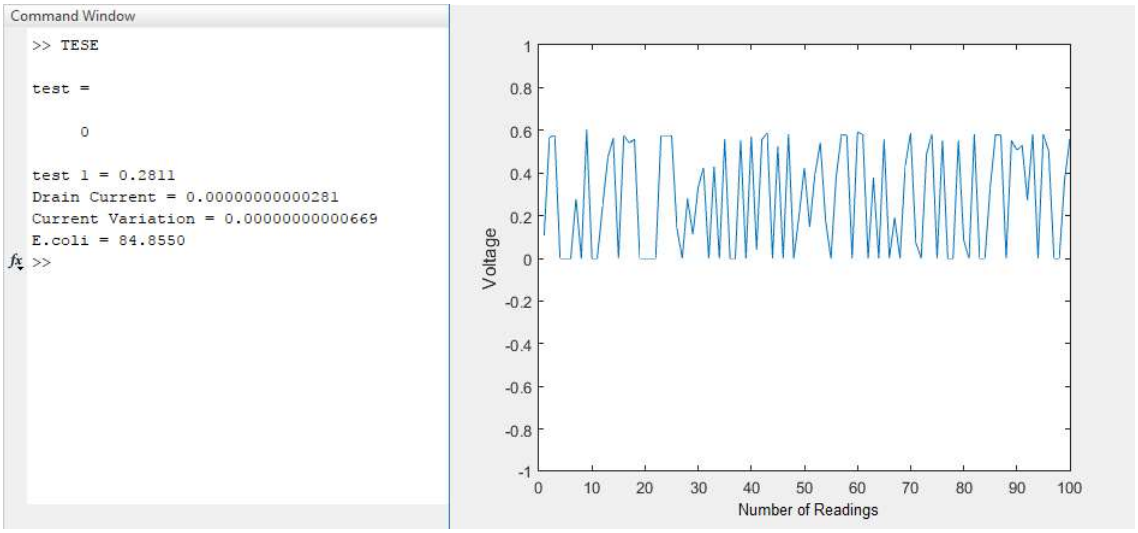

Figure 61 - Test results for a CNT-FET with 100 UFC / 2μL *E. coli* concentration.

Chapter 7

Conclusions

CNT-FETs are, in fact, very powerful tools for biosensing applications, and, in this study it was concluded that CNT-FETs can be used to assess water quality, even though these sensors still require further research, it was proven that they are capable of detecting bacteria or other molecules. Althoght the lower threshold of detection of these sensor was set at 50 UFC / 2μL (Chapter 4, section 4.7), this was done mainly to ensure a better working of the point-of-care device. From 50 UFC / 2μL until 200 UFC / 2μL the CNT-FETs showed a very good behaviour, almost linear. For low concentrations the CNT-FETs showed a irregular behaviour, none-the-less, with the increase in *E. coli* concentration the $\mid \Delta I \mid$ also increased, however for these low concentrations it was not possible to discriminate the *E. coli* values based on the ,measured drain-currents (Chapter 4, section 4.7). This was because although the average $\mid \Delta I \mid$ value of the 3 UFC / 2μL was lower than the one for 6 UFC / 2μL. Their standard deviations overlapped between *E. coli* concentrations. This made it extremely difficult to discriminate the lower concentrations from each other.

For the higher concentrations the discrimination of *E. coli* concentration was easier, because the average $\mid \Delta I \mid$ were very distanced and the standard deviation for each *E. coli* concentration value showed minimal overlap Figure 51.

7.1 Major Achievements

In this study the major achievements were, reaching the objective of effectively manufacture a CNT-FET biosensor capable of detecting waterborne bacteria, which was accomplished.

Nonetheless to be able to fabricate such device several steps were crucial, one of which was obtaining a good Carbon Nanotube dispersion this was achieved by using sodium cholate and several dilutions until a final dispersion was achieved, showing the ideal characteristics. Another great step in this study was obtaining a method of deposition for the Carbon Nanotubes that ensured that the CNT-FETs were working in the same range of values, achieving this also increased the reproducibility of results, this objective was achieved with a dielectrophoretic deposition method, and it ultimately allowed for the creation of a point-of-care device that could not only sense the drain-current of the CNT-FET but also correlate this

current to the *E. coli* concentration present in the water sample.

In conclusion, this study was able to successfully develop a CNT-FET capable of detecting bacteria quantities as low as 50 bacterias in water samples.

References

1. Pandey PK, Kass PH, Soupir ML, Biswas S, Singh VP. Contamination of water resources by pathogenic bacteria. *AMB Express*. 2014:1-16.

2. Taylor P, Bradford SA, Morales VL, et al. Transport and Fate of Microbial Pathogens in Agricultural Settings. *Crit Rev Environ Sci Technol*. 2013;43(December 2014):775-893. doi:10.1080/10643389.2012.710449.

3. Prevention C for DC and. Surveillance Surveillance for Waterborne-Disease Outbreaks — United States , 1993 – 1994. *Morb Mortal Wkly Rep*. 1996:1-45.

4. Ali SH. A socio-ecological autopsy of the E . coli O157 : H7 outbreak in Walkerton , Ontario , Canada. *Elsevier*. 2004;58:2601-2612. doi:10.1016/j.socscimed.2003.09.013.

5. Hu P, Zhang J, Li L, Wang Z, Estrela P. Carbon Nanostructure-Based Field-Effect Transistors for Label-Free Chemical/Biological Sensors. *Sensors*. 2010:5133-5159. doi:10.3390/s100505133.

6. Yang N, Chen X, Ren T, Zhang P, Yang D. Carbon nanotube based biosensors. *Sensors Actuators, B Chem*. 2015;(PartA):690-715. doi:10.1016/j.snb.2014.10.040.

7. Grove-rasmussen K. *Electrical Properties of Carbon Nanotubes*.; 2000.

8. Tîlmaciu C, Morris MC. Carbon nanotube biosensors. *Front Chesmitry*. 2015;3(October):1-21. doi:10.3389/fchem.2015.00059.

9. Zhang X, Wang D, Yang D, Li S, Shen Z. Electronic Detection of Escherichia coli O157 ： H7 Using Single-Walled Carbon Nanotubes Field-Effect Transistor Biosensor. *Sci Res*. 2012;2012(October):94-98. doi:10.4236/eng.2012.410B024.

10. Li J, Lu Y. Carbon Nanotube Based Chemical Sensors for Space and Terrestrial Applications. *ECS Trans*. 2009;19:7-15.

11. Molaie M. Field effect transistor nanobiosensors : State-of-the-art and key challenges as point of care testing devices. *Nanomed*. 2016;3(2):69-82. doi:10.7508/nmj.2016.02.001.

12. Pujadó MP. *Carbon Nanotubes as Platforms for Biosensors with Electrochemical and Electronic Transduction*.; 2012.

13. Yang D, Wang L, Zhao Q, Li S. Fabrication Of Single-Walled Carbon Nanotubes (SWNTs) Field-Effect Transistor (FET) Biosensor. *Int Conf Biomed Eng Informatics*. 2010:1482-1485.

14. Kang D, Park N, Ko J, Bae E, Park W. Oxygen-induced p-type doping of a long individual single-walled carbon nanotube. *Nano*. 2005:1048-1052. doi:10.1088/0957-4484/16/8/008.

15. Sagadevan S, Periasamy M. Recent trends in nanobiosensors and their applications – A Review. *Rev Adv Mater Sci*. 2014;36:62-69.

16. Rao CNR, Voggu R. Charge-transfer with graphene and nanotubes. *Mater Today*. 2010;13(9):34-40. doi:10.1016/S1369-7021(10)70163-2.

17. Agarwal S. Metal Carbon Nanotube Schottky Barrier Diode with Detection of Polar Non-Polar Gases. *15th Int Conf Embed Syst*. 2016:361-366. doi:10.1109/VLSID.2016.107.

18. Jiménez D, Cartoixà X, Miranda E, Suñé J, Chaves F a, Roche S. A simple drain current model for Schottky-barrier carbon nanotube field effect transistors. *Nanotechnology*. 2007;18(41):419001. doi:10.1088/0957-4484/18/41/419001.

19. Ali Javey JK. *Carbon Nanotube Electronics*.; 2009.

20. Saito R, Fujita M, Dresselhaus G, et al. Electronic structure of chiral graphene tubules structure of chiral graphene tubules. *Applies Phys Lett*. 2012;2204(May):67-70. doi:10.1063/1.107080.

21. M. S. Dresselhaus, G. Dresselhaus PCE. *Science of Fullerenes and Carbon Nanotubes. Their Properties and Applications (1996)*.; 1996.

22. Aldrich S. CAS 308068-56-6|704121. :63103.

23. Heller I, Janssens AM, Ma J, Minot ED, Lemay SG, Dekker C. Identifying the Mechanism of Biosensing with Carbon Nanotube Transistors. *Nano Lett*. 2008;8(2):591-595.

24. Chen J, Klinke C, Afzali A, Avouris P, Heights Y. Air-Stable Chemical Doping of Carbon Nanotube Transistors. *IEEE*. 2003:137-138.

25. Derycke V, Martel R, Appenzeller J, Avouris P. Controlling doping and carrier injection in carbon nanotube transistors. *Appl Phys Lett*. 2002;80(15):2773-2775. doi:10.1063/1.1467702.

26. Dang T, Anghel L, Leveugle R. CNTFET basics and simulation. *Int Conf Des Test Integr Syst Nanoscale Technol*. 2006:28-33. doi:10.1109/DTIS.2006.1708731.

27. Gong M, Shastry TA, Cui Q, et al. Understanding Charge Transfer in Carbon Nanotube-Fullerene Bulk Heterojunctions. *ACS Appl Mater Interfaces*. 2015:2-26. doi:10.1021/acsami.5b01536.

28. Lee K, Kong J. Chemical Sensing with SWNT FETs. *IEEE*. 2009:191-207. doi:10.1007/978-0-387-69285-2.

29. Villamizar RA, Maroto A, Rius FX. Chemical Improved detection of Candida albicans with carbon nanotube field-effect transistors. *Sensors Actuators B*. 2009;136:451-457. doi:10.1016/j.snb.2008.10.013.

30. Liu W, Hierold C, Haluska M. Electrical contacts to individual SWCNTs : A review. *Beilstein J Nanotechnol*. 2014:2202-2215. doi:10.3762/bjnano.5.229.

31. Pachauri V, Ingebrandt S. Biologically sensitive field-effect transistors : from ISFETs to NanoFETs. *Essays Biochem*. 2016;(June):81-90. doi:10.1042/EBC20150009.

32. Lee CY, Baik S, Zhang J, Masel RI, Strano MS. Charge Transfer from Metallic Single-Walled Carbon Nanotube Sensor Arrays. *J Phys Chesmistry B*. 2006:11055-11061.

33. Zhao J, Buldum A, Han J, Lu JP. Gas molecule adsorption in carbon nanotubes and nanotube bundles. *Nanotechnology*. 2002;13:195-200.

34. Bushmaker AW, Oklejas V, Walker D, Hopkins AR, Chen J, Cronin SB. Single-ion adsorption and switching in carbon nanotubes. *Nat Commun*. 2016;7:1-8. doi:10.1038/ncomms10475.

35. Belkhamssa N, Justino CIL, Santos PSM, et al. Label-free disposable immunosensor for detection of atrazine. *Talanta*. 2016;146:430-434. doi:10.1016/j.talanta.2015.09.015.

36. Strano MS, Moore VC, Miller MK, et al. The Role of Surfactant Adsorption during Ultrasonication in the Dispersion of Single-Walled Carbon Nanotubes. *J Nanosci Nanotechnol*. 2003;3(1):81-86. doi:10.1166/jnn.2003.194.

37. Aldrich S. Exfoliation and Debundling Procedure for Single-walled Carbon Nanotubes.

38. Shi Y, Ren L, Li D, Gao H, Yang B. Optimization Conditions for Single-Walled Carbon Nanotubes Dispersion. *Sci Res*. 2013;(January):6-12.

39. Aldrich S. CAS 206986-87-0 | 24892867. :63103.

40. Maehashi K, Matsumoto K. Label-free electrical detection using carbon nanotube-based biosensors. *Sensors*. 2009;9(7):5368-5378. doi:10.3390/s90705368.

41. Gmbh P. Absorption Spectroscopy as a Powerful Technique for the Characterization of Single-Walled Carbon Nanotubes. *Perkin Elmer*. 2007:4-9.

42. Jason Moscatello, Vijaya Kayastha, Archana Pandey, Benjamin Ulmen and YKY. Dielectrophoretic Deposition of Carbon Nanotubes with Controllable Density and Alignment. *Mater Res Soc*. 2008;1057:2-7.

43. Sarker BK, Shekhar S, Khondaker SI. Semiconducting enriched carbon nanotube align arrays of tunable density and their electrical transport properties. *Nano Lett*.:23-26.

44. Moraes MC, Galeazzo E, Peres HEM, Dantas MOS, Ramirez-Fernandez FJ. Electrical behavior of devices composed by dielectrophoretically deposited carbon nanotubes for gas sensing applications. *2014 29th Symp Microelectron Technol Devices Chip Aracaju, SBMicro 2014*. 2014:5-8. doi:10.1109/SBMicro.2014.6940131.

45. Zhang X, Wang D, Yang D, Li S. Field-effect Transistor Biosensor Fabricated With Selective Enrichment of Semiconducting Single- Walled Carbon Nanotubes. *2012 Int Conf Biomed Eng*. 2012;(February):27-28.

46. AbCam. Product datasheet Anti-E . coli antibody ab13627. :1-2.

47. Yates A. Alan Yates' Laboratory - Picoammeter. http://www.vk2zay.net/article/251. Published 2010.

48. EEVblog Electronics Community Forum. Picoammeter Design. https://www.eevblog.com/forum/projects/picoammeterdesign/msg790045/?PHPSESSID=onm5o5fg8ov5edgj0tr6mcpl2#msg790045. Published 2015.

49. Craftycoder. Precision Low Current Measurement w/ Feedback Ammeter. https://www.youtube.com/watch?v=YfB1hZ44B20. Published 2012.

50. Diagram C, Application T. LMC662 CMOS Dual Operational Amplifier LMC662. 2013;(March).

51. Instructables. Dual Voltage Supply (9V Batteries. http://www.instructables.com/id/Dual-Voltage-Supply-9V-batteries/.

52. Exchange EES. +/- 9V DC Power Supply. https://electronics.stackexchange.com/questions/2734/9v-dc-power-supply. Published 2013.